# HYDROTHERMAL SYNTHESIS AND STRUCTURAL STUDIES OF COBALT AND VANADIUM OXIDE COMPOUNDS

**Mr. Kittipong Chainok**

**A Thesis Submitted in Partial Fulfillment of the Requirements for the Degree of Master of Science in Chemistry**

**Suranaree University of Technology**

**Academic Year 2004**

**ISBN 974-533-356-5**

# การสังเคราะห์โดยวิธีไฮโดรเทอร์มัล และศึกษาโครงสร้างของสารประกอบโคบอลต์และเวนาเดียมออกไซด์

นายกิตติพงศ์ ไชยนอก

วิทยานิพนธ์นี้เป็นส่วนหนึ่งของการศึกษาตามหลักสูตรปริญญาวิทยาศาสตรมหาบัณฑิต

สาขาวิชาเคมี

มหาวิทยาลัยเทคโนโลยีสุรนารี

ปีการศึกษา 2547

ISBN 974-533-356-5

# HYDROTHERMAL SYNTHESIS AND STRUCTURAL STUDIES OF COBALT AND VANADIUM OXIDE COMPOUNDS

Suranaree University of Technology has approved this thesis submitted in partial fulfillment of the requirements for a Master's Degree.

Thesis Examining Committee

(Asst. Prof. Dr.Malee Tangsathitkulchai)

Chairperson

(Assoc. Prof. Dr.Kenneth J. Haller)

Member (Thesis Advisor)

(Asst. Prof. Dr.Kunwadee Rangsriwatananon)

Member

(Asst. Prof. Dr.Adrian E. Flood)

Member

(Assoc. Prof. Dr.Sarawut Sujitjorn)

Vice Rector for Academic Affairs

(Assoc. Prof. Dr.Prasart Suebka)

Dean of Institute of Science

กิตติพงศ์ ไชยนอก : การสังเคราะห์โดยวิธีไฮโดรเทอร์มัลและศึกษาโครงสร้างของสารประกอบโคบอลต์และเวนาเดียมออกไซด์ (HYDROTHERMAL SYNTHESIS AND STRUCTURAL STUDIES OF COBALT AND VANADIUM OXIDE COMPOUNDS) อาจารย์ที่ปรึกษา : รองศาสตราจารย์ ดร.เค็นเนท เจ. แฮลเลอร์, 135 หน้า. ISBN 974-533-356-5

วิทยานิพนธ์นี้รายงานการสังเคราะห์ผลึกเชิงเดี่ยวด้วยวิธีไฮโดรเทอร์มัล และพิสูจน์เอกลักษณ์โครงสร้างซุปราโมเล็กคิวลาร์ของโลหะที่เกิดจากอันตรกิริยาแบบไม่ใช่โควาเลนต์ โดยวิธีทางเอ็กซเรย์ สารประกอบยังได้ศึกษาด้วยวิธีการถ่ายภาพพื้นผิวและวิเคราะห์ธาตุ ฟูริเออร์ทรานสฟอร์มอินฟราเรดสเปกโทรสโกปี และการวิเคราะห์หาน้ำหนักของสารที่หายไปโดยความร้อน อีกด้วย

ผลึกของ $[Co(picoline)_3]\cdot H_2O$ อยู่ในระบบมอโนคลินิกกลุ่ม *C2/c* สารประกอบเชิงซ้อนเกิดโครงสร้างที่บิดเบี้ยวไปจากรูปทรงแปดหน้าด้วย *เมอร์* สามอะตอมไนโตรเจนจากไพริดีนและ *เมอร์* สามอะตอมออกซิเจนจากคาร์บอกซิลเลต เมื่อหลายๆ โมเลกุลถูกสร้างรวมกันขึ้นในทิศทาง [001] วงเอริลซ้อนทับกันมีอันตรกิริยาชนิดไพ-ไพ ($\pi\cdots\pi$) เกิดโครงสร้างแบบหนึ่งมิติลักษณะเป็นสายโซ่คล้ายหวีสองอันซ้อนกัน ถูกเชื่อมกลายเป็นแผ่นแบบสองมิติด้วยอันตรกิริยาชนิดคาร์บอนิล-คาร์บอนิล ไดโพล-ไดโพล ($C(\delta^+)\cdots O(\delta^-)$) และพันธะไฮโดรเจนชนิดแข็งแรง ($O-H\cdots O$) โดยใช้โมเลกุลของน้ำ พันธะไฮโดรเจนชนิดอ่อน ($C-H\cdots O$ และ $C-H\cdots\pi$) เชื่อมต่อกับแผ่นเกิดเป็นโครงสร้างซุปราโมเล็กคิวลาร์แบบสามมิติ

ผลึกของ $(H_2dap)^{2+}[(V^{IV}O)_2(V^{V}O_4)_2]^{2-}$ อยู่ในระบบมอโนคลินิกกลุ่ม $P2_1/c$ โครงสร้างผลึกประกอบด้วยโครงร่างสองมิติแบบเป็นชั้นๆ ของเวนาเดียม (IV) และเวนาเดียม (V) ออกไซด์ (เวนาดิล (IV) พีระมิดฐานสี่เหลี่ยม เวนาเดียม (V) ทรงสี่หน้า) ระหว่างชั้นสลับด้วยสองไอออนบวกของ 1,3-dap$H_2$ ซึ่งเชื่อมกันด้วยอันตรกิริยาพันธะไฮโดรเจนชนิดแข็งแรง ($N-H\cdots O$)

สาขาวิชาเคมี
ปีการศึกษา 2547

ลายมือชื่อนักศึกษา _____
ลายมือชื่ออาจารย์ที่ปรึกษา _____

KITTIPONG CHAINOK : HYDROTHERMAL SYNTHESIS AND STRUCTURAL STUDIES OF COBALT AND VANADIUM OXIDE COMPOUNDS. THESIS ADVISOR : ASSOC. PROF. KENNETH J. HALLER, Ph.D. 135 PP. ISBN 974-533-356-5

This thesis reports hydrothermal synthesis and single crystal X-ray structural characterization of metal containing supramolecular structures formed using noncovalent interactions. The compounds were also studied by scanning electron microscopy/energy dispersive X-ray analysis, Fourier transform infrared spectrophotometry, and thermogravimetric analysis.

$[Co(picoline)_3]\cdot H_2O$ crystallizes in monoclinic space group *C2/c*. The complex has distorted octahedral coordination geometry with tri *mer* pyridine nitrogen atoms and tri *mer* carboxylate oxygen atoms. The molecules pack in offset face-to-face $\pi$–$\pi$ stacks of aryl rings along [001] to form one-dimensional double comb chain motifs, bridged into two-dimensional sheets by $C(\delta^+)\cdots O(\delta^-)$ carbonyl-carbonyl dipole-dipole interactions and strong O–H···O hydrogen bonds with the water molecule. C–H···O and C–H···$\pi$ hydrogen bonding connect the sheets into the three-dimensional supramolecular assembly.

$(H_2dap)^{2+}[(V^{IV}O)_2(V^VO_4)_2]^{2-}$ crystallizes in monoclinic space group $P2_1/c$. The crystal structure consists of a two-dimensional anionic mixed valence $V^{IV}/V^V$ oxide network (square pyramidal $V^{IV}$ vanadyl and tetrahedral $V^V$) alternating with organic layers of 1,3-dap$H_2$ dications, extensively interconnected by strong N–H···O hydrogen bonding interactions.

School of Chemistry

Academic Year 2004

Student's Signature K. Chainok.

Advisor's Signature Kenneth J. Haller

# Acknowledgments

I would like to gratefully thank my advisor, Assoc. Prof. Dr. Kenneth J. Haller for the unique opportunity to accomplish an M.Sc. degree with him and to pursue my interests in materials science, and especially his specialty, X-ray crystallography and crystal engineering. In particular, I would like to thank him for offering several precious opportunities to attend international academic conferences and to make presentations in local and overseas meetings. He has helped provide a rich graduate experience, showing me the world, and opening many doors for me. Without his support and suggestions, this thesis would not have been possible.

Thanks to the members of my thesis examination committee: Asst. Prof. Dr. Malee Tangsathitkulchai (chairperson), Asst. Prof. Dr. Kunwadee Rangsriwatananon, and Asst. Prof. Dr. Adrian E. Flood for sparing their precious time for examining my thesis.

Many thanks also go to Prof. Ian D. Williams and Dr. Herman H.-Y. Sung for additional training in hydrothermal synthesis and crystallographic methods during a study visit at the Hong Kong University of Science and Technology.

In addition, special thanks are due to the other members of our research group, especially: Mr. Winya Dungkaew, Ms. Weenawan Somphon, Ms. Samroeng Krachodnok, Ms. Saiphon Chanpaka, and Mrs. Nongnaphat Khosavithitkul for their help.

Finally, I am deeply indebted to my parents, my brothers and sisters, and my girl friend for their support, patience and love.

Kittipong Chainok

# Contents

Page

Abstract in Thai ..... I

Abstract in English ..... II

Acknowledgements ..... III

Contents ..... IV

List of Tables ..... VII

List of Figures ..... IX

List of Symbols and Abbreviations ..... XII

**Chapters**

**I Introduction** ..... 1

1.1 Overview ..... 1

1.2 Supramolecular Chemistry ..... 2

**II Theoretical Background** ..... 27

2.1 Hydrothermal Crystal Growth Technology ..... 27

2.2 Single Crystal X-Ray Diffraction Technique ..... 33

**III Experimental** ..... 43

3.1 Chemicals ..... 43

3.2 Instrumentation and Instrumental Methods ..... 45

3.3 Procedures ..... 49

# Contents (Continued)

**Chapters** Page

**IV Hydrothermal Synthesis and Characterization of**

**[Co(picoline)$_3$]·H$_2$O** ..... 56

4.1 Introduction ..... 56

4.2 Hydrothermal Crystallization ..... 56

4.3 X-Ray Crystallographic Study ..... 57

4.4 Description of Structure ..... 58

4.5 Further Physical Characterization ..... 70

**V Hydrothermal Synthesis and Characterization of**

**$(H_2dap)^{2+}[(V^{IV}O)_2(V^VO_4)_2]^{2-}$** ..... 76

5.1 Introduction ..... 76

5.2 Hydrothermal Crystallization ..... 77

5.3 X-Ray Crystallographic Study ..... 78

5.4 Results and Discussion ..... 81

5.5 Further Physical Characterization ..... 91

**VI Conclusions** ..... 95

6.1 Conclusions ..... 95

6.2 Suggestions for Future Work ..... 97

References ..... 100

# Contents (Continued)

Page

Appendices ..... 119

Appendix A Supplementary Data for $[Co(picoline)_3]\cdot H_2O$ ..... 120

Appendix B Supplementary Data for $(H_2dap)^{2+}[(V^{IV}O)_2(V^{V}O_4)_2]^{2-}$ .... 127

Appendix C Submitted Abstracts and Presentations ..... 133

Curriculum Vitae ..... 135

# List of Tables


| Table | | Page |
|---|---|---|
| 1.1 | The van der Waals Radii Used for Observing Hydrogen Bonds | 13 |
| 1.2 | Properties of Hydrogen Bond Interactions | 17 |
| 2.1 | Target Materials and Associated Constants | 40 |
| 3.1 | Details of Experimental Preparations by the Hydrothermal Method | 53 |
| 3.2 | Results from Hydrothermal Synthesis, OM, and SEM-EDX Analysis | 54 |
| 4.1 | Summary of Crystal Data, Data Collection, and Structure Refinement Details for $[Co(picoline)_3]\cdot H_2O$ | 59 |
| 4.2 | Fractional Monoclinic Coordinates and Isotropic Atomic Displacement Parameters for the Refined Atoms in $[Co(picoline)_3]\cdot H_2O$ | 61 |
| 4.3 | Anisotropic Atomic Displacement Parameters in $[Co(picoline)_3]\cdot H_2O$ | 62 |
| 4.4 | Selected Interatomic Bond Lengths | 63 |
| 4.5 | Selected Interatomic Bond Angles | 63 |
| 4.6 | Intermolecular Hydrogen Bonds in $[Co(picoline)_3]\cdot H_2O$ | 64 |
| 4.7 | Vibrational Frequency Data of $[Co(picoline)_3]\cdot H_2O$ | 74 |
| 4.8 | Potential Decomposition Products of $[Co(picoline)_3]\cdot H_2O$ | 74 |
| 5.1 | Summary of Crystal Data, Data Collection, and Structure Refinement Details for $(H_2dap)^{2+}[(V^{IV}O)_2(V^{V}O_4)_2]^{2-}$ | 79 |
| 5.2 | Fractional Monoclinic Coordinates and Isotropic Atomic Displacement Parameters for the Refined Atoms in $(H_2dap)^{2+}[(V^{IV}O)_2(V^{V}O_4)_2]^{2-}$ | 80 |

# List of Tables (Continued)


| Table | | Page |
|---|---|---|
| 5.3 | Anisotropic Atomic Displacement Parameters in $(H_2dap)^{2+}[(V^{IV}O)_2(V^{V}O_4)_2]^{2-}$ | 82 |
| 5.4 | Selected Bond Lengths and Angles for $(H_2dap)^{2+}[(V^{IV}O)_2(V^{V}O_4)_2]^{2-}$ | 83 |
| 5.5 | Intermolecular Hydrogen Bonds in $(H_2dap)^{2+}[(V^{IV}O)_2(V^{V}O_4)_2]^{2-}$ | 85 |
| 5.6 | Bond Valence Sums for $(H_2dap)^{2+}[(V^{IV}O)_2(V^{V}O_4)_2]^{2-}$ | 86 |
| 5.7 | Potential Decomposition Products of $(H_2dap)^{2+}[(V^{IV}O)_2(V^{V}O_4)_2]^{2-}$ | 94 |
| A1.1 | Derived Fractional Monoclinic Coordinates and Isotropic Atomic Displacement Parameters for the Unrefined Hydrogen Atoms in $[Co(picoline)_3]\cdot H_2O$ | 120 |
| A1.2 | Selected Torsional Angles for $[Co(picoline)_3]\cdot H_2O$ | 121 |
| A1.3 | Principal Mean Square Atomic Displacements for $[Co(picoline)_3]\cdot H_2O$ | 123 |
| A1.4 | Mean Planes Calculated for $[Co(picoline)_3]\cdot H_2O$ | 124 |
| B1.1 | Derived Fractional Monoclinic Coordinates and Isotropic Atomic Displacement Parameters for the Hydrogen Atoms in $(H_2dap)^{2+}[(V^{IV}O)_2(V^{V}O_4)_2]^{2-}$ | 127 |
| B1.2 | Selected Torsional Angles for $(H_2dap)^{2+}[(V^{IV}O)_2(V^{V}O_4)_2]^{2-}$ | 128 |
| B1.3 | Principal Mean Square Atomic Displacements for $(H_2dap)^{2+}[(V^{IV}O)_2(V^{V}O_4)_2]^{2-}$ | 130 |
| B1.4 | Mean Planes Calculated for $(H_2dap)^{2+}[(V^{IV}O)_2(V^{V}O_4)_2]^{2-}$ | 131 |

# List of Figures


Figure Page

1.1 Structure-function relationship between molecular and supramolecular chemistry ..... 3

1.2 Self-assembly of an organic linker with metal-containing corners ..... 5

1.3 Aromatic-aromatic interactions ..... 7

1.4 Fourfold phenyl embraces of $Ph_4P^+$ pairs ..... 10

1.5 Schematic representation of the aryl embraces in $M(phen)_n$ complexes . 11

1.6 Hydrogen bond geometry and partial charges ..... 12

1.7 Structures of common hydrogen bond types ..... 15

1.8 Graph set notation for hydrogen bonds ..... 16

1.9 Representative examples of N,O-donor ligand types ..... 19

1.10 Hydrogen bonds in the supramolecular structure of $[Cu(picoH)_2]$ ..... 21

1.11 π–π stacking interactions in $[Cu(phen)Cl(HL)_{2/2}]$ and $[Cu(phen)(NO_3)(HL)_{2/2}]$ ..... 23

1.12 Two-dimensional structures of $[Cu(dap)VO_3]$, and $[Co(Hdpa)_2V_4O_{12}]$ ... 25

2.1 Temperature-density diagram of pure water ..... 31

2.2 Experimental autoclave apparatus for hydrothermal crystal growth ..... 33

2.3 The relationship of X-rays to other electromagnetic radiation ..... 35

2.4 A sealed tube X-ray source ..... 36

2.5 Continuous X-ray spectra as a function of accelerating voltage ..... 37

2.6 X-ray spectra with characteristic peaks for Mo and Cu x-radiation ..... 38

# List of Figures (Continued)


| Figure | | Page |
|---|---|---|
| 2.7 | Reflection of X-rays from lattice planes and diffraction by crystals | 42 |
| 3.1 | N,O-containing organic template molecules for experimental research | 45 |
| 3.2 | Teflon-lined stainless steel autoclave for hydrothermal synthesis | 49 |
| 3.3 | Variation of water pressure with temperature for various autoclave filling factors | 50 |
| 3.4 | Schematic diagram of the experimental research | 52 |
| 3.5 | SEM pictures of chosen crystalline materials | 55 |
| 4.1 | Perspective drawing of $[Co(picoline)_3]\cdot H_2O$ | 64 |
| 4.2 | Projection diagram down [010] showing the π–π stacking of rings **R1** along *c* | 65 |
| 4.3 | Projection diagram down the π–π stacking direction | 66 |
| 4.4 | P4AE interaction between two $[Co(picoline)_3]$ complex molecules | 67 |
| 4.5 | Space-filling model of the P4AE interaction between two $[Co(picoline)_3]$ complex molecules | 67 |
| 4.6 | Carbonyl-carbonyl antiparallel interaction motif | 68 |
| 4.7 | Schematic representation of the 2-D carbonyl-carbonyl linked π–stacked columns | 69 |
| 4.8 | Water bridging two molecules, showing strong O−H···O hydrogen bonds | 70 |
| 4.9 | The 2-D network of $[Co(picoline)_3]\cdot H_2O$ connected by hydrogen bonds | 71 |
| 4.10 | SEM picture of $[Co(picoline)_3]\cdot H_2O$ | 71 |

# List of Figures (Continued)


| Figure | | Page |
|---|---|---|
| 4.11 | EDX spectrum of $[Co(picoline)_3]\cdot H_2O$ | 72 |
| 4.12 | FTIR spectrum of $[Co(picoline)_3]\cdot H_2O$ | 73 |
| 4.13 | TGA curve of $[Co(picoline)_3]\cdot H_2O$ | 75 |
| 5.1 | ORTEP drawing of $(H_2dap)^{2+}[(V^{IV}O)_2(V^{V}O_4)_2]^{2-}$ | 85 |
| 5.2 | View of ball and stick model of the building unit with $\{V_4O_{10}\}^{2-}$ | 87 |
| 5.3 | A polyhedral representation of one unit of the tetravanadate network | 89 |
| 5.4 | The 2-D single layer structure of $\{V_4O_{10}\}^{2-}$ | 89 |
| 5.5 | View along the *b* axis of the alternating layers of anionic vanadium oxide and organic amine cations in the interlayer spaces | 90 |
| 5.6 | Edge view of the layers of $(H_2dap)^{2+}[(V^{IV}O)_2(V^{V}O_4)_2]^{2-}$ | 90 |
| 5.7 | SEM picture of $(H_2dap)^{2+}[(V^{IV}O)_2(V^{V}O_4)_2]^{2-}$ | 91 |
| 5.8 | EDX spectrum of $(H_2dap)^{2+}[(V^{IV}O)_2(V^{V}O_4)_2]^{2-}$ | 91 |
| 5.9 | FTIR spectrum of $(H_2dap)^{2+}[(V^{IV}O)_2(V^{V}O_4)_2]^{2-}$ | 92 |
| 5.10 | TGA curve of $(H_2dap)^{2+}[(V^{IV}O)_2(V^{V}O_4)_2]^{2-}$ | 93 |

# List of Symbols and Abbreviations

## Symbols

| | |
|---|---|
| ··· | noncovalent interaction or nonbonded interatomic separation |
| − | primarily covalent interaction or coordination interaction |
| −H··· | hydrogen bond interaction |
| ∠[ − ] | interplanar dihedral angle |
| ∠[ − − ] | interatomic angle for normal bonded atoms |
| ∠[ − ··· ] | interatomic angle involving a noncovalent interaction |
| ∠[ − − − ] | interatomic torsional angle |
| $\alpha$, $\beta$, $\gamma$ | unit cell angles |
| $\theta$ | Bragg angle or scattering angle |
| $\lambda$ | wavelength of x-radiation |
| $\mu$ | linear absorption coefficient |
| $\rho$ | electron density |
| $a$, $b$, $c$ | unit cell dimensions |
| d[ − ] | interatomic bond distance for normal bonded atoms |
| d[ ··· ] | interatomic bond distance involving a noncovalent atom |
| $U$[ ] | isotropic atomic displacement parameter for the indicated atom |
| $z$ | charge on an ionic species |
| $Z$ | number of formula units in the unit cell or<br>atomic number of an atom |

# List of Symbols and Abbreviations (Continued)

## Abbreviations

| | |
|---|---|
| 1-D | one-dimensional |
| 2-D | two-dimensional |
| 2PE | twofold phenyl embrace |
| 3-D | three-dimensional |
| 4AE | fourfold aryl embrace |
| 6AE | sixfold aryl embrace |
| 6PE | sixfold phenyl embrace |
| ACS | American Chemical Society |
| azpy | azobispyridine |
| bipy | bipyridine |
| bpe | 1,2-bis(4-pyridyl)ethane |
| btc | 1,3,5-benzenetricarboxylic acid |
| dap | 1,3-diaminopropane |
| dcb | dicyanobenzene |
| dpa | dipyridyl amine |
| DPE | Double Phenyl Embrace |
| EDX | Energy Dispersive X-ray analysis |
| *ef* | Edge-to-Face interaction\ |
| EvalCCD | data reduction software from Bruker Nonius |
| FTIR | Fourier transform infrared spectroscopy |

# List of Symbols and Abbreviations (Continued)

## Abbreviations

| | |
|---|---|
| gof | estimated standard deviation of an observation of unit weight, or goodness of fit |
| Hdpa | protonated di-2-pyridylamine |
| HL | maleic acid |
| Im | imidazole |
| ip | isophthalate |
| ISO | International Standards Organization |
| kV | kilovolts |
| mA | milliamperes |
| *off* | Offset Face-to-Face interaction |
| OM | Optical Microscopy |
| O4PE | Orthogonal Fourfold Phenyl Embrace |
| ORTEP | Oak Ridge Thermal Ellipsoid Plot program |
| OSPE | Offset Sextuple Phenyl Embrace |
| OTf | trifluoromethanesulfonate, triflate |
| pdc | pyridinedicarboxylic acid |
| phen | phenanthroline |
| picoH | protonated picolinate |
| P4AE | Parallel Fourfold Aryl Embrace |
| PQPE | Parallel Quadruple Phenyl Embrace |
| P4PE | Parallel Fourfold Phenyl Embrace |

# List of Symbols and Abbreviations (Continued)

## Abbreviations

| | |
|---|---|
| $R_1$ | conventional crystallographic discrepancy index |
| RPE | analytical grade reagent chemical |
| SEM | scanning electron microscope |
| SHELXL97 | least squares structure refinement program |
| SIR97 | direct methods structure solution software |
| SPE | Sextuple Phenyl Embrace |
| TGA | thermogravimetric analysis |
| TMA | trimesic acid |
| TQPE | Translational Quadruple Phenyl Embrace |
| tp | teraphatlate |
| tptz | 2,4,6-tri(2-pyridyl)-s-triazine |
| *vf* | Vertex-to-Face interaction |
| $wR_2$ | weighted crystallographic discrepancy index |

# Chapter I

# Introduction

## 1.1 Overview

Currently, the solid state structure of materials is attracting considerable attention. The main objective being to solve the questions of why the materials perform as they do, and how to make new materials that have functions useful for technology, science, engineering, and daily life. Knowledge of the structure of materials is one of the fundamental aims of chemistry, and is an excellent route to profound understanding of the physical and chemical properties of materials, supporting development of new materials and leading to important new applications and discoveries.

The overall research goal is the design and synthesis of new organic-inorganic hybrid supramolecular compounds by the hydrothermal approach with an emphasis on understanding the fundamental issues of structural assembly and growth that will enable the rational control of material composition, property, and functionality as evidenced by single crystal X-ray diffraction analyses. It is expected that, these supramolecular compounds, with special geometric and topological character, have various potential applications in catalysis (Bugnet, Nixon, Kilner, Greatrex & Kee, 2003), electrooptic or magnetic devices (Moulton & Zaworotko, 2001), liquid crystal or mesogen applications (Serrano & Sierra, 2003), sensor materials (Dickert & Sikorski, 1999), and molecular recognition (Hosseini, 2003; Rathore, Lindeman & Kochi, 1997).

## 1.2 Supramolecular Chemistry

Supramolecular chemistry is one of the most popular and fastest growing areas of experimental science. It combines knowledge from chemistry, biology, and physics while utilizing the most modern research technology (Steed & Atwood, 2000). One precise definition of supramolecular chemistry has been given by Jean-Marie Lehn, who received a Noble Prize for his pioneering work on supramolecular chemistry in 1987, as "chemistry of the intermolecular bond, covering the structures and functions of the entities formed by association of two or more chemical species" (Lehn, 1988). More extended definitions, including the nature of the interactions have been subsequently offered; "…the chemistry of the intermolecular bond, covering the structures and functions of the entities formed by association of two or more chemical species through weaker noncovalent bond interactions such as hydrogen bonding, electrostatic interaction, electron-donor/electron-acceptor interactions, and π–π stacking interactions" (Dinolfo & Hupp, 2001).

**Self-Assembly**

Supramolecular self-assembly has been used as a powerful tool by natural organisms in assembling small subunits into complex macroscopic structures (Papaefstathiou & MacGillivray, 2003). It has been defined in a number of ways. Lehn (1988) defined supramolecular self-assembly as the "spontaneous association of either a few or many components resulting in the generation of either discrete oligomolecular supramolecular or of extended polymolecular assemblies". Self-assembly involves many noncovalent intermolecular interactions that might be arranged in the following four categories (Desiraju, 2003):

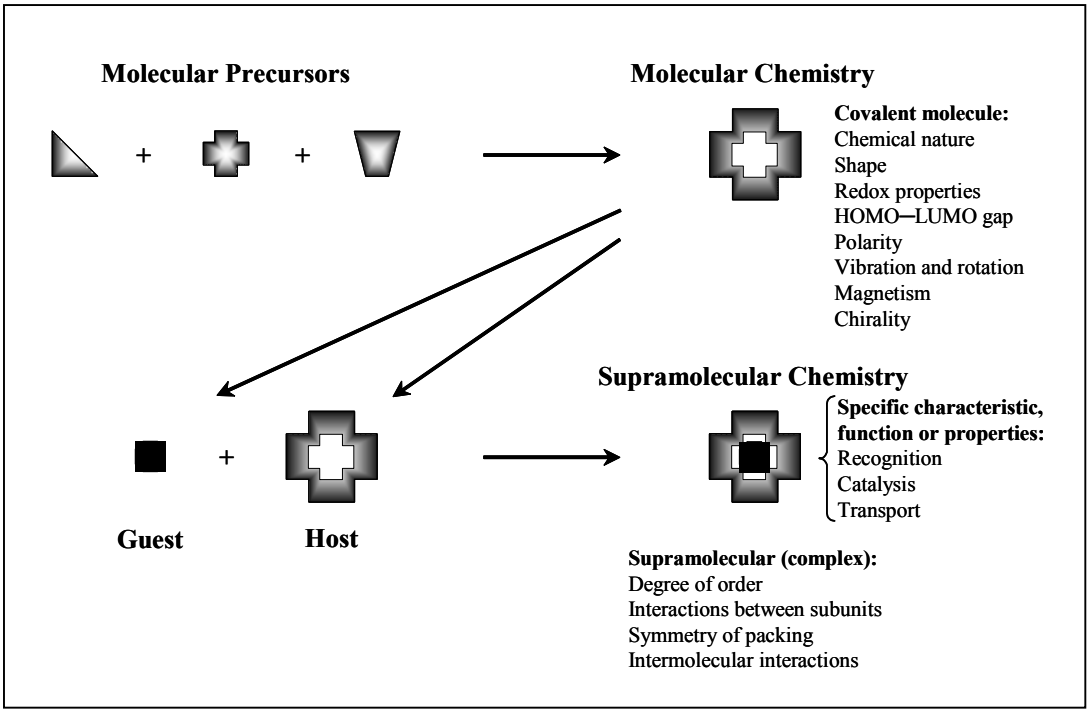


Figure 1.1. Structure-function relationship between molecular and supramolecular chemistry. (Reproduced with permission from Steed & Atwood, 2001, *Supramolecular Chemistry*, John Wiley & Sons, New York).

(i) coordination bonding (metal-ligand),

(ii) hydrogen bonding,

(iii) electrostatic forces (π–π stacking, van der Waals, and dipole-dipole interactions), and

(iv) hydrophobic/hydrophilic interactions.

Recently, self-assembly of well-defined inorganic architectures has been considered to result from the operation of programmed supramolecular systems, based on suitably designed ligands, resulting in a variety of inorganic entities (Erxleben, 2003).

Ferrer, Rodriguez, and Rossell (2003) have used the diaza ligand, 1,4-bis(4-pyridyl)-butadiyne, as a linker in self-assembly reactions with different diphosphine Pd(II) and Pt(II) triflates to build metallo supramolecular squares and triangles as illustrated in Figure 1.2. Other self-assembled metallosupramolecular squares, where 90° angles at the four vertices of the polygon are provided by transition metals, hypervalent iodine, or organic frameworks, have been experimentally studied and the results quantified (Leininger, Olenyuk & Stang, 2000; Cotton, Lin & Murillo, 2001).

**Supramolecular Interactions**

The noncovalent interactions involved in supramolecular entities may be a combination of several types of interaction as follows:

*Ion-ion interactions* (40-380 kJ $mol^{-1}$) are attractive interactions between a positive ion and a negative ion or repulsion between two ions of the same charge. An example of supramolecular ion-ion interaction can be seen in the interaction of the organic terephthalate anion with copper(II) to produce the structure of the missing $[Cu_2(terephthalate)_4]$ paddle-wheel coordination polymer (Chainok, Haller & Williams, 2002).

*Ion-dipole attractions* (40-210 kJ $mol^{-1}$) are the electrostatic attractions between ions and dipoles (the separation of charge in a bond or a molecule with a positively charged end and a negatively charged end) of the molecules. Simple examples of ion-dipole interaction are the alkali metal cations, $Li^+$, $Na^+$, $K^+$, $Rb^+$ and $Cs^+$, interacting with polar macrocyclic crown ether molecules, reviewed by Steed, 2001.

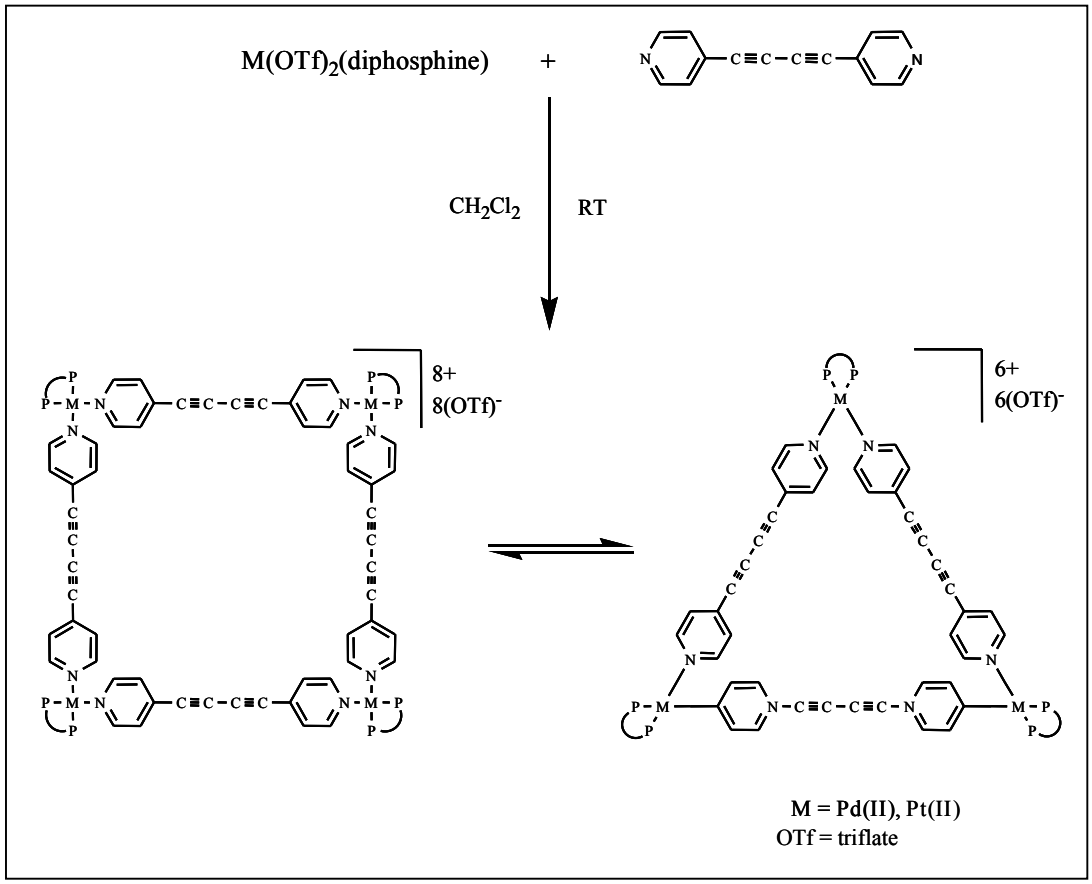


Figure 1.2. Self-assembly of an organic linker with metal-containing corners. (after Ferrer, Rodriguez & Russell, 2003).

*Dipole-dipole interactions* (4-40 kJ $mol^{-1}$) are intermolecular or intramolecular interactions between molecules or groups of atoms having permanent electric dipole moments. The strength of the interaction depends on the distance, strength of the dipoles, and relative orientation of the dipoles. The term also applies to intramolecular interactions between bonds having permanent dipole moments. For example, the attraction between the positive polarity carbon atom and the negative polarity oxygen atom of adjacent carbonyl groups in pyridine-3,5-dicarboxylic acid(Krachodnok & Haller, 2004).

*Cation–π interactions* (4-85 kJ $mol^{-1}$) are the attractions of positive charges toward the π-electron clouds of aromatic moieties. Ethylene, acetylene, and other simple π systems are documented to be involved in cation–π interactions. A review of cation–π interactions has recently been published (Ma & Dougherty, 1997).

*π–π stacking interactions* (4-20 kJ $mol^{-1}$) are weak electrostatic interactions that occur between aromatic moieties which can interact in different physical arrangements: face-to-face stacked arrangement (offset, slipped, or parallel displaced), and edge-to-face or point-to-face, T-shaped conformation; These orientations come from C−H···π interactions between positively charged hydrogen atoms (the C−H bond generally having a small dipole moment) and a negatively charged π-cloud of the aromatic system. The perfect facial alignment of an eclipsed face-to-face orientation is unlikely because all the electrostatic interactions would be repulsive between the two negatively charged π-systems of the aromatic rings (Hunter & Sanders, 1990) and between the positive ends of the C−H dipoles. The distance between the aromatic faces in a π–π interaction is about 3.3-3.8 Å (Janiak, 2000). Types of aromatic-aromatic interactions are illustrated in Figure 1.3.

Concerted aromatic-aromatic interactions were first identified by Dance and Scudder in 1995 as multiple phenyl embrace motifs. These supramolecular motifs are named as multiple phenyl (aryl) embraces because they are multi-armed, concerted, and attractive (Scudder & Dance, 2002). The individual intermolecular phenyl-phenyl conformations are offset face-to-face (*off*), and edge-to-face (*ef*) or vertex-to-face (*vf*) geometries. Five classes of supramolecular multiphenyl interaction motifs were identified (1996a) by Dance and Scudder:

(i) the sextuple phenyl embrace (SPE) with $(ef)_6$,

(ii) offset sextuple phenyl embrace (OSPE) with $(off)_1(ef)_2(ef/vf)_2$,

(iii) the translational quadruple phenyl embrace (TQPE) with $(ef)_4$,

(iv) the parallel quadruple phenyl embrace (PQPE) with $(off)_1(vf)_2$, and

(v) the double phenyl embrace (DPE) with $(off)_1$.

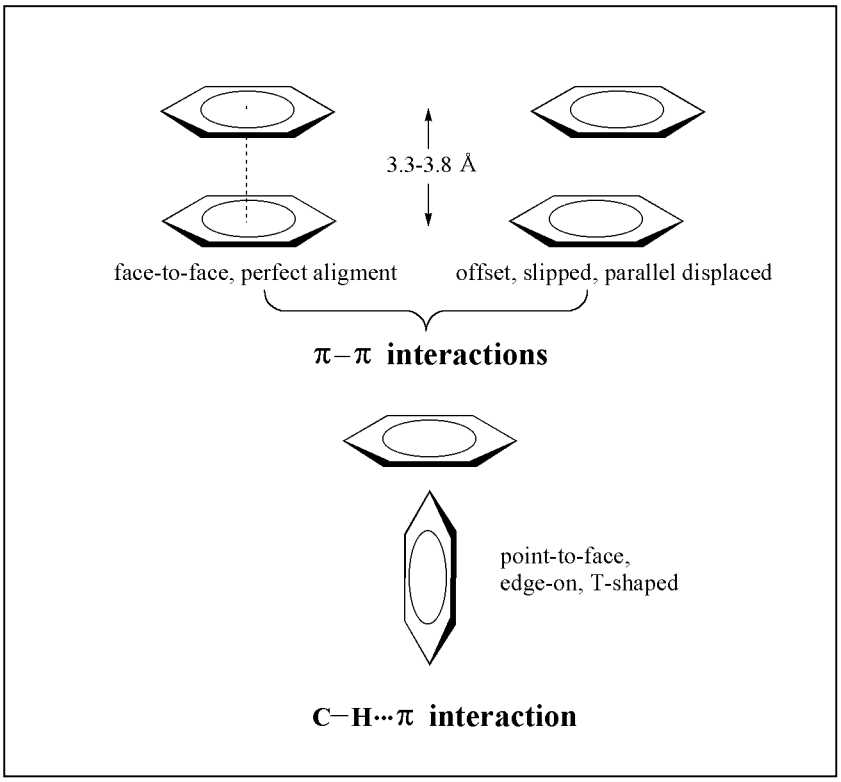


Figure 1.3. Aromatic-aromatic interactions.

Several additional motifs have subsequently been identified (Dance & Scudder, 1996b), and the original motifs have been renamed in an attempt to develop an unambiguous systematic naming system (sextuple (S) became sixfold (6), quadruple (Q) became fourfold (4), and aryl (A) was added as an alternative to phenyl (P); thus,

SPE, TQPE, PQPE, and DPE became 6PE, O4PE, P4PE, and 2PE, respectively). However, to date the most common supramolecular motif embraces remain the sixfold (6PE, 6AE) and fourfold (4PE, 4AE) phenyl or aryl embraces based on intermolecular *ef* interactions between phenyl or aryl groups.

In the sixfold phenyl embrace, three phenyl rings on one molecule are oriented between three phenyl rings on another molecule such that there is a supramolecular concert of six *ef* intermolecular phenyl-phenyl interactions (often across a center of inversion). Each interaction is from the edge of one ring to the face of another, across the intermolecular space. Each ring is the donor in one *ef* interaction and the acceptor in another. Sixfold phenyl embraces in tetraphenyl-phosphonium salts typically have net attractive energies in the range 60 to 85 kJ $mol^{-1}$ per $[Ph_4P^+]_2$ pair, and P···P separations in the range 5.8 to 6.8 Å (Dance & Scudder, 1996a). Multiple phenyl/aryl embraces formed by metal complexes with 2,2′-bipyridine (bipy), 1,10-phenanthroline (phen), tridentate terpyridine (terpy) and/or other aryl N-donor chelating ligands provide elaborate examples for π–π interaction that have been extensively studied by Dance and coworkers (Dance & Scudder, 1998; Scudder, Goodwin & Dance, 1999; Horn, Scudder & Dance, 2001; Russell, Scudder & Dance, 2001).

When the sixfold aryl embrace forms, for example, between the octahedral tris-ligand complexes, $[M(bipy)_3]^z$ (where M = V, Cr, Ni, Zn, Ru, Rh), where three aryl sections protruding in a threefold array from one end of the complex can form a concerted cycle of six *ef* interactions with the threefold array from another complex. The other end of the $[M(bipy)_3]^z$ complex (along the threefold axis) is the same, and it

can form another 6AE embrace, thereby forming an infinite 1-D supramolecular structure chain of complexes connected by 6AE embraces. The M···M distance for a pair of $[M(bipy)_3]^z$ complexes is *ca* 7.7 Å for $z = 0$, and 8.1 ± 0.1 Å for $z = 2$ and at least 1 Å longer than the P···P distance of a 6PE (Dance & Scudder, 1998). Another example of the infinite chain 6AE occurs in $[Fe(phen)_3]^{2+}(I_8)^{2-}$ (Horn, Scudder & Dance, 2001).

In the fourfold phenyl embrace (4PE) only two phenyl rings from each cation are used. As shown in Figure 1.4, there are two variant subclasses, that is the parallel (P4PE) and orthogonal (O4PE) embraces named according to the parallel or orthogonal relationship between the relevant C−P−C planes on each molecule. In P4PE there is one *off* interaction across the center of the embrace, and two *ef* interactions between rings, while in O4PE there is a concerted cycle of four *ef* interactions between rings as illustrated in Figure 1.4. In addition, 4PE are usually centrosymmetric, and therefore heterochiral. 4AE embraces occurring in $M(phen)_2$, and $M(phen)_3$, complexes vary in geometry between a single *off* at one extreme to $(ef)_2$ at the other. The principal embrace types for M-phen complexes are represented diagrammatically in Figure 1.5.

The P4AE motif occurs in the *C2/c* crystals of $[Os(phen)_3][ClO_4]_2{\cdot}2H_2O$. There are segregated hydrophobic and hydrophilic slabs, the latter containing the $ClO_4^-$ and $H_2O$, while the former contains the $[Os(phen)_3]^{2+}$ complexes associated in chains of P4AE, but with a variation of the local P4AE geometry such that there is an *off* stack of phen ligands also propagated along the P4AE chain axis. This one-dimensional motif is therefore an alternation of the *off* interactions and P4AE motifs,

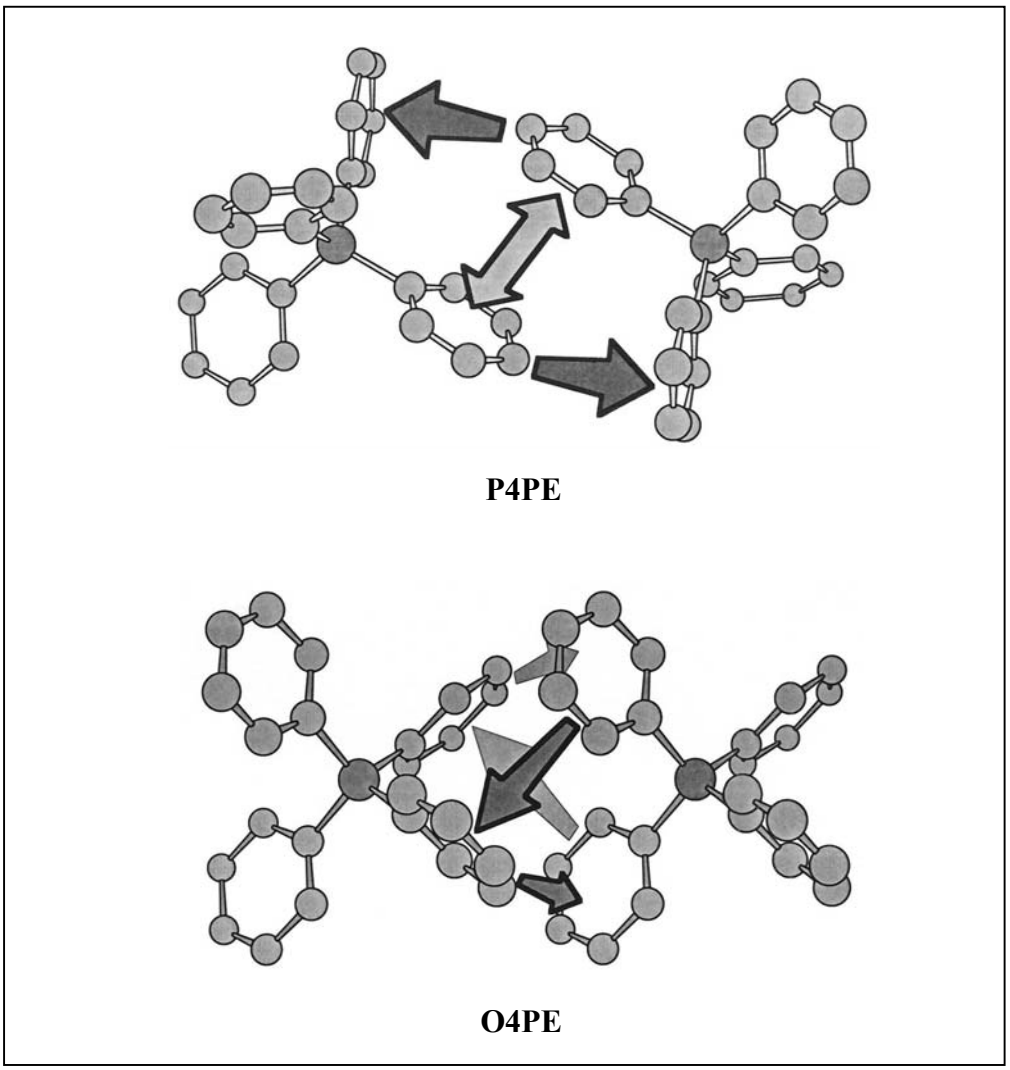


Figure 1.4. Fourfold phenyl embraces of $Ph_4P^+$ pairs. Above is the parallel fourfold phenyl embrace (P4PE), and below is the orthogonal fourfold phenyl embrace (O4PE). Hydrogen atoms have been omitted for clarity. (Dance & Scudder, 1996a).

P4AE-*off* chain type I in Figure 1.5. Another P4AE-*off* chain, type II, illustrated in Figure 1.5 occurs in the *C2/c* lattice structure types of $[Co(phen)_3][ClO_4]_2 \cdot H_2O$ and $[Co^{III}(phen)_3][ClO_4]_3 \cdot 2H_2O$ (Russell, Scudder & Dance, 2001).

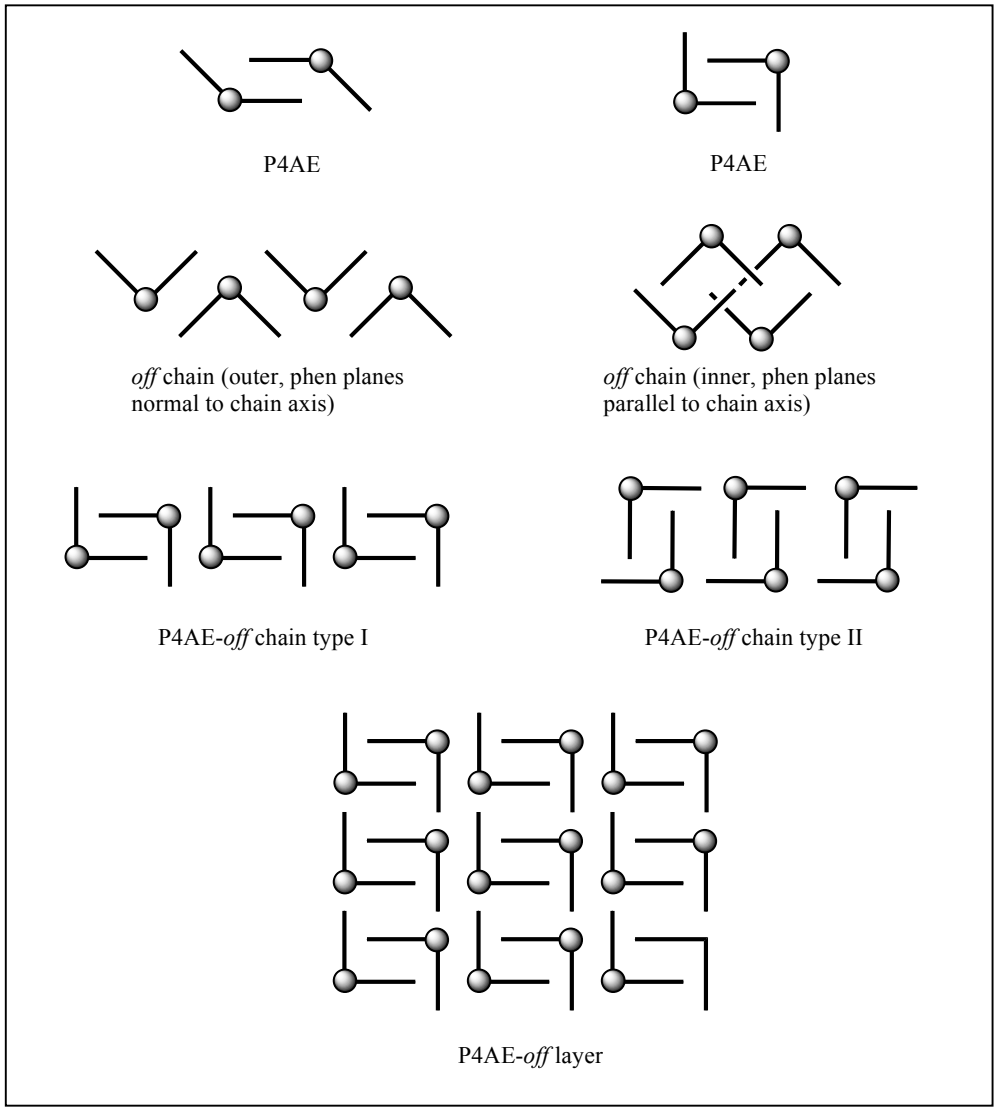


Figure 1.5. Schematic representation of the aryl embraces in M(phen)$_n$ complexes. The dot is metal, and the lines are phen ligand planes (Russell, Scudder & Dance, 2001).

*Hydrogen bond interactions* (4-65 kJ mol$^{-1}$) are bonding interactions between acidic hydrogen atoms and negatively charged or negatively polarized atoms with (or without) lone-pairs as depicted in Figure 1.6 (left). They are described by the formula

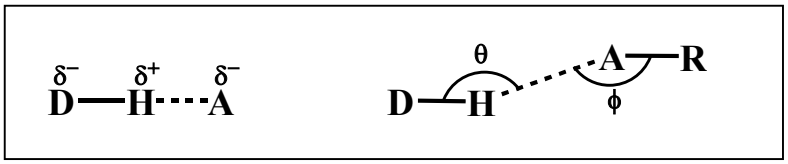


Figure 1.6. Hydrogen bond geometry and partial charges. Donor and acceptor atoms in a hydrogen bond (left), and angular dependence in hydrogen bonds (right).

D−H···A (where D represents the donor atom that is bonded to the acidic hydrogen atom, and A represents the acceptor atom to which the acidic hydrogen atom is bonded). Hydrogen bonds are widely exploited in molecular crystal engineering (Braga, Grepioni & Desiraju, 1998; Desiraju, 2002; Beatty, 2003), have been used extensively in molecular recognition applications (Hosseini, 2003), and are especially important because they best combine both strength and directionality (Braga & Grepioni, 2001). The most commonly used criteria for identification of a strong hydrogen bond, are the interatomic distances H···A and D···A, and the angle (θ), illustrated in Figure 1.6 (right). If the distance between the hydrogen and acceptor atoms is significantly shorter than the sum of van der Waals radii, and if θ is close to 180°, a hydrogen bond is usually present. Several studies have shown the angular dependence of θ to be related to the strength of the hydrogen bond (Bernstein, Etter, Leiserowitz, 1994). Stronger hydrogen bonds tend to show a shorter H···A distance, correlated with an elongated D−H bond and a θ between 170-180°. In cases where the acceptor is a carbonyl (C═O), the ϕ angle is most frequently between 110° and 130°, corresponding to the regions of the lone electron pairs (Braga, Grepioni, Sabatino & Desiraju, 1994). Irrespective of the criteria listed above, it has become widely

accepted that there is a hydrogen bond interaction whenever the H···A and/or the D···A distances are less than the sum of the van der Waals radii. Accordingly, a list of van der Waals radii, such as that in Table 1.1 for some common atoms, with comparison between Pauling (1945), Bondi (1964), and Rowland and Taylor (1996) radii, is an essential tool for observing hydrogen bonds.

Table 1.1. The van der Waals Radii (in Å) Used for Observing Hydrogen Bonds.

| Element | Pauling (1945) | Bondi (1964) | Rowland and Taylor (1996) |
|---|---|---|---|
| H | 1.20 | 1.20 | 1.09 |
| C | | 1.70 | 1.75 |
| N | 1.50 | 1.55 | 1.61 |
| O | 1.40 | 1.52 | 1.56 |
| F | 1.35 | 1.47 | 1.44 |
| S | 1.85 | 1.80 | 1.79 |
| Cl | 1.80 | 1.75 | 1.74 |
| Br | 1.95 | 1.85 | 1.85 |
| I | 2.15 | 1.98 | 2.00 |

The structure and strength of hydrogen bonds in inorganic solids has recently been examined by Lutz (2003). He remarked that they depend on several factors, including the various D−H···A motifs possible, the inherent hydrogen bond donor strength of the acid hydrogen atom, the inherent acceptor capability of the respective acceptor groups, collective phenomena (cooperative, competitive, and synergetic effects), and structural features, such as the number of acceptors *e*.g. two-center, three-center (bifurcated), *etc.* hydrogen bonds, and the hydrogen bond angles

D−H···A (linear or bent) and H···A−R. As already mentioned, the nature and strength of hydrogen bonds strongly depends on both the hydrogen-bond donors and acceptors involved and the structural arrangement of the hydrogen bonds. Therefore, structural arrangement including geometry, coordination, and configuration is essential for understanding hydrogen bonding. Figure 1.7 illustrates the structures of several common hydrogen bond types.

Graph theory is one convenient method for analyzing, manipulating, and understanding hydrogen-bond patterns in crystals (Kuleshova & Zorkii, 1980). There are four basic pattern types for the three types of intermolecular hydrogen bonds including C (chain or catemer), R (ring), and D (dimer or other finite set) and one for intramolecular hydrogen bonds, denoted S (self). The number of donors (*d*) and acceptors (*a*) used in each motif are assigned as subscripts and superscripts, respectively, and the size or degree of the motif (*n*) in which corresponding to the number of atoms in the repeat unit is indicated in parentheses, *e.g.* $R_2^2(8)$. Examples of graph set hydrogen bond patterns are depicted in Figure 1.8.

Several experimental techniques are useful to study hydrogen bonding. X-ray and neutron diffraction, inelastic neutron scattering, infrared and Raman spectroscopy, and nuclear magnetic and nuclear quadrupole resonance measurements are used for studying type, structural arrangement, distances and angles involved, and strength of hydrogen bonds (Lutz & Haeuseler, 1999; Huyskens, Sobczyk & Majerz, 2002; Godzisz, Ilczyszyn & Ilczyszyn, 2002). The experimental methods have been nicely supplemented with theoretical approaches, such as *ab initio* and density functional methods, variational methods, quantum diffusion Monte Carlo methods, and so on

(Császár & Mills, 1997; Pejov, 2002; Grabowski, 2001). The distances, in terms of long, medium, and short D···A and H···A, used for classification of the strength of hydrogen bonds, along with other properties of hydrogen bonds, are summarized in Table 1.2.

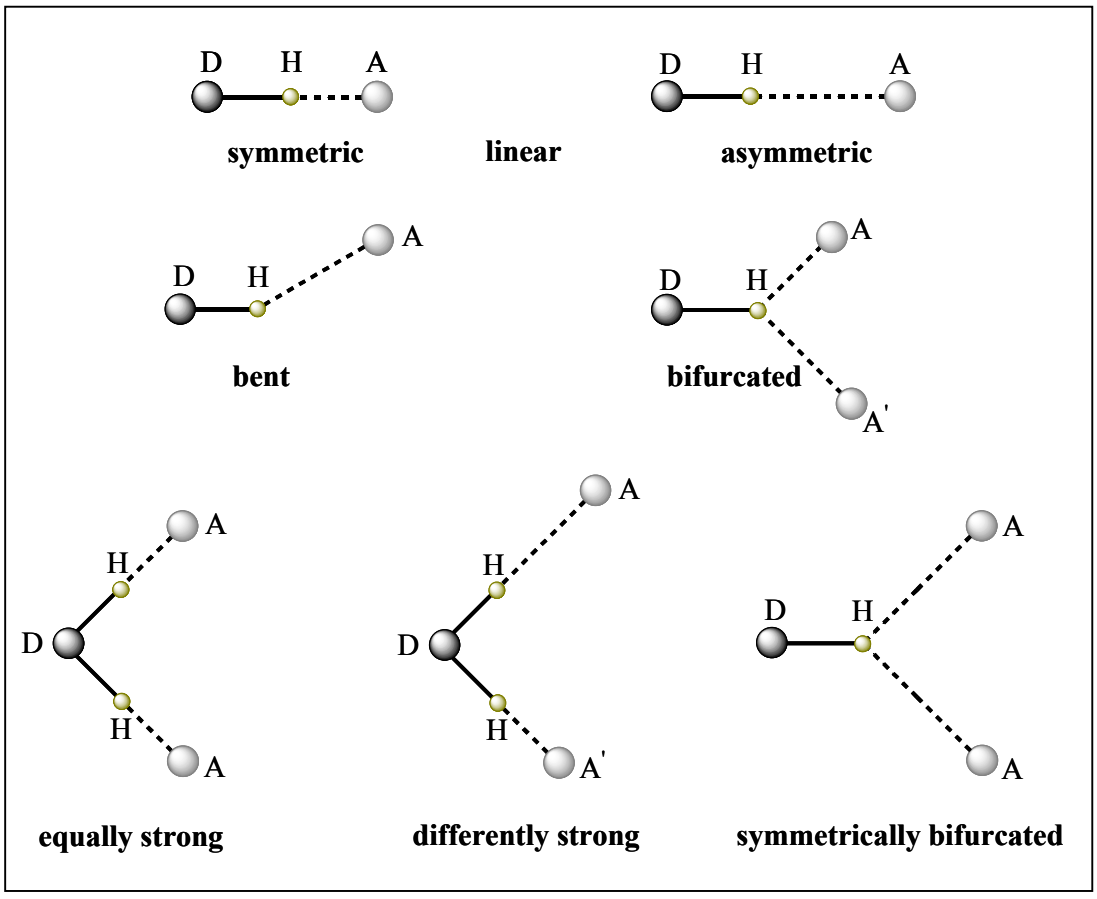


Figure 1.7. Structures of common hydrogen bond types (Lutz, 2003).

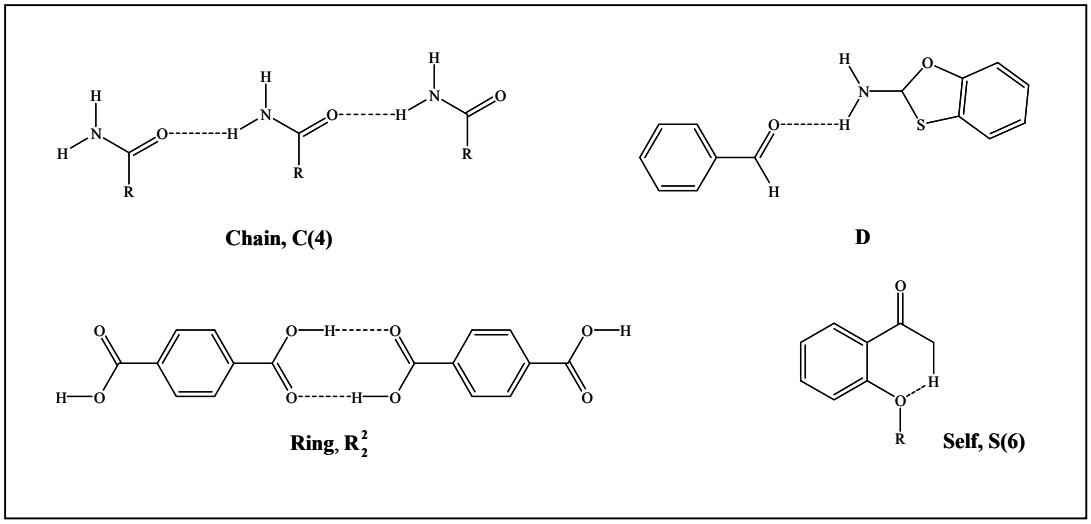


Figure 1.8. Graph set notation for hydrogen bonds.

Solvophobic effects (in polar solvents) leading to desolvation can stabilize and cause aggregation of lipophilic molecular surfaces, especially with compounds containing aromatic π system (Waters, 2002). It has been reported that the strength of π-stacking interaction is very sensitive to solvent and strongly influenced by the electrostatic properties of the interacting rings (Leonard, 1979; Hunter & Sanders, 1990). Moore and coworkers (2000, 2002) has designed both cyclic and linear systems made up of *m*-phenylene ethynylene units that spontaneously associate in polar solvents. The driving forces for these associations are believed to be stacking of the aromatic rings. The fact that association occurs preferentially in polar solvents suggests that solvophobic forces influence this system significantly. The same phenomenon has also been observed in *m*-diethynylbenzene macrocycles (Tobe, Utsumi, Kawabata, Nagano, Adechi, Araki, Sonoda, Hirose & Naemura, 2002).

Table 1.2. Properties of Hydrogen Bond Interactions.

| | Strong | Moderate | Weak |
|---|---|---|---|
| D─H···A interaction | Mainly covalent | Mainly electrostatic | Electrostatic |
| Bond energy (kJ $mol^{-1}$) | 60−120 | 16-60 | <12 |
| Bond lengths (Å) | | | |
| H···A | 1.2−1.5 | 1.5−2.2 | 2.2−3.2 |
| H···D | 2.2−2.5 | 2.5−3.2 | 3.2−4.0 |
| Bond angles (°) | 175−180 | 130−180 | 90−150 |
| Relative IR vibration shift (symmetrical stretching mode, $cm^{-1}$) | 25% | 10−25% | <10% |
| $^{1}H$ NMR chemical shift (downfield ppm) | 14−22 | <14 | ? |
| Examples | Gas phase dimers with strong acids/bases<br>Proton sponge<br>HF complexes | Acids<br>Alcohols<br>Biological molecules | Minor components of bifurcated bonds<br>C−H···A hydrogen bonds<br>O−H···π hydrogen bonds |

(Steed & Atwood, 2000)

Supramolecular chemistry research has exploded during the last decade. The syntheses of various supramolecular compounds has helped to obtain new information on intermolecular interactions. Such noncovalent interactions provide the key to understanding the relationship between structure and function in chemistry, biology, and materials science. Understanding of interactions in crystal packing has been important in developing new tools for the rational design and construction of new framework structures with desired physical and chemical properties for potential applications in various fields.

The use of transition metal ions, coordination chemistry, and selected ligand molecules to control assembly of molecular architectures is a burgeoning area, so much so, that the *Annual Reports on Progress in Chemisry* recently replaced the series on "Coordination of Polydentate Ligands" with "Supramolecular Coordination Chemistry" (Ward, 2000). The design of bridging ligands is at the heart of this area of supramolecular chemistry. Several rigid ligands containing either N-donor or O-donor atoms have been widely used because of their physiological activity and rich noncovalent interaction possibilities. These ligands have played an important role in the formation of 1-D, 2-D, and 3-D supramolecular architectures. For example, the protonated amino group of 2,6-pyridinedicarboxylic acid (2,6-pdc) may be a hydrogen bond donor and the (deprotonated) carboxylate group may be an acceptor, while in 1,10-phenanthroline, the C–H groups can act as hydrogen bond donors, and the π-clouds as hydrogen bond acceptors. Some examples of N-donor or O-donor ligands that have been widely used in the formation of supramolecular architectures are depicted in Figure 1.9.

Recently, inherently rigid space ligands, such as 2,4-pdc, 2,5-pdc, 3,5-pdc, and 2,6-pdc which possess diverse functional groups and have more possibility to form bridging hydrogen bonds were employed as building blocks, because of their potential for self-assembly. Whitfield, Zheng, Wang & Jacobson (2001) reported the hydrothermal synthesis and single crystal X-ray structural characterization of $[Co(pdc)(H_2O)_2]$ and $[Ni(pdc)(H_2O)]$, where pdc = 3,5-pdc. The structure of $[Co(pdc)(H_2O)_2]$ is composed of honeycomb layers built up from $\{CoO_4N\}$ trigonal

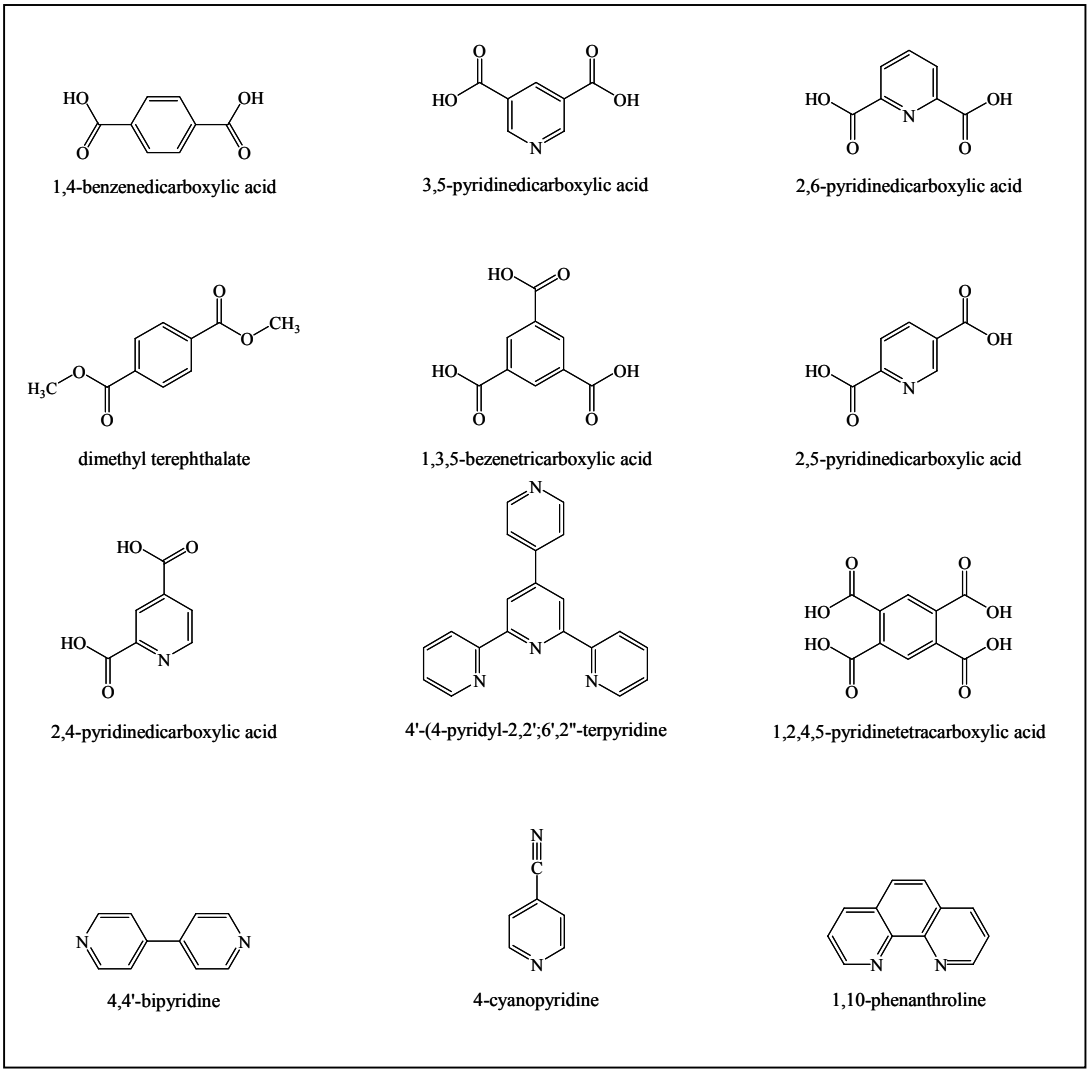


Figure 1.9. Representative examples of N,O-donor ligand types.

bipyramids and pdc bridges, while the structure of [Ni(pdc)($H_2O$)] adopts a 3-D framework in which the Ni atoms are coordinated by pdc bridges both within the honeycomb layer and between the layers. Plater, Roberts & Howie, (1998) reported the hydrothermal reaction between $Co(OAc)_2 \cdot 4H_2O$ and 3,5-pdc in a 1:1 mole ratio to give a 2-D cobalt polymer $[Co(pdc)] \cdot 2H_2O$, in which the seven-coordinate cobalt metal is bonded to two bidentate carboxylate groups, one pyridine nitrogen, and two water molecules. In the same year, they also employed the hydrothermal method to

synthesize coordination polymers of $[M(pdc)]\cdot 3H_2O$, where M = $Co^{II}$, $Ni^{II}$, or a mixture of $Co^{II}_{(0.4\text{-}0.6)}$ and $Ni^{II}_{(0.6\text{-}0.4)}$, and pdc = 2,5-pdc. These mixed metal Co–Ni coordination polymers are the first examples that have been prepared by hydrothermal synthesis (Plater, Forman, Howie & Lachowski, 1998).

Numerous other examples of pyridinedicarboxylic acid as a bridging ligand in transition metal systems have been synthesized by hydrothermal methods and characterized, and can be found in the literature, including 3-D $[Co(pdc)H_2O]$ (Min, Yoon, Lee, Suh & Lee, 2001), 3-D $[Tb_2(3,5\text{-pdc})_2(H_2O)_4(C_2O_4)]\cdot 2H_2O$, and $[Tb(2,4\text{-pdc})(H_2O)(C_2O_4)_{0.5}]$ (Min & Lee, 2002), 1-D $[Cu(2,5\text{-pdc})(H_2O)]$, and $[Cu(2,4\text{-pdc})_2]$ (Min, Yoon, Jung, Lee, Kim, Han & Lee, 2001), and 2-D $[Mn(3,5\text{-pdc})\cdot 2H_2O]$ (Haitao, Nengwu, Hanhuia, Yonggang, Ruyi, Enyi & Xianglin, 2002).

More recently, 3-hydroxypicolinic acid (pico) has been used for fabricating extended structures. It can coordinate as a monodentate or bridging ligand through the oxygen atoms of the deprotonated carboxylic anion, as a six-member ring O,O-chelating ligand through the carboxylate group and the deprotonated hydroxyl group, or as a five-member ring N,O-chelating ligand through the pyridine nitrogen and the carboxylate group. For example, $[Cu(picoH)_2]$ was synthesized by the hydrothermal method (Sun, Zheng & Jin, 2003). The copper(II) ion is strongly coordinated by four atoms ($N_2O_2$) in a square-planar fashion, and also interacts weakly with two other oxygen atoms, forming a '4 + 2' distorted octahedron. The weak Cu–O coordination bonds and hydrogen bonds bring the moieties into a 3-D supramolecular network, as shown in Figure 1.10.

Terephathalates (tp) have been used in many synthetic systems because they can form short bridges *via* one carboxylate end or long bridges *via* the benzene ring. The helical metal complex of $[Fe(phen)(ip)]_n$ has been hydrothermally synthesized from isophthalate (ip), 1,10-phenanthroline, $FeCl_2 \cdot 4H_2O$, and water (Hou, Shen, Wang, Wang, Xiao, Li, Xu & Hu, 2003). The structure is composed of left-handed and right-handed helical chains in which phen ligands project above and below into the interlamellar region and strong π–π stacking interaction occurs between adjacent chains. Moreover, mixed between phen and maleic acid with $CuCl_2 \cdot 2H_2O$ and $Cu(NO_3)_2 \cdot 3H_2O$ in $CH_3OH/H_2O$ (1:1 v/v) at pH = 2.0 under hydrothermal synthesis

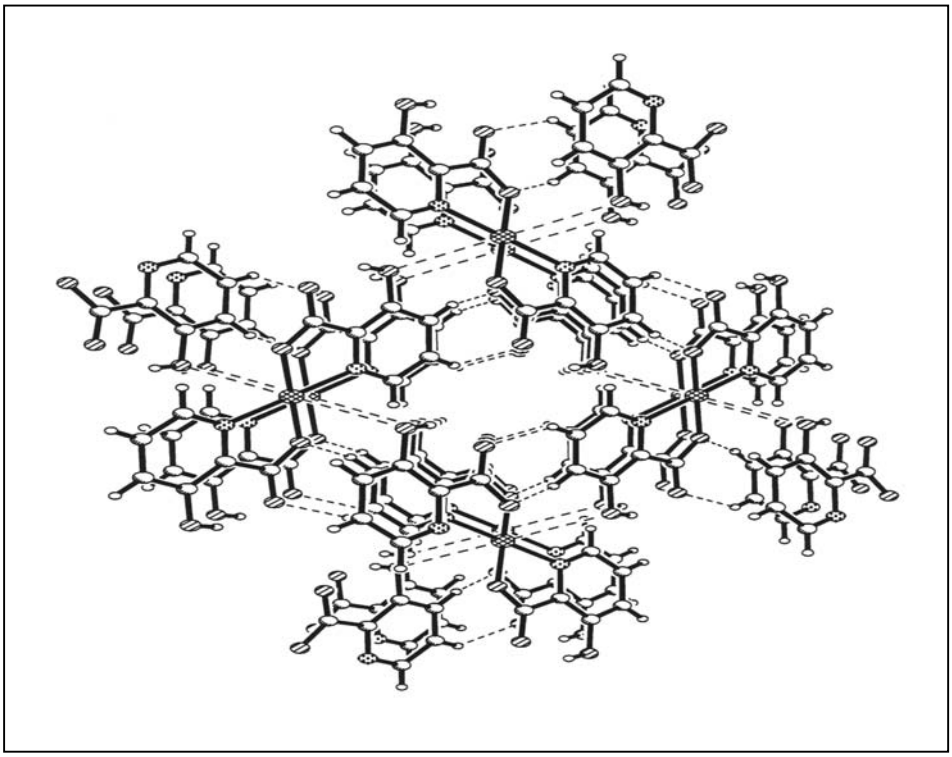

Figure 1.10. Hydrogen bonds in the supramolecular structure of $[Cu(picoH)_2]$ (Sun, Zheng & Jin, 2003).

produced maleato (HL) bridged Cu(II) complexes [Cu(phen)Cl$(HL)_{2/2}$ ] and [Cu(phen)$(NO_3)(HL)_{2/2}$] (where HL = maleic acid), respectively (Zheng, Sun & Lin, 2003). In both complexes, the square pyramidally coordinated Cu atoms are bridged by hydrogen maleato ligands into 1-D chains with the coordinating phen ligands parallel on one side. Interdigitation of the chelating phen ligands of two neighboring chains *via* π–π stacking interactions forms supramolecular double chains, which are then arranged in the crystal structures according to pseudo 1-D close packing patterns, as illustrated in Figure 1.11. Other linear spacer ligands such as 4,4′-bipyridine (bipy) or 4,4′-azobispyridine (azpy) have been synthesized, such as two-dimensional square network, interwoven, honeycomb, 3-D square grid, simple, and interpenetrated ladder (Lu, Paliwala, Lim, Yu, Niu, & Jacobson, 1997; Schmaltz, Jouaiti, Hosseini & Cian, 2001; Erxleben, 2003).

However, even when the same multifunctional ligand is used, structures with different dimensionalities can be formed. For example, $[Cu(btcH)(H_2O)_3]_n$ (where btc = 1,3,5-benzenetricarboxylic acid) has a chain structure but $[Cu_3(btc)_2H_2O)_3]_n$ has a three-dimensional microporous structure, even though both contain the same btc ligand (Pech & Pickardt, 1988; Chui, Lo, Chrmant, Orpen & Williams, 1999). Small changes in the synthesis conditions can lead to changes in supramolecular associations and therefore different structures. There have been some suggestions with regard to the role of a large number of critical variables such as pH, temperature, time, solvent and starting materials that need to be controlled in the synthesis method (Whittingham, Guo, Chen, Chirayil, Janauer & Zavalij, 1995; Chirayil, Boylan, Mamak, Zavalij & Whittingham, 1997).

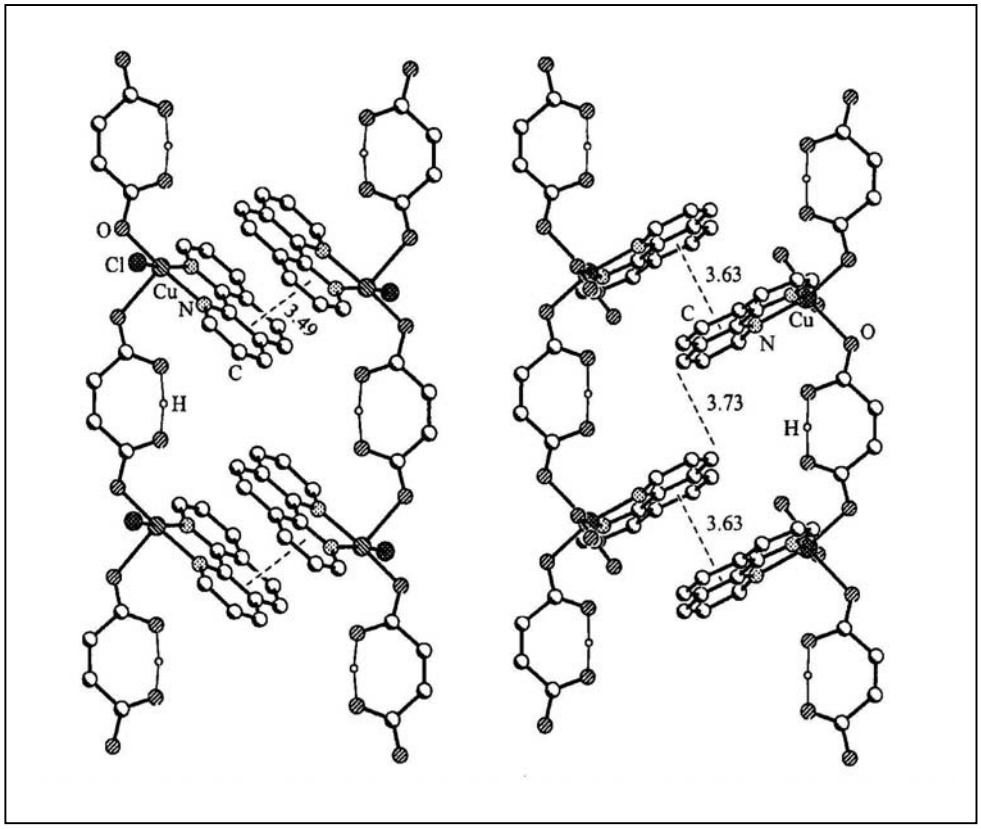


Figure 1.11. π–π stacking interactions in (left) $[Cu(phen)Cl(HL)_{2/2}]$ and (right) $[Cu(phen)(NO_3)(HL)_{2/2}]$ (Zheng, Sun & Lin, 2003).

The synthesis of organic-inorganic vanadium oxide hybrid open-framework materials by the hydrothermal approach has been the subject of intense research owing to their interesting structural chemistry and potential applications in ion exchange, adsorption, and catalysis. A common approach for the design of such materials is the use of metal centers coordinated to rigid multidentate ligands containing N- and/or O-donor atoms. The organic amine besides being a charge-compensating cation and space-filling moiety may also function as a ligand to the metal (Liu, Hou, Zhang & Gao, 2002). The amine molecules occupy the cavities and

channels within the frameworks and, in some cases, can be removed by post-synthesis treatments such as calcination or acid leaching. There have been some suggestions with regard to the role of the amine in the formation of these structures, with pH of the medium and the p$K_a$ of the amine as important parameters (Natarajan, 2003).

There are a large number of critical variables such as pH, temperature, time, solvent, starting materials, and concentrations of starting materials that need to be controlled in the hydrothermal synthesis method for reproducibility. Often, pH controls not only what phase is formed, but also whether a phase is formed at all. Whittingham, Guo, Chen, Chirayil, Janauer & Zavalij (1995) suggested that use of nitric rather than hydrochloric acid for pH control precludes the incorporation of chloride ion into the oxide lattice, and nitric acid is less likely to lead to Keggin-like clusters being formed. Williams (2004) made the further observation that use of acetates rather that nitrates or chlorides can be important if want a neutral or basic pH. The temperature chosen for a reaction can be optimized for phase formation; higher temperatures tend to give higher quality crystals, *i.e*. larger crystallites, but some of the desired structures may not be stable. The temperature is typically chosen in the range 100 °C to 200 °C. In most cases water used as the solvent is also effective, particularly if reduced phases are desired. Reduced phases can also be formed by the addition of lower valent transition metal reactants, such as molybdenum metal. Time has also been shown to be critical if one phase is an intermediate in the formation of another.

Ligand influences and secondary metal coordination preferences are even more pronounced in the 2-D structure (sheet or plane) of $[Cu(dpa)VO_3]$ (LaDuca, Finn & Zubieta, 1999). As shown in Figure 1.12(a), the dipodal dipyridylamine ligand serves to bridge Cu(I) sites to produce $[Cu(dpa)]_n^{n+}$ infinite chains as structural motifs. These link to the chains of corner-sharing V(V) tetrahedra both to decorate the periphery of the vanadate chains and to link vanadate chains. Thus, one $[Cu(dpa)]_n^{n+}$ chain runs parallel to the vanadate chains and links to every fourth vanadium tetrahedron to confer a distorted T-shaped geometry at each Cu(I) site forming a ladder-like double chain motif. Two sets of $[Cu(dpa)]_n^{n+}$ chains make an angle of *ca.* 73° with respect to these double chains and serve to link the assembly into an unusual double layer structure. In contrast, if one end of the dpa ligand is

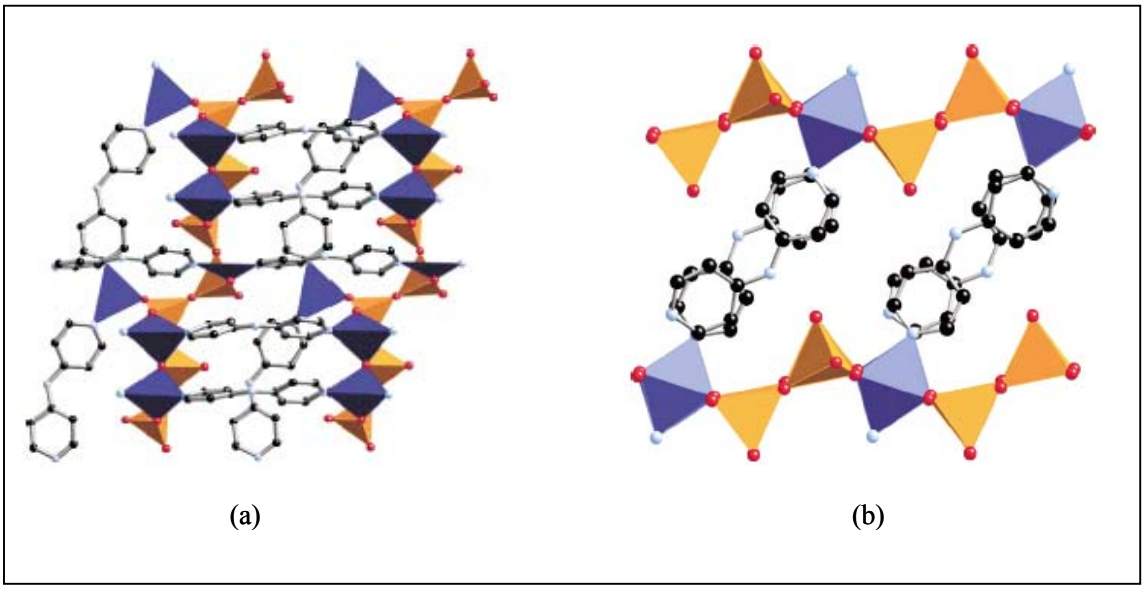


Figure 1.12. Two-dimensional structures of (a) $[Cu(dap)VO_3]$, and (b) $Co(Hdpa)_2$-$V_4O_{12}]$ (LaDuca, Finn & Zubieta, 1999; LaDuca, Rarig & Zubieta, 2001).

protonated and the metal oxidized to the divalent metal state, M(II), the structure which emerges exhibits vanadate chains linked through $[M'(II)O_4(Hdap)_2]^{4+}$ octahedra into the network assembly, as shown in Figure 1.12(b) for $[Co(Hdpa)_2V_4O_{12}]$ (LaDuca, Rarig & Zubieta, 2001). These bimetallic oxide network $[CoV_4O_{12}]_n^{2n-}$ with $Hdpa^+$ monodentrate ligands projecting into the interlamellar region and hydrogen bonding to the adjacent.

Many important applications of materials chemistry continue to be found in the electronics, communications, structural materials, environmental, energy aerospace, medical, and processing industries. As with materials developed over the past century, new materials designed by chemistry will certainly continue to have a large impact on our economy and the world. Supramolecular inorganic coordination chemistry has established itself as one of the most important and exciting parts of this new World.

# Chapter II

# Theoretical Background

## 2.1 Hydrothermal Crystal Growth Technology

The importance of the role of crystals in the development of many branches of physics and chemistry is well known and is receiving increasing attention (Chen, 1998). The importance of crystals in technology and in the national economy is also appreciated. Accordingly, various innovative techniques of growing single crystals have been developed. One recent process innovation is the use of hydrothermal methods (Demianets, 1991).

Hydrothermal synthesis grew out of the discovery by the British geologist, Sir Roderick Impey Murchisin in 1849 that the action of water at elevated temperature and pressure could bring about changes in the earth's crust leading to the formation of various rocks and minerals. The first use of hydrothermal synthesis in Asia was in the 1920s in Japan. However, it was not until the last four decades, when hydrothermal research became popular in several countries such as Australia, China, Canada, France, Germany, India, Korea, Russia, Switzerland, Spain, Sweden, Taiwan, UK, USA, and so on, leading to applications in various branches of science.

The term hydrothermal is purely of geological origin. However, there is no unanimity on the definition of the term hydrothermal. Morey and Niggli (1913) defined hydrothermal synthesis as synthesis subjected to the action of water at a temperature, generally near, though often considerably above, the critical temperature of water (~370 °C) in closed bombs, and therefore, also under the correspondingly

high pressures developed by such solutions. More recently this has been considerably relaxed. Lobachev (1973), defined it is a group of methods in which crystallization is carried out from superheated aqueous solutions at high pressures. Lobachev dropped the requirement that it be near the critical temperature of water. Rebenau (1985) relaxed the conditions even more, removing reference to superheated conditions, but still requiring aqueous conditions, declaring that hydrothermal synthesis is the heterogeneous reaction in aqueous media at temperatures above 100 °C and pressures greater than one atm. During the 1980's and early 1990's, hundreds of reports of synthetic techniques, similar to those described by Lobachev and Rabenau, using water and other solvents at a variety of temperature and pressure conditions were reported.

Consequently, several related techniques were developed with strong roots attached to the hydrothermal technique, *i.e*. hydrothermal crystal growth, hydrothermal treatment, hydrothermal alternation, hydrothermal decomposition, hydrothermal dehydration, hydrothermal extraction, hydrothermal reaction sintering, hydrothermal precipitation−hydrothermal crystallization, hydrothermal electro-chemical reaction, hydrothermal mechanochemical reaction, and so on (Sōmiya & Roy, 2000). Today, the consensus of the authors seems to be that a hydrothermal reaction is any heterogeneous chemical reaction in the presence of a solvent (whether aqueous or nonaqueous) above room temperature and at a pressure greater than 1 atm in a closed system.

As reported in the literature by Rabenau (1985), hydrothermal techniques, in contrast to other conventional techniques, offer several advantages:

(i) The hydrothermal method can be used to prepare compounds with elements in oxidation states that are difficult to obtain, especially important for transition metal compounds, *e.g.* ferromagnetic chromium(IV) oxide.

(ii) The hydrothermal method is also useful for the so-called low temperature phases, *e.g.*, α-quartz, α-berlinite, and others.

(iii) The hydrothermal method is unique in its ability to synthesize metastable compounds, such as the subiodide of tellurium, $Te_2I$.

More particularly, hydrothermal technology offers many advantages over conventional and nonconventional synthesis methods for inorganic materials. All forms of inorganic materials can be prepared with hydrothermal synthesis, namely single crystals, powders, fibers, monolithic ceramic bodies, and coatings on metals, polymers, and ceramics. Hydrothermal technology is more environmentally friendly than many other synthesis methods, in part due to energy saving low processing temperatures, the ability to recycle wastes, and the safe and convenient disposal of wastes that cannot be recycled.

In addition to lowering the overall cost of the synthesis process, the low reaction temperatures avoid common problems encountered with high-temperature technologies, such as poor stoichiometic control due to volatilization of components, presence of thermally induced defects, formation of undesired phases, and unwanted phase transformations. From the standpoint of ceramic powder production, additional advantages of the hydrothermal method are minimal aggregation levels and excellent control of crystal size and morphology, leading one author to suggest that, perhaps, the largest potential growth area for commercialization of the hydrothermal technique

is ceramic powder production (Kaya, Hea, Gub & Butlera, 2002). So far, one of the best examples of well-established commercial applications of hydrothermal synthesis is the growth of single crystals of quartz (Byrappa & Gopalakrishna, 1985).

Originally, hydrothermal synthesis used pure water as a solvent in the reaction system. Water is still favored for use because it is environmentally the safest material and the cheapest of all solvents. It also can act as a mineralizer, or a catalyst under elevated pressure and temperature conditions. Liquid water can be regarded as an array of molecules and atoms which has a short-range order and which resembles the lattice of a solid by the thermal motion of its particles.

The behavior of water at high temperatures and pressures is represented by its thermodynamic properties. In 1982 Millero studied the thermophysical properties of pure water, including its density, viscosity, diffusity, and thermal conductivity. A temperature-density diagram of water with pressure as a parameter, from his work is given in Figure 2.1. The dotted isobars are interpolated, and CP and TP signify critical point and triple point, respectively. There is evidence that water at 150-200 kbar and 1000 °C has a density of 1.7-1.9 g $cm^{-3}$ and is completely dissociated into $H_3O^+$ and $OH^-$ (Rabenau, 1985).

At temperature greater than 374 °C, pressure greater than 221 bar, and density greater than 0.322 g $cm^{-3}$ water is called supercritical. At this point water possesses properties of both liquid and gas states, and can dissolve most liquids and gases (such as oxygen, which makes it a promising solvent for oxidation reactions). The density and the dielectric constant of liquid water decrease with increasing temperature or pressure, therefore, the mobility of molecules and ions in the supercritical range is

much higher than under normal conditions because the viscosity also decreases with temperature. Thus, in supercritical water, mobility and reactivity are both enhanced at high temperature, and diffusion of the dissolved species is faster.

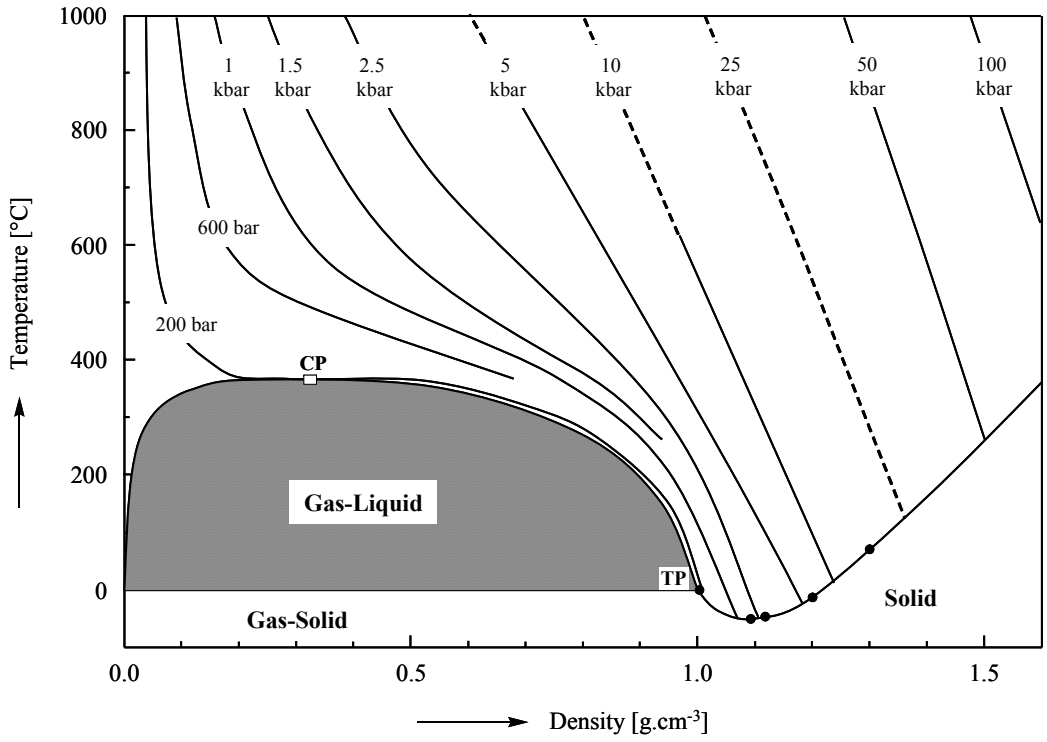


Figure 2.1. Temperature-density diagram of pure water (after Millero, 1982).

Various experimental devices for hydrothermal crystal growth have been designed. The high-temperature, high-pressure apparatus called an 'autoclave' or a 'bomb' resulted from early experimental work by Morey (1953). The basic types of autoclave can be classified on the basis of pressure/temperature ranges and volume. Sōmiya and Roy (2000) report that in the United States, there are three companies:

(i) Tem-Press is the best source for research vessels of all kinds including test tube bombs and gas intensifiers for specialized gases, $H_2$, $O_2$, $NH_3$, *etc*.

(ii) Autoclave Engineers makes a complete line of lab-scale valves, tubing, collars, all fittings for connections, and also, very large autoclaves (1-3 m) for quartz and other chemical processes, and

(iii) Parr Instrument makes simple, low-pressure, low-temperature laboratory scale autoclaves, including vessels lined with Teflon.

The simple autoclave is most popular to use for synthesis or crystallization of inorganic solids and/or organic-inorganic hybrid materials. Figure 2.2 depicts a slightly more complex hydrothermal crystal growth technique in an autoclave. The apparatus consists of a steel cylinder; the cone set closure is kept at a low temperature, outside of the heater. The temperature differential between the hot zone (bottom) and the cool zone (top) of the autoclave results in a solubility gradient to ensure the transport of materials from the nutrient (bottom) to the crystallization zone (top). In the case of inverse solubility, the nutrient is solubilized at low temperature which is slowly increased. When the crystal growth conditions are optimized, crystal seeds can be installed in the growth zone of lager autoclaves. Oriented crystallization is then promoted. Diffusion and convection flows are limited by baffles in order to separate the dissolving and growth zones and to obtain low and uniform growth rates for all seeds.

However, in the more general use, the autoclave is simply placed in a constant or programmed temperature oven. The reaction and/or crystallization then proceeds by equilibration processes to produce crystalline products. Several parameters are important in the synthesis, in particular the pH of the reaction medium, the ratio of

the reactants, the ions present in solution (including shape-directing/templating ions), and the temperature of the reaction (Chirayil, Zavalij & Whittingham, 1998).

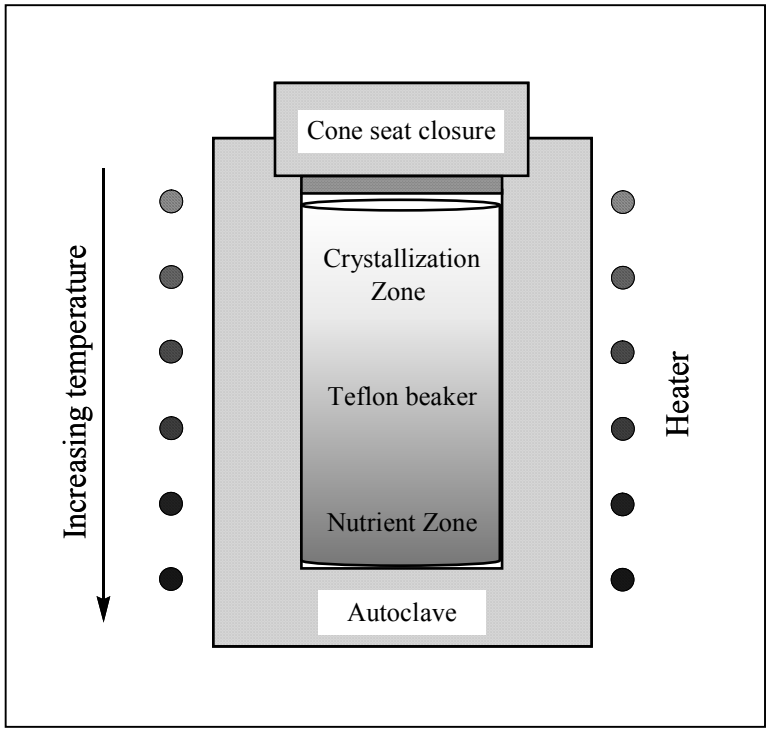


Figure 2.2. Experimental autoclave apparatus for hydrothermal crystal growth.

## 2.2 Single Crystal X-Ray Diffraction Technique

### Historical Introduction

X-rays are a type of electromagnetic radiation between ultraviolet light and gamma rays in wavelength, frequency, and energy. They were discovered by Wilhelm Röntgen (who received the first Nobel Prize for Physics in 1901 for their discovery) in 1895 while performing experiments with cathode rays or electron beams (Hellman, 1996). He called them X-rays because "X" stood for the unknown.

In 1912, Max von Laue demonstrated X-ray diffraction by crystals (Noble Prize for Physics in 1914). Walther Friedrich, and Paul Knipping, and the father-son research team of William Henry and William Lawrence Bragg (Nobel Prize for Physics in 1915) analyzed crystal structures by means of X-rays, giving birth to modern crystallography, and laying the foundations for the field of X-ray crystallography.

X-rays have shorter wavelengths and therefore higher energy than ultraviolet waves. They have played a very important role in science and in our lives, mostly because they can go through most solid objects. Medical and dental X-rays were an early method to make the invisible in our bodies visible; screening systems use X-rays to improve our security when traveling; X-ray diffraction and fluorescence help us explore beneath the surface of old paintings or identify archeological artifacts; and X-ray crystallography allows us to investigate the structure of matter at the atomic and molecular levels. In addition, X-ray images of celestial objects are one way of learning about their high-energy properties.

**Origin of X-Ray Spectra**

As illustrated in Figure 2.3, as the wavelengths of light decrease, they increase in energy. The energy of X-rays, like all electromagnetic radiation, is inversely proportional to their wavelength as given by the Einstein equation:

$$E_{\max} = h\upsilon_{\max} = \frac{hc}{\lambda_{\min}} = eV$$

where $E$ = energy, $h$ = Planck's constant, 6.62517 x $10^{-27}$ erg sec, $\upsilon_{max}$ = the photon frequency and the subscript max indicates that this is the maximum possible energy, $c$

= velocity of light = 2.99793 x $10^{10}$ cm $sec^{-1}$, $\lambda$ = wavelength, $e$ = the charge of the electron, and $V$ = the accelerating potential.

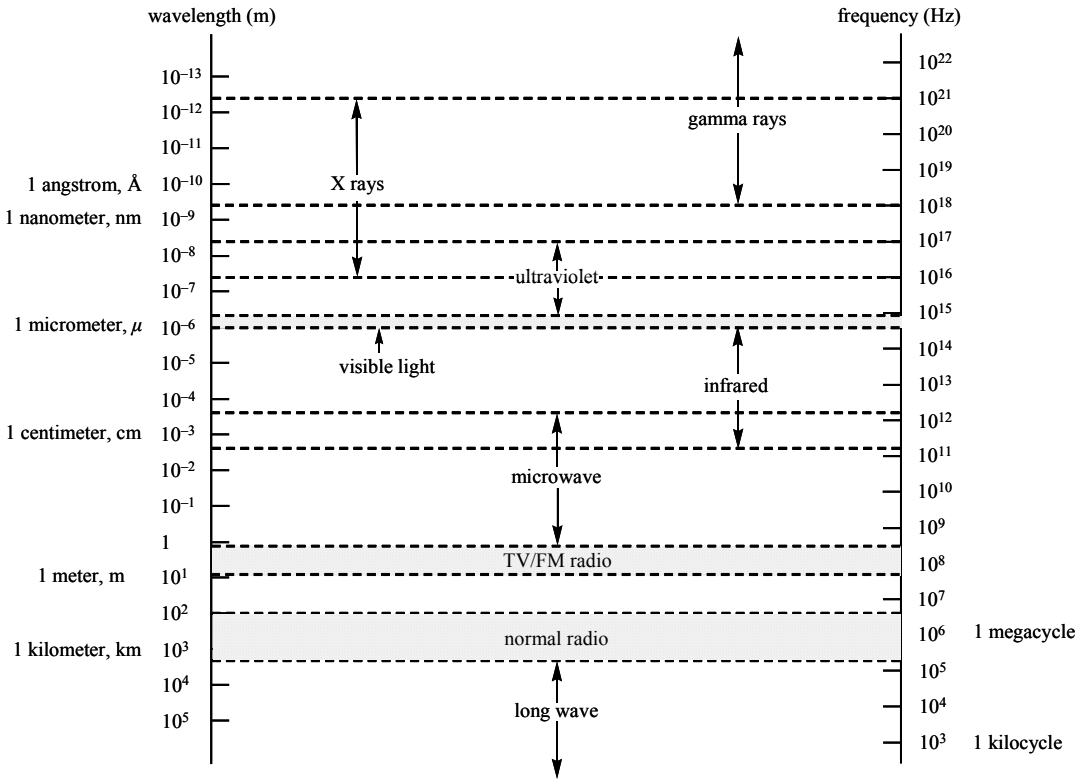


Figure 2.3. The relationship of X-rays to other electromagnetic radiation.

A standard laboratory X-ray source is a sealed tube device as shown schematically in Figure 2.4. X-rays are produced by accelerating electrons into a target anode at high energy. Typical accelerating voltages are tens to hundreds of kilovolts of potential. The bombarding electrons can eject electrons from the inner shells of the atoms of the metal target. Those vacancies will be quickly filled by

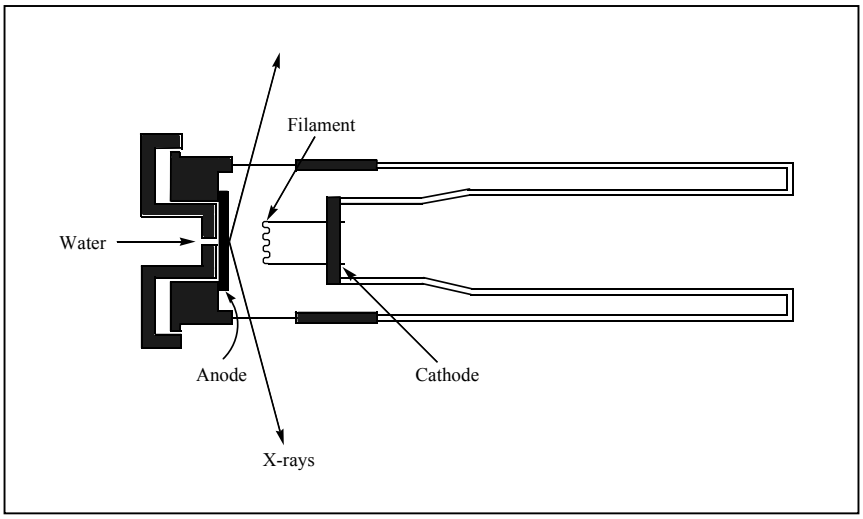


Figure 2.4. A sealed tube X-ray source.

electrons dropping down from higher levels, emitting X-rays, as depicted in Figure 2.5, with sharply defined frequencies associated with the difference between the atomic energy levels of the target atoms. The broad emission extending under the characteristic peaks is due to the Bremstrallung effect of the deceleration of the majority of the electron beam. The minimum wavelength of the resulting radiation can be calculated from the equation:

$$\lambda_{\min} = \frac{hc}{eV} = \frac{12{,}398}{V} \text{ Å}$$

The potential $V$ is measured in volts and the minimum wavelength is obtained in Å. This equation gives the minimum value for the wavelength of the X-rays that can be obtained by the process as a function of the electron accelerating voltage. Figure 2.6, shows some continuous X-ray spectra as a function of the accelerating voltage.

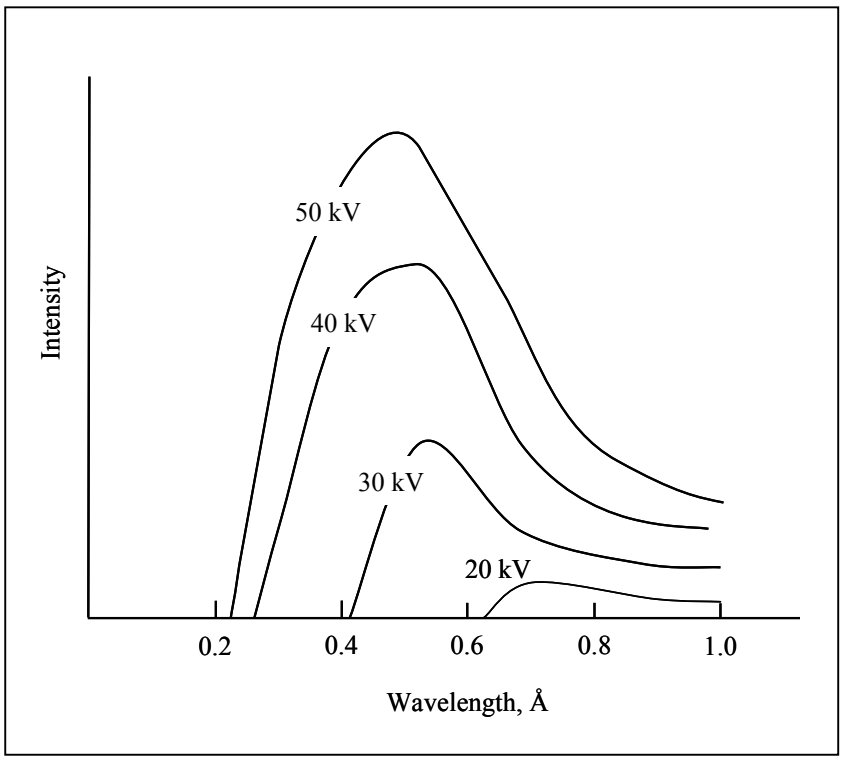


Figure 2.5. Continuous X-ray spectra as a function of accelerating voltage (Giacovazzo, Monaco, Artioli, Viterbo, Ferraris, Gilli, Zanotti & Catti, 2002).

Notice that as the accelerating voltage is increased, both the minimum wavelength and the position of the intensity maximum shift to the left.

The interpretation of X-ray spectra are according to the Bohr Theory of electronic levels (Douglas, McDaniel & Alexander, 1994). The electrons in an atom are arranged in shells (K, L, M, N, ... corresponding to n = 1, 2, 3, 4, ...). Theory predicts that the energy differences between successive shells increase with decreasing n and that the electron transition from n = 2 to n = 1 results in the

emission of very energetic (short wavelength) radiation, while outer shell transitions (*e.g.* from n = 5 to n = 4) yield low energy (long wavelength) radiation.

Characteristic X-rays are emitted from heavy elements when their electrons make transitions between the lower atomic energy levels. Figure 2.6 shows the characteristic X-ray emissions for Cu and Mo x-radiation sources. The sharp peak which occurs to the right results when vacancies are produced in the $n$ = 1 or $K$-shell of the atom and electrons drop down from above to fill the gap. The X-rays produced by transitions from the $n$ = 2 to $n$ = 1 levels are called $K_\alpha$ X-rays, and those for the n = 3 to n = 1 level are called $K_\beta$ X-rays. Transitions to the n = 2 or L-shell are designated as $L$ X-rays ($n = 3$ to $n = 2$ is $L_\alpha$, $n = 4$ to $n = 2$ is $L_\beta$, *etc.*). The

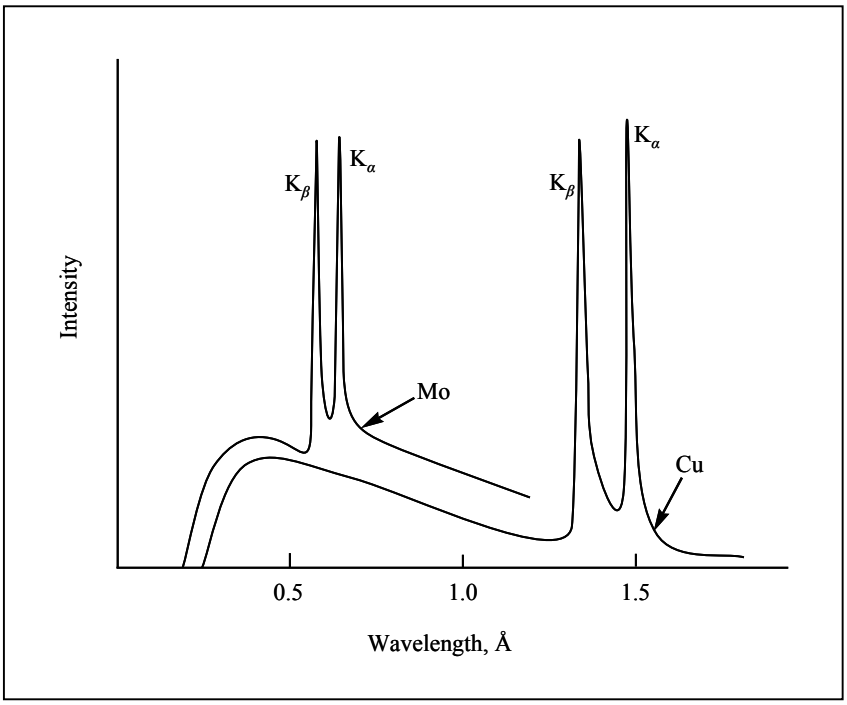


Figure 2.6. X-ray spectra with characteristic peaks for Mo and Cu x-radiation. MoKα, 50 kV; CuKα, 35 kV. (Stout & Jensen, 1989).

continuous distribution of X-rays which forms the base for the two sharp peaks at left is called Bremsstrahlung or white radiation.

Cu $K_\alpha$ radiation has a weighted average wavelength of 1.5418 Å, from the $2p \rightarrow 1s$ transition and its $K_\beta$ radiation has a wavelength of 1.3922 Å from the $3p \rightarrow 1s$ transition. The $K_\alpha$ transition occurs much more frequently than the $K_\beta$ transition and this more intense $K_\alpha$ radiation is a doublet, $K_{\alpha 1}$ = 1.54051 Å and $K_{\alpha 2}$ = 1.54433 Å, because the transition has a slightly different energy for the two possible spin states of the $2p$ electron which makes the transition, relative to the spin of the vacant $1s$ orbital. In some X-ray experiments, diffraction by the $K_{\alpha 1}$ and $K_{\alpha 2}$ radiation is not resolved and a single line or spot is observed instead of a doublet *e.g.* diffraction at low angle.

**Selection of Radiation and X-Ray Tubes**

The useful wavelength of the X-rays generated by conventional equipment is limited to the values of the characteristic $K_\alpha$ lines of the metals commonly used as targets. Targets are limited to materials that are conductive, solid, dense, and high-melting. Fortunately, the transition elements of the first and second long periods ($Z$ = 21-30 and 39-48) meet these requirements and have characteristic radiation in the region that is most useful for crystal structure analysis.

Copper and molybdenum are the metals that are most frequently used. Copper $K_\alpha$ radiation was traditionally used as a source for macromolecular work and for the structure determination of organic molecules that do not contain atoms that absorb this radiation strongly. It is sufficiently penetrating that it does not suffer too badly from absorption in the crystal or while passing through air, and at the same time it is

recorded with reasonable efficiency on film. When used with diffraction apparatus that can record all of the reflections theoretically accessible, it can provide enough data to adequately determine a structure for most chemical purposes. Molybdenum is a more penetrating radiation and is less well adapted to use with film because of the lower efficiency of recording. However, it gained acceptance when scintillation counter diffractometers became the norm, and today is the radiation of choice for small molecule laboratory diffractometers (but not at synchrotrons). The resolution standards of *Acta Crystallographica* preclude the use of copper $K_\alpha$ radiation for routine X-ray structure work today. Silver radiation, which is harder (has shorter wavelength) than molybdenum radiation, is sometimes used in electron density studies because of the greater number of data theoretically available. Some of the most common targets and their characteristic $K_\alpha$ average wavelengths are given in Table 2.1.

Table 2.1 Target Materials and Associated Constants.

| | Cr | Fe | Cu | Mo |
|---|---|---|---|---|
| $Z$ | 24 | 26 | 29 | 42 |
| $K_{\alpha 1}$ | 2.2896 | 1.9360 | 1.5405 | 0.70926 |
| $K_{\alpha 2}$ | 2.2935 | 1.9399 | 1.5443 | 0.71351 |
| $\langle\alpha\rangle$ [a] | 2.29092 | 1.9373 | 1.5418 | 0.71069 |
| $K_{\beta 1}$ | 2.0848 | 1.7565 | 1.3922 | 0.63225 |
| $\beta$ filter | V, 0.4 mil [b] | Mn, 0.4 mil | Ni, 0.6 mil | Nb, 3 mils |
| $\alpha$ filter | Ti | Cr | Co | Y |
| Resolution (Å) | 1.15 | 0.95 | 0.75 | 0.35 |
| Critical potential | 5.99 | 7.11 | 8.98 | 20.0 |

[a] $\langle\alpha\rangle$, the intensity-weighted average of $K_{\alpha 1}$ and $K_{\alpha 2}$, is the figure usually used for the wavelength when the two lines are not resolved, [b] 1 mil = 0.001 in. = 0.025 mm.

**Single Crystal X-Ray Crystallography**

Single crystal X-ray diffraction is an analytical technique that is able to determine the precise atomic positions and therefore the bond lengths and angles of the atoms within a single crystal specimen. It is Extremely powerful in that the results are very accurate, giving bond lengths to a few tens of a picometer and bond angles to a few hundreths of a degree. Distances are reported in this thesis in Ångstroms (1 Å = 100 pm) in accordance with the historical tradition for reporting distances determined by X-ray analysis. The pattern produced by the diffraction of X-rays through the closely spaced lattice of atoms in a crystal is recorded and then analyzed to reveal the nature of that lattice. X-ray crystallographic systems generally include dedicated computers with associated hardware and software for instrument control, data reduction, solution and refinement of molecular structures, and display and plotting of final results.

Characteristic X-rays are used for the investigation of crystal structure by X-ray diffraction. Crystal lattice dimensions may be determined with the use of Bragg's law:

$$2d_{\mathrm{H}}\sin\theta = n\lambda$$

where $n$ is an integer, lambda ($\lambda$) is the wavelength of a beam of radiation incident on a crystal with lattice planes separated by distance $d_H$, and theta ($\theta$) is the Bragg angle.

As illustrated in Figure 2.7, when a monochromatic X-ray beam with wavelength $\lambda$ is projected onto a crystalline material at an angle $\theta$, constructive

interference occurs only when the distance traveled by the rays reflected from successive planes of atoms differs by a complete number $n$ of wavelengths. By varying the angle $\theta$, the Bragg's Law conditions are satisfied by different $d$-spacings in polycrystalline materials. Plotting the angular positions and intensities of the resultant diffracted peaks of radiation produces a pattern which is characteristic of the sample. Where a mixture of different phases is present, the resultant diffractogram is formed by addition of the individual patterns.

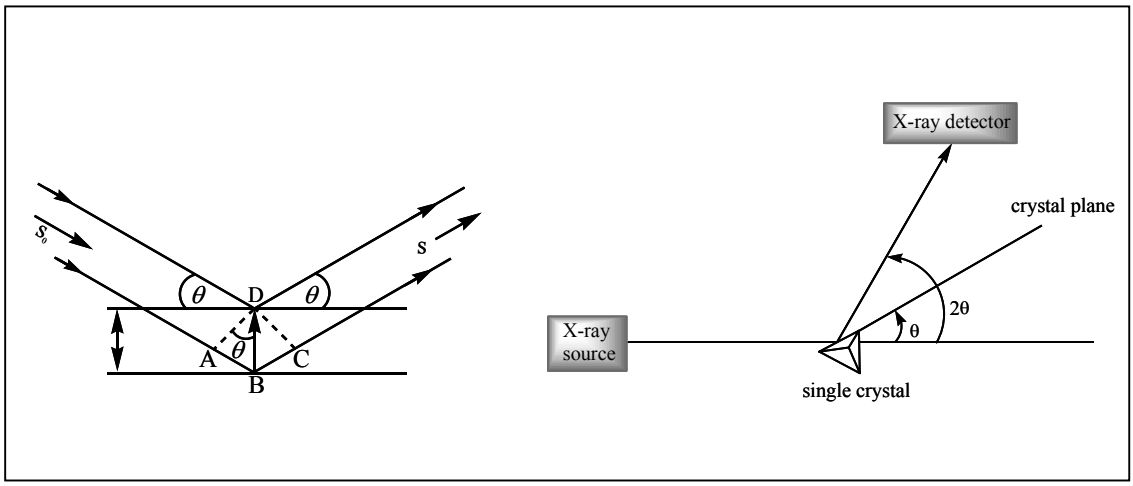


Figure 2.7. (a) Reflection of X-rays from lattice planes and (b) diffraction by crystals.

# Chapter III

# Experimental

## 3.1 Chemicals

1. Vanadium pentoxide ($V_2O_5$)

Carlo Erba, RPE for analysis, minimum assay 99%, carbonate ($CO_2$) ≤ 0.02%, Cl (chloride) ≤ 0.005%, sulphate ≤ 0.02%, As (arsenic) ≤ 0.005%, Fe (iron) ≤ 0.005%, Pb (lead) ≤ 0.002%

2. Cobalt(II) chloride hexahydrate ($CoCl_2 \cdot 6H_2O$)

Carlo Erba, RPE-ACS for analysis, minimum assay 99%, ammonium ≤ 0.005%, nitrate ≤ 0.01%, sulphate ≤ 0.01%, water insoluble matter ≤ 0.01%, Ca (calcium) ≤ 0.005%, Cu (copper) ≤ 0.002%, Fe (iron) ≤ 0.005%, potassium ≤ 0.01%, Mg (magnesium) ≤ 0.005%, Na (sodium) ≤ 0.05%, Ni (nickel) ≤ 0.1%, Zn (zinc) ≤ 0.03%

3. Cobalt(II) acetate tetrahydrate ($(CH_3CO_2)_2Co \cdot 4H_2O$)

Strem Chemical, 98+%

4. Manganese(II) chloride tetrahydrate ($MnCl_2 \cdot 4H_2O$)

Carlo Erba, ACS for analysis, minimum assay 98%, water insoluble matter ≤ 0.005%, heavy metals (Pb) ≤ 0.0005%, sulphate ≤ 0.005%, pH of a 5% solution at 25 °C 3.5-6.0, Ca (calcium) ≤ 0.005%, Fe (iron) ≤ 0.0005%, K (potassium) ≤ 0.01%, Na (sodium) ≤ 0.05%, zinc (Zn) ≤ 0.0005%

5. 1,3-Diaminopropane ($H_2NCH_2CH_2CH_2NH_2$), (**1** in Figure 3.1)

Fluka, puriss, minimum assay ≥ 99% (GC)

6. 1,4-Dicyanobenzene ($C_8H_4N_2$), (**2** in Figure 3.1)

Acros Organics, 98%, water ≤ 0.2% (K.F.)

7. 2,4,6-Tri(2-pyridyl)-s-triazine ($C_{18}H_{12}N_6$), (**3** in Figure 3.1)

Acros Organics, 98%, water ≤ 0.5% (K.F.)

8. 2,5-pyridine-dicarboxylic acid ($C_7H_5NO_4$), (**4** in Figure 3.1)

Acros Organics, 98%, water ≤ 1% (K.F.)

9. Imidazole ($C_3H_4N_2$), (**5** in Figure 3.1)

Acros Organics, 99%, water ≤ 1% (K.F.)

10. 1,2-Bis(4-pyridyl)ethane ($C_{12}H_{12}N_2$), (**6** in Figure 3.1)

Acros Organics, 97%

11. Hydrochloric acid (HCl)

Carlo Erba, RPE-ISO for analysis, minimum assay 36.5%, ammonium ≤ 0.0001%, bromide (Br) ≤ 0.005%, color (APHA) 10, Free chloride (Cl) 0.00005%, heavy metal (Pb) ≤ 0.00001%, residue on ignition ≤ 0.0005%, phosphate ≤ 0.00005%, sulfate ≤ 0.0001%, sulphite ≤ 0.00005%, Al (aluminum) ≤ 0.000005%, As (arsenic) ≤ 0.000001%, Ba (barium) ≤ 0.00001%, Cu (copper) ≤ 0.000001%, Fe (iron) ≤ 0.00002%, Mg (magnesium) ≤ 0.00003%, Ni (nickel) ≤ 0.000002%, Pb (lead) ≤ 0.000005%, Zn (zinc) ≤ 0.000005%, K (potassium) ≤ 0.00001%, Na (sodium) ≤ 0.00005%, Sr (strontium) ≤ 0.000002%, Be (beryllium) ≤ 0.000002%, Bi (bismuth) ≤ 0.000005%, Ca (calcium) ≤ 0.00005%, Cd (cadmium) ≤ 0.0000005%, Co (cobalt) ≤ 0.000001%, Cr (chromium) ≤ 0.000002%, Hg (mercury) ≤ 0.00001%, Li (lithium) ≤ 0.000002%, Mn (manganese) ≤ 0.000001%, Mo (molybdenum) ≤ 0.000005%, Tl (thallium) ≤ 0.000005%, V (vanadium) ≤ 0.000002%, Zr (zirconium) ≤ 0.000005%

12. Water

Deionized water

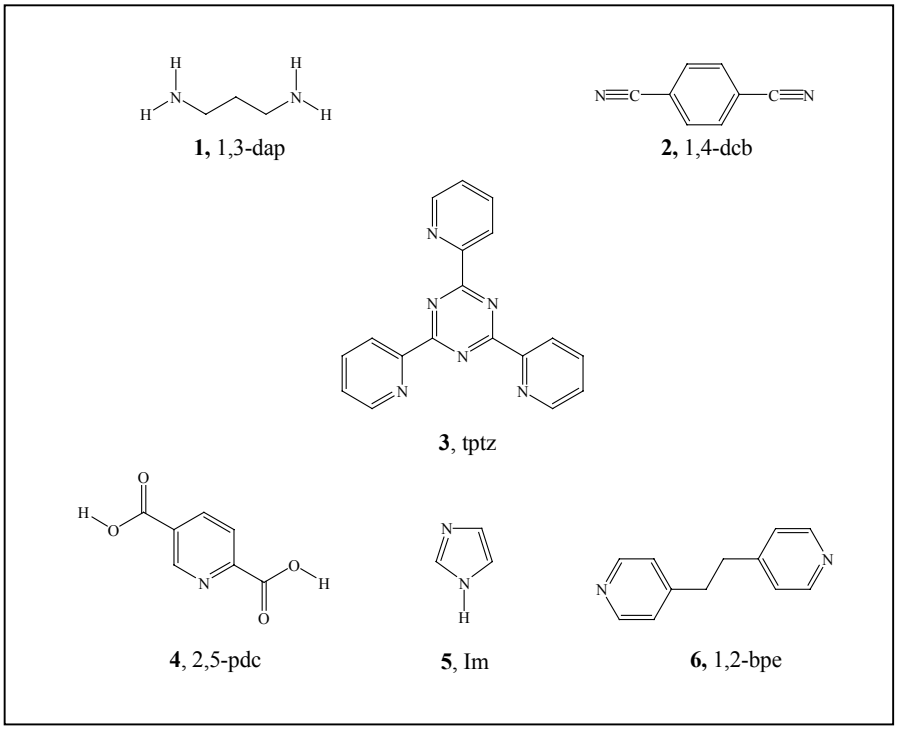


Figure 3.1. N,O-containing organic template molecules for experimental research.

## 3.2 Instrumentation and Instrumental Methods

### Single Crystal X-ray Diffraction

Reflection intensities were collected on a Bruker-Nonius KappaCCD four-circle area-detector diffractometer equipped with a graphite crystal monochromator, an *ifg* focusing capilliary collimator, and a fine focus X-ray tube (Mo $K_\alpha$ radiation, $\bar{\lambda}$ = 0.71073 Å) using the COLLECT software (Nonius, 1998). The frame images were reduced to intensity data using the EvalCCD package (Duisenberg, Kroon-Batenburg & Schreurs, 2003).

Structure solution and refinement follows a general pattern similar to the detailed description that follows. At each of the discrete steps the model is carefully evaluated based on criteria of chemical reasonability and on features in the electron density maps. Model deficiencies are corrected before proceeding to the next step. The following paragraph describes the basic steps for the $[Co(picoline)_3]\cdot H_2O$ structure reported in chapter IV. This structure was straightforward without model deficiencies at any step.

All 29 nonhydrogen atoms were located by SIR97 direct methods program (Altomare, Burla, Camalli, Cascarano, Giacovazzo, Guagliardi, Moliterni, Polidori & Spagna, 1999) and their position coordinates and individual atom atomic displacement parameters refined isotropically to convergence (117 variables; $R_1$(obs) = 0.0825; $R_1$(all) = 0.1149; $wR_2$(all) = 0.2402; gof = 1.629). Positions for 12 hydrogen atoms on the complex and two water hydrogen atoms were located from a difference electron density map calculated from this model. The hydrogen atoms in the complex were included in the model in idealized positions (d[C–H] = 0.93 Å; $U$[H] = 1.1$U$[$C_{attached}$]) constrained to ride on the atoms to which they are bonded, the hydrogen atoms in the water molecule were included with refinable positions ($U$[H] = 1.1$U$[$O_{water}$]), and the model refined to convergence (123 variables; $R_1$(obs) = 0.0745; $R_1$(all) = 0.1070; $wR_2$(all) = 0.2143; gof = 1.447). Examination of an electron density difference map calculated from this model did not reveal any problems with the model. Atomic displacement parameters for all nonhydrogen atoms were converted to anisotropic form and the model refined to convergence (268 variables $R_1$(obs) = 0.0369; $R_1$(all) = 0.0683; $wR_2$(all) = 0.1239; gof = 0.840). Least squares refinement,

electron density calculations, and idealized geometric parameters for hydrogen atom positions were provided by SHELXL-97 (Sheldrick, 1997).

The accuracy of numerical data reported in fractional coordinate tables, atomic displacement parameter tables, distance and angle tables, and other tables generally follows the convention of 29, the *de facto* standard in crystallographic publications. This convention means that the number of significant digits reported is such that the estimated standard deviations in the least significant digits are in the range of 3 to 29.

**Fourier Transform Infrared Spectrophotometry**

FTIR spectra were recorded with a Perkin-Elmer model Spectrum GX FTIR Fourier transform infrared spectrophotometer with Win-IR software. The samples were prepared by mixing 1.0 mg of sample with 100 mg of dried potassium bromide and grinding to a very fine power with an agate mortar and pestle. The ground powder was pressed into a transparent disk (16 mm diameter) using a hydraulic press at 10 tons of pressure for 1 min. The pellet was placed in the sample holder in the instrument beam and the mid IR range (4000-370 $cm^{-1}$) spectrum was recorded.

**Thermogravimetric Analysis**

TGA spectra were recorded on a TGA7 thermogravimetric analyzer from Perkin-Elmer using the SCO UNIX System V/386 software to measure the change of mass of the sample (10-15 mg) as a function of increasing temperature from room temperature to 800 ºC with a heating rate of 10 ºC/min under air flow.

**Scanning Electron Microscopy/Energy Dispersive X-ray Analysis**

Scanning Electron Microscopy utilized a Jeol model JSM-6400 SEM, running with an electron beam accelerating voltage of 20 kV, vacuum pressure $10^{-4}$ Pa, and a tungsten filament with a working distance of 39 mm. The SEM was equipped with an Oxford WDX-100 energy dispersive x-ray fluorescence microanalyzer (EDX), and the Link ISIS Version 1.04 software. The fluorescence attachment is capable of analyzing sodium and heavier elements.

Teflon-lined Stainless Steel Autoclave (Parr bomb)

Stainless steel bombs with inner Teflon container liners from Parr Instrument Company (model 452HC T316), Figure 3.2, were used for hydrothermal syntheses. The maximum temperature and pressure are 350 °C, and 2950 psi, respectively. The inner dimensions of the Teflon cup are 3.10 cm diameter and 12.5 cm deep. The bomb does not have a safety rupture disk so reaction mixtures are generally limited to less than 10% of the capacity of the bomb.

**Thermoline Oven**

The heat source for the hydrothermal synthesis is a Thermoline Model 060GD gravity convection oven with a BTC-9090 digitally controlled microprocessor based temperature controller. The controller maintains the set temperature within ±1 °C of the set point temperature, which may range from room temperature up to 200 °C.

**Optical Microscopy (OM)**

An Olympus model SZ–ST optical stereo microscope was used for the first physical characterization technique to recognize the morphologies and colors of the crystalline products that resulted from hydrothermal synthesis. The stereo zoom body

covers a continuous magnification range of 0.7 to 4.7, the objectives are 1x, and the eyepieces lenses are 10x, giving a magnification range of 7 to 47.

Figure 3.2. Teflon-lined stainless steel autoclave (125 mL Parr bomb) for hydrothermal synthesis.

## 3.3 Procedures

**Safety Information for Hydrothermal Bomb Techniques**

The pressure-temperature diagram of water including the filling factor (degree of fill) of the autoclave as a parameter is given in Figure 3.3. Understanding of this diagram is important in designing hydrothermal syntheses or other reaction to be carried out in pressurized vessels. The chain-dotted line is the equilibrium line of vapor and liquid, and $T_{cr}$ is the critical temperature of water, 374 °C. A representation of P = *f*(T) for a given amount of water can be given as a function of volume or as a function of the filling factor, $\tau$, the fraction of the vessel that is filled at room temperature. At the critical filling factor, $\tau_c$ = 0.322 (or 32.2% or 0.322 g $cm^{-3}$), the

level of the meniscus remains constant on heating, and disappears at $T_{cr}$. When $\tau > \tau_c$ the fluid-gas meniscus is curved upwards and the reaction vessel is completely filled with the fluid phase below the critical temperature, *e.g.* with a degree of fill of 0.80, the reaction vessel is completely filled at 245 °C. When $\tau < \tau_c$, the behavior is reversed, and the liquid phase disappears at a temperature less than $T_{cr}$, *i.e.* the autoclave boils dry at a sufficiently high temperature less than $T_{cr}$.

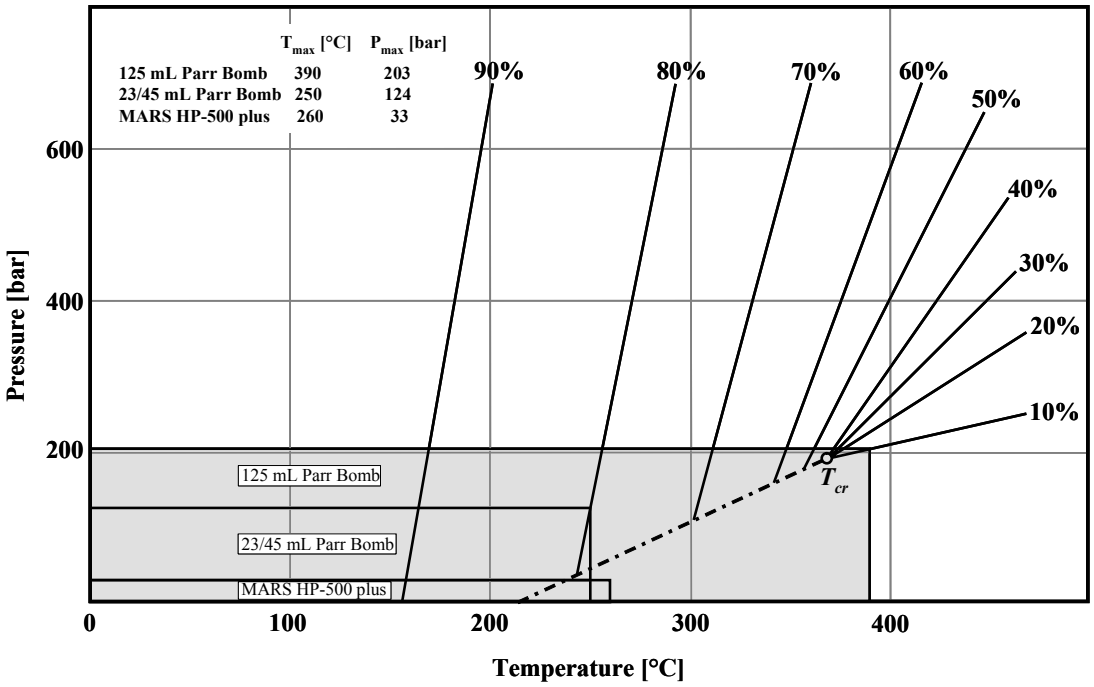


Figure 3.3. Variation of water pressure with temperature for various autoclave filling factors (after Rabenau & Rau, 1969).

As the sealed system is heated, more of the liquid phase is transferred to the vapor phase; the pressure and the density of the vapor phase increase. When $\tau > \tau_c$ and the liquid-vapor equilibrium curve is crossed, only one fluid phase is present and the rate of pressure change with temperature increases dramatically as shown in Figure 3.3. One must take account of this behavior when planning experiments so the

reaction vessel does not explode. In addition, one must remember that reactions may produce unexpected gaseous products which also add to the pressure inside the reaction vessel. Consideration of the pressure-temperature diagram in conjunction with the filling factor gives control over the solvent pressure, while use of millimolar quantities of reactants minimizes effects from unexpected reactions.

The 125 mL Parr model 452HC T316 reactor can be operated at temperatures up to 390 °C and pressures up to 203 bar, and thus can operate just above the critical point of water (supercritical condition). The other reactors available at Suranaree University of Technology have lower specifications; 250 °C and pressure up to 124 bar for the 23 mL Parr model 4749 T316 and 45 mL Parr model 4744 T316 reactors, and 260 °C and pressure up to 33 bar for the MARS (Microwave Accelerated Reaction System from CEM Corporation) HP-500 Plus reactors. The regions included within the limits for these reactors have been indicated on Figure 3.3 as an aid for designing syntheses conditions that will be within the safe limits for the reactors. All syntheses reported in this thesis were carried out on millimolar scale at relatively low temperature (maximum of 180 °C) and with filling factors significantly less than $\tau_c$ (maximum $\tau = 0.26$), thus ensuring the presence of a liquid phase for all reactions, as well as pressures within the design limits of the reactors being used.

**Sample preparation**

Hydrothermal preparations were carried out in the 125 mL Teflon-lined stainless steel autoclave (Parr bomb). All chemicals were commercially purchased and used without further purification. A schematic for the preparation of crystalline

samples is given in Figure 3.4. A typical procedure began with mixing vanadium pentoxide, a divalent transition metal salt, and an organic template with distilled water in probable stoichiometric proportions and stirring for a few minutes to form a reaction mixture, then adjusting the pH of the mixture/solution with hydrochloric acid

Figure 3.4. Schematic diagram of the experimental research.

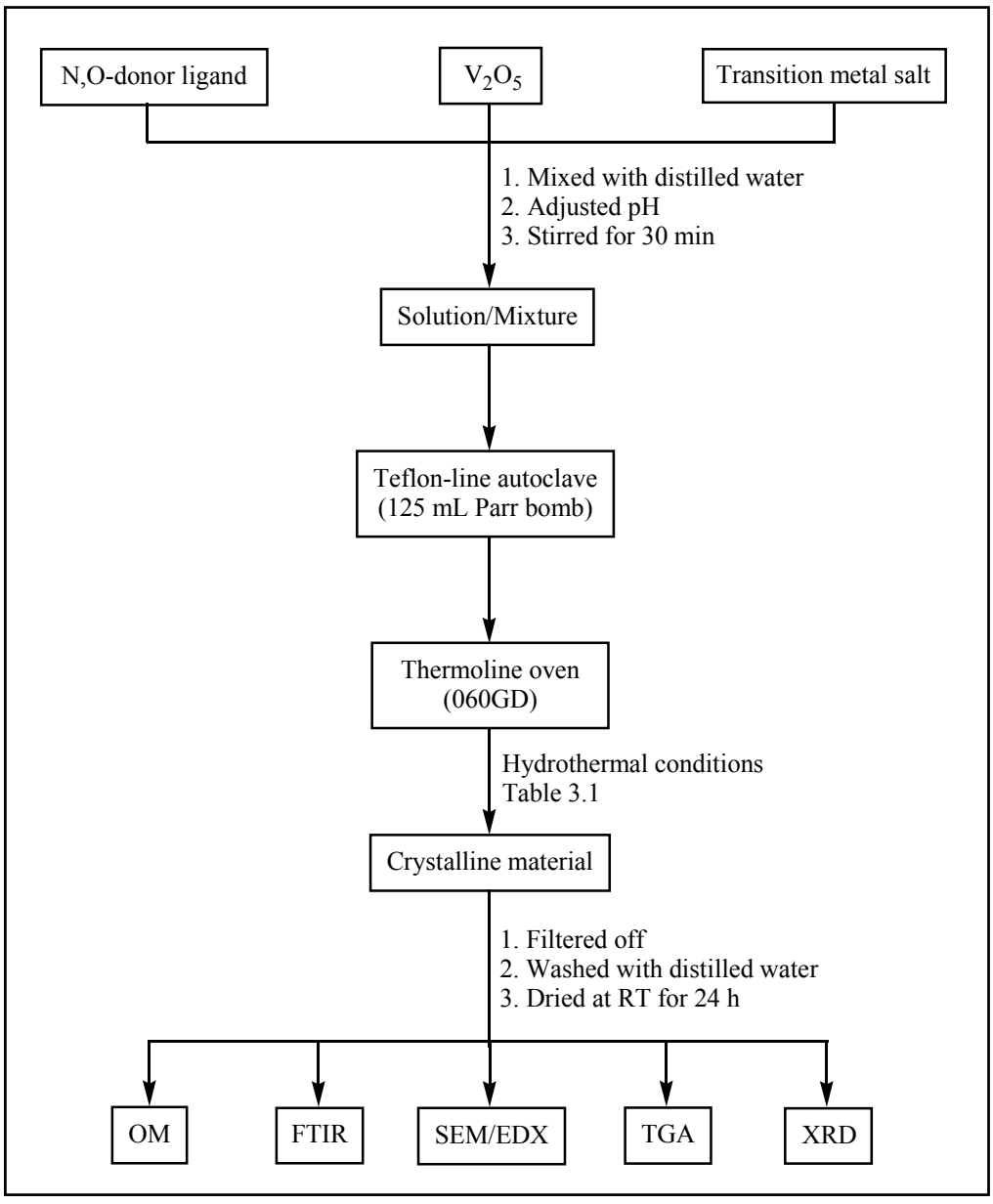

and stirring for 30 minutes. The final reaction mixture/solution was placed in the Teflon container, sealed in a 125 mL Parr bomb, and placed in the Thermoline oven. The mixture was heated to the reaction temperature indicated in Table 3.1 and held there for the indicated time. After the heating period, the oven was switched off and cooled to room temperature, and the Parr reactor removed from the oven. The crystalline materials were filtered off, washed with distilled water, and dried in air. The details of the synthesis and experimental results are shown in Tables 3.1 and 3.2.

Table 3.1. Details of Experimental Preparations by the Hydrothermal Method.

| No. | $V_2O_5$ | Metal ($M^{2+}$) salt | | Ligand [a] | | $H_2O$ | Adjusting pH | | Condition |
|---|---|---|---|---|---|---|---|---|---|
| 1 | 0.50 g | $CoCl_2 \cdot 6H_2O$ | 0.75 g | dap | 0.46 mL | 30 mL | HCl | 0.08 mL | 180 °C, 4 days |
| 2 | 0.10 g | $CoCl_2 \cdot 6H_2O$ | 0.75 g | dcb | 0.71 g | 20 mL | HCl | 2.00 mL | 180 °C, 4 days |
| 3 | 0.10 g | $CoCl_2 \cdot 6H_2O$ | 0.13 g | bpe | 0.20 g | 10 mL | HCl | 0.02 mL | 180 °C, 7 days |
| 4 | 0.25 g | $MnCl_2 \cdot 4H_2O$ | 0.27 g | tptz | 0.86 g | 30 mL | HCl | 2.00 mL | 180 °C, 3 days |
| 5 | 0.50 g | $CoCl_2 \cdot 6H_2O$ | 0.75 g | dap | 0.46 g | 30 mL | pdc | 0.92 g | 180 °C, 3 days |
| 6 | 0.09 g | $(CH_3CO_2)_2Co \cdot 4H_2O$ | 0.25 g | Im | 0.28 g | 5 mL | - | - | 120 °C, 6 days |
| 7 | 0.09 g | $(CH_3CO_2)_2Co \cdot 4H_2O$ | 0.25 g | Im | 0.54 g | 5 mL | - | - | 120 °C, 6 days |
| 8 | 0.09 g | $(CH_3CO_2)_2Co \cdot 4H_2O$ | 0.25 g | Im | 0.61 g | 5 mL | - | - | 120 °C, 6 days |

[a] bpe = 1,2-bis(4-pyridyl)ethane, dap = 1,3-diaminopropane, dcb = 1,4-dicyanobenzene, Im = imidazole
pdc = pyridine-2-dicarboxylic acid, tptz = 2,4,6-tri(2-pyridyl)-s-triazine

The shapes and colors of crystalline material were carefully selected and separated under the optical microscope. The morphologies of the crystalline products were further observed by scanning electron microscopy, and the presence of elements with atomic number equal to or greater than sodium was confirmed by energy dispersive X-ray fluorescence microanalysis. The presence or absence of the template molecule and water molecules, as well as knowledge on the functional groups and the

nature of the noncovalent bonding was inferred from the FTIR spectra. A Perkin-Elmer TGA7 thermogravimetric analyzer was used to measure mass change of materials exposed to a temperature program and also records the temperature or time of the mass loss region and the temperature at maximum transition.

Table 3.2. Results from Hydrothermal Synthesis, OM, and SEM-EDX Analysis.

| No. | Mass of Product | Description of Products | Figure | Typical Size | Elements Observed and % of Sample |
|---|---|---|---|---|---|
| 1 | 0.40 g | Black-brown hexagonal plate, green-brown powder, | 3.5a - | 100 μm | 3% Co, 97% V |
| 2 | 0.18 g | Bright brown plate, green-brown powder | - - | | 2% Co, 98% V |
| 3 | 0.03 g | Orange plate, green-brown powder | - - | | 4% Cl, 2% V, 94% Co |
| 4 | 0.08 g | Black dense rosettes plates, black powder | 3.5b - | 10 μm | 48% Mn, 52% V |
| 5 | 0.65 g | Red-violet hexagonal plate, yellow-brown powder | 3.5c - | 100 μm | 100% Co |
| 6 | 0.13 g | Bright yellow needle, yellow-brown powder | 3.5d - | 100 μm | 37% Co, 63% V |
| 7 | 0.21 g | Bright violet plate, red-violet powder | 3.5e - | 100 μm | 35% Co, 65% V |
| 8 | 0.20 g | Violet hexagonal, red-violet powder | 3.5f - | 240 μm | 37% Co, 63% V |

**SEM pictures**

The crystal morphologies for a selection of the products given in Table 3.2 are presented in Figure 3.5. Nice looking crystalline materials were chosen for SEM/EDX analysis using the optical microscope.

**a.** $V_2O_5 + Co^{2+} + dap + H_2O + HCl$
(1:1:2:593:1)

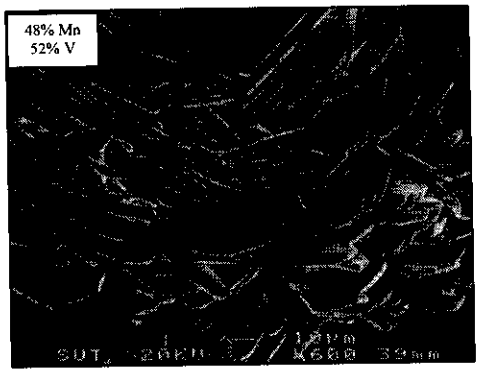


**b.** $V_2O_5 + Mn^{2+} + tptz + H_2O + HCl$
(1:1:2:593:2)

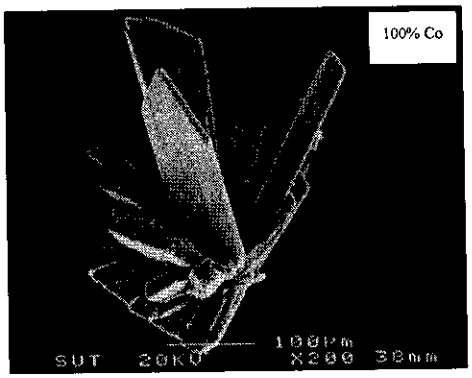


**c.** $V_2O_5 + Co^{2+} + dap + H_2O + pdc$
(1:1:2:593:2)

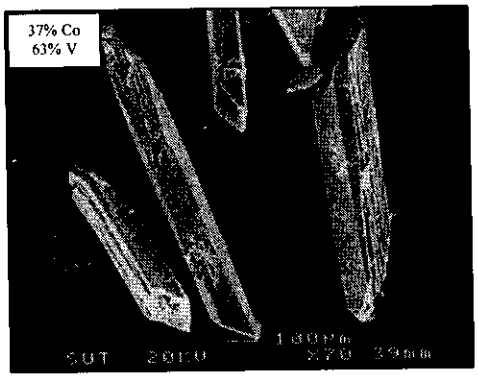


**d.** $V_2O_5 + Co^{2+} + Im + H_2O$
(0.5:1:8:400)

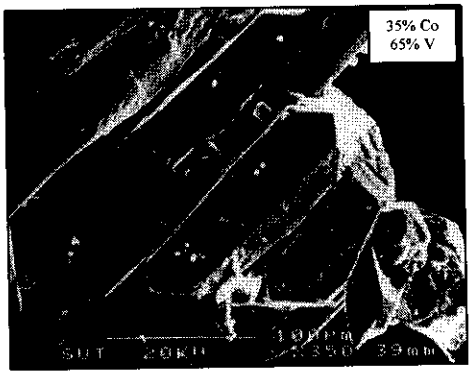


**e.** $V_2O_5 + Co^{2+} + Im + H_2O$
(0.5:1:16:400)

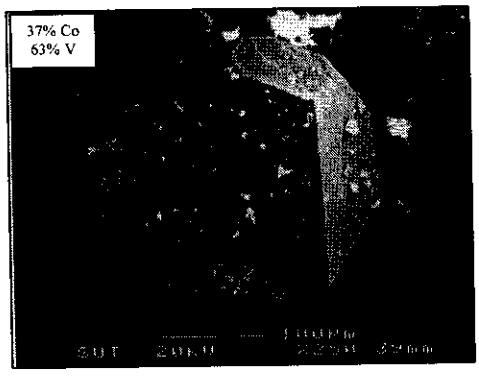


**f.** $V_2O_5 + Co^{2+}$ Im $+ H_2O$
(0.5:1:18:400)

Figure 3.5. SEM pictures of chosen crystalline materials.

# Chapter IV

# Hydrothermal Synthesis and Characterization of $[Co(picoline)_3]\cdot H_2O$

## 4.1 Introduction

Supramolecular chemistry is a rapidly developing research area because of the functional applications of many of the resulting materials (Sun & Lees, 2002). Recently, multidimensional supramolecular architectures have been constructed from N,O-donor chelating ligands such as pyridinedicarboxylic acids and transition metals using water as a solvent (Plater, Foreman, Howie, Lachowski, 1998; Min, Yoon, Lee, Suh & Lee, 2001; Whitfield, Zheng, Wang & Jacobson, 2001). Here we report the hydrothermal synthesis using 2,5-pyridinedicarboxylic acid (pdc) as donor chelating ligand source to produce the Co(III) complex, $[Co(picoline)_3]\cdot H_2O$, where significant $\pi$–$\pi$ stacking, O–H···O, C–H···O and C–H···$\pi$ hydrogen bonding interactions, and $C(\delta^+)\cdots O(\delta^-)$ carbonyl-carbonyl interactions are responsible for the supramolecular assembly.

## 4.2 Hydrothermal Crystallization

Hydrothermal synthesis of the complex carried out at SUT utilized the 125 mL Teflon-lined stainless steel autoclave (bomb). $V_2O_5$ (0.3 mmol, 0.50 g), $CoCl_2\cdot 6H_2O$ (0.3 mmol, 0.75 g), 1,3-diaminopropane (0.6 mmol, 0.46 ml), 2,5-pyridiendicarboxylic acid, (0.6 mmol, 0.92 g), and $H_2O$ (1.6 mol, 30 mL) in a molar

ratio of 1:1:2:2:593 was stirred for a few minutes in air, transferred and sealed in a 125 mL bomb, and heated to 180 °C under autogenous pressure for 6 days to allow the reaction and crystallization to proceed under hydrothermal conditions. The mixture was cooled to room temperature (final pH = 6), and the crystalline solid filtered off, washed with water, and air-dried at room temperature. The yield (0.65 g) was 84% based on cobalt.

## 4.3 X-Ray Crystallographic Study

A single crystal fragment of the red-violet compound with size, 0.04 x 0.16 x 0.23 mm was cut from a larger hexagonal plate and mounted to the end of a hollow glass fiber with cyanoacrylate glue. Reflection intensities were collected on a Bruker-Nonius KappaCCD four-circle area-detector diffractometer using the COLLECT (Nonius, 1998) software. The diffractrometer was equipped with a graphite monochromator, a 0.3 mm *ifg* capilliary collimator, and a fine focus X-ray tube (Mo $K_\alpha$ radiation, $\bar{\lambda}$ = 0.71073 Å) operating at 40 kV and 25 mA. The frame images were reduced to intensity data using the EvalCCD package (Duisenberg, Kroon-Batenburg & Schreurs, 2003). The structure was solved by direct methods using SIR97 (Altomare, Burla, Camalli, Cascarano, Giacovazzo, Guagliardi, Moliterni, Polidori & Spagna, 1999) and all the hydrogen atoms easily located from a subsequent difference electron density map.

In the final model all nonhydrogen atoms were given anisotropic atomic displacement parameters, while all hydrogen atoms of the complex were included as indealized riding model isotropic atomic contributions to the structure, and the

positions of the water hydrogen atoms were refined. Crystal data and details of the data collection, and structure refinement are summarized in Table 4.1. Fractional monoclinic coordinates and (equivalent) isotropic atomic displacement parameters for the refined atoms are given in Table 4.2. Anisotropic atomic displacement parameters for the nonhydrogen atoms are given in Table 4.3. Selected interatomic bond distances and angles are complied in Tables 4.4 and 4.5, respectively, and hydrogen bond parameters are given in Table 4.6. Derived hydrogen atom positions and isotropic atomic displacement parameters, torsional angles, principal mean square atomic displacements, and mean planes calculated through selected groups of nominally planar atoms are given as supplementary material in Appendix A as Tables A1.1, A1.2, A1.3, and A1.4, respectively.

## 4.4 Description of Structure

The contents of one asymmetric unit of the $[Co(picoline)_3]\cdot H_2O$ crystal structure are shown in Figure 4.1 with the atomic labeling scheme indicated thereon. The $[Co(picoline)_3]$ complex has distorted octahedral coordination geometry with three *mer* pyridyl nitrogen atoms and three *mer* carboxylate oxygen atoms. The bidentate anion ligands chelate (N, O-chelating) to cobalt; the Co–N bond distances vary from 1.912(1) to 1.926(1) Å, and the Co–O distances are constant (within $3\sigma$) at 1.888(1) to 1.890(1) Å. While the Co–N bond distances vary $14\sigma$, they are within the range of distances previously observed for similar six-coordinate cobalt(III) complexes with oxygen and nitrogen donor atoms (Sreelanth, Kala, Nayer & Kurup, 2004).

Table 4.1 Summary of Crystal Data, Data Collection, and Structure Refinement Details for $[Co(picoline)_3]\cdot H_2O$.

| | | |
|---|---|---|
| *Crystal data* | | |
| Structure formula | | $[Co(picoline)_3]\cdot H_2O$ |
| Chemical formula | | $C_{18}H_{12}N_3O_6Co\cdot H_2O$ |
| Chemical formula weight | | 443.25 |
| Crystal color / habit | | red-violet / plate |
| Crystal size (mm) | | 0.04 x 0.16 x 0.23 |
| Crystal system and space group | | monoclinic *C2*/c (No. 15) |
| Unit cell | $a$ (Å) | 29.727(4) |
| | $b$ (Å) | 8.5401(6) |
| | $c$ (Å) | 13.8024(11) |
| | $\beta$ (°) | 95.862(9) |
| | $V$ (Å$^3$) | 3485.7(6) |
| $Z$ | | 8 |
| $D_{calc}$ (Mg m$^{-3}$) | | 1.689 |
| Temperature (K) | | 298(2) |
| Absorption coefficient, $\mu$ (cm$^{-1}$) | | 10.4 |
| *F(000)* | | 1808 |
| *Data collection* | | |
| Diffractometer | | Bruker-Nonius KappaCCD |
| Radiation type / Wavelength (Å) | | Mo $K_\alpha$ / 0.71073 |
| Generator settings (kV/mA) | | 40 / 25 |
| Absorption correction: | | multiscan (SADABS; Sheldrick, 1996) |
| | | $T_{min}$ = 0.7944, $T_{max}$ = 0.9578 |
| Measured reflections | | 44627 |
| Theta range for data collection | | 2.48-29 |
| $R_{int}$ | | 0.0705 |
| Range of *h, k, l* | | $-40 \le h \le 40$, $-11 \le k \le 11$, $-18 \le l \le 18$ |

Table 4.1. (Continued)

| | |
|---|---|
| *Refinement* | |
| Refinement on | $F^2$ |
| No. of unique reflections | 4635 |
| No. of observed reflections ($F_o > 4\sigma F_o$) | 3314 |
| Final: $R$ indices ($F_o > 4\sigma F_o$) | $R_1 = 0.0364$, $wR_2 = 0.0734$ |
| $R$ indices (all data) | $R_1 = 0.0678$, $wR_2 = 0.0823$ |
| goodness of fit | 1.013 |
| Number of variables | 268 |
| Weighting scheme | $w = 1/[\sigma^2 F_o^2 + (0.0355P)^2 + 2.61P]$ where $P = [\max(F_o^2, 0) + 2F_c^2]/3$ |
| $\Delta\rho_{max}$ / $\Delta\rho_{min}$ / $\Delta\rho_{err}$ (e Å$^{-3}$) | 0.29 / –0.31 / 0.06 |
| Refinement program | SHELXL97 (Sheldrick, 1997) |
| Drawing program | ORTEP–III v 1.076 (Farrugia, 1997) (Burnett & Johnson, 1996) Diamond v 2.1e (Brandenburg, 2001) |

Table 4.2. Fractional Monoclinic Coordinates[a] and Isotropic Atomic Displacement Parameters[b] for the Refined Atoms in [Co(picoline)$_3$]·$H_2O$.

| Atom[c] | $x$ | $y$ | $z$ | $U_{eq}$ |
|---|---|---|---|---|
| Co | 0.112528(8) | 0.21883(3) | 0.626538(18) | 0.02283(8) |
| N1 | 0.05630(5) | 0.32888(20) | 0.61981(11) | 0.0248(4) |
| C1 | 0.04968(7) | 0.48296(25) | 0.62112(14) | 0.0314(5) |
| C2 | 0.00724(8) | 0.54564(29) | 0.62489(16) | 0.0388(5) |
| C3 | –0.02895(8) | 0.4465(3) | 0.62702(16) | 0.0414(6) |
| C4 | –0.02233(7) | 0.28731(29) | 0.62539(15) | 0.0359(5) |
| C5 | 0.02075(7) | 0.23193(25) | 0.62167(14) | 0.0277(4) |
| C6 | 0.03276(7) | 0.06269(26) | 0.61887(15) | 0.0304(5) |
| O1 | 0.07569(5) | 0.03840(16) | 0.61387(10) | 0.0302(3) |
| O2 | 0.00512(5) | –0.04080(20) | 0.62096(13) | 0.0501(4) |
| N2 | 0.16573(5) | 0.09011(19) | 0.64967(11) | 0.0254(4) |
| C7 | 0.18950(7) | 0.01655(28) | 0.58696(16) | 0.0357(5) |
| C8 | 0.22788(8) | –0.0663(3) | 0.61687(18) | 0.0457(6) |
| C9 | 0.24287(8) | –0.0699(3) | 0.71384(19) | 0.0487(7) |
| C10 | 0.21846(8) | 0.00545(29) | 0.77956(16) | 0.0397(5) |
| C11 | 0.17987(7) | 0.08230(24) | 0.74514(14) | 0.0266(4) |
| C12 | 0.14927(7) | 0.16225(26) | 0.80894(15) | 0.0311(5) |
| O3 | 0.11292(5) | 0.21731(18) | 0.76353(10) | 0.0321(3) |
| O4 | 0.15920(6) | 0.16832(23) | 0.89632(10) | 0.0521(5) |
| N3 | 0.11643(5) | 0.24365(19) | 0.48956(12) | 0.0252(4) |
| C13 | 0.09404(7) | 0.16555(26) | 0.41562(15) | 0.0311(5) |
| C14 | 0.10124(8) | 0.19753(28) | 0.32045(15) | 0.0402(6) |
| C15 | 0.13156(8) | 0.3107(3) | 0.30054(16) | 0.0439(6) |
| C16 | 0.15400(8) | 0.3931(3) | 0.37711(16) | 0.0405(6) |
| C17 | 0.14555(6) | 0.35680(26) | 0.47077(14) | 0.0286(4) |
| C18 | 0.16747(7) | 0.43801(26) | 0.55995(15) | 0.0316(5) |
| O5 | 0.15060(5) | 0.39650(17) | 0.63898(10) | 0.0297(3) |
| O6 | 0.19762(6) | 0.53124(21) | 0.55534(12) | 0.0501(5) |
| O7 | 0.10967(8) | –0.25473(23) | 0.55407(17) | 0.0639(6) |
| H7a | 0.0950(10) | –0.156(4) | 0.5614(20) | 0.0702 |
| H7b | 0.1237(10) | –0.243(3) | 0.4997(24) | 0.0702 |

[a] Estimated standard deviations of the least significant digits are given in parentheses.

[b] Equivalent isotropic atomic displacement parameters for the atoms refined anisotropically. $U$ values for H7a and H7b were fixed at 10% larger than $U_{eq}$[O7]. $U_{eq} = 1/3(U_{11} + U_{22} + U_{33})$

Table 4.3. Anisotropic Atomic Displacement Parameters[a] in

$[Co(picoline)_3]\cdot H_2O$ ($Å^2$).

| Atom | $U_{11}$ | $U_{22}$ | $U_{33}$ | $U_{23}$ | $U_{13}$ | $U_{12}$ |
|---|---|---|---|---|---|---|
| Co | 0.01837(13) | 0.02821(14) | 0.02186(14) | –0.00015(11) | 0.00175(9) | –0.00023(12) |
| N1 | 0.0220(8) | 0.0303(9) | 0.0222(8) | 0.0019(7) | 0.0023(6) | 0.0008(8) |
| C1 | 0.0331(12) | 0.0297(12) | 0.0313(11) | 0.0004(9) | 0.0022(9) | –0.0006(9 |
| C2 | 0.0451(14) | 0.0371(13) | 0.0337(12) | 0.0010(10) | 0.0026(10) | 0.0136(11) |
| C3 | 0.0306(12) | 0.0577(16) | 0.0356(12) | 0.0009(11) | 0.0017(10) | 0.0167(11) |
| C4 | 0.0225(10) | 0.0504(14) | 0.0349(12) | 0.0031(11) | 0.0034(9) | 0.0008(10) |
| C5 | 0.0226(10) | 0.0357(11) | 0.0247(10) | 0.0043(9) | 0.0024(8) | 0.0010(9) |
| C6 | 0.0247(11) | 0.0362(12) | 0.0302(11) | 0.0040(9) | 0.0023(8) | –0.0027(9) |
| O1 | 0.0246(7) | 0.0284(8) | 0.0377(8) | 0.0022(6) | 0.0038(6) | –0.0011(6) |
| O2 | 0.0324(9) | 0.0403(10) | 0.0780(12) | 0.0065(9) | 0.0082(8) | –0.0114(8) |
| N2 | 0.0190(8) | 0.0303(9) | 0.0268(9) | –0.0028(7) | 0.0020(7) | –0.0010(7) |
| C7 | 0.0294(12) | 0.0458(14) | 0.0324(11) | –0.0071(10) | 0.0050(9) | 0.0036(10) |
| C8 | 0.0335(13) | 0.0527(16) | 0.0524(15) | –0.0101(12) | 0.0110(11) | 0.0109(11) |
| C9 | 0.0286(13) | 0.0568(17) | 0.0602(16) | 0.0087(13) | 0.0024(11) | 0.0175(12) |
| C10 | 0.0333(13) | 0.0484(15) | 0.0365(12) | 0.0068(11) | –0.0006(10) | 0.0070(11) |
| C11 | 0.0247(10) | 0.0288(11) | 0.0259(10) | 0.0012(8) | 0.0009(8) | –0.0021(8) |
| C12 | 0.0352(12) | 0.0335(11) | 0.0251(11) | 0.0036(9) | 0.0048(9) | –0.0004(10) |
| O3 | 0.0298(8) | 0.0438(9) | 0.0235(7) | 0.0015(6) | 0.0070(6) | 0.0073(7) |
| O4 | 0.0597(12) | 0.0748(13) | 0.0210(8) | 0.0002(8) | 0.0010(7) | 0.0184(10) |
| N3 | 0.0196(8) | 0.0309(10) | 0.0246(8) | –0.0002(7) | 0.0002(6) | 0.0003(7) |
| C13 | 0.0306(11) | 0.0301(11) | 0.0312(11) | –0.0026(9) | –0.0043(9) | –0.0004(9) |
| C14 | 0.0480(14) | 0.0441(15) | 0.0260(11) | –0.0074(10) | –0.0083(10) | 0.0087(11) |
| C15 | 0.0482(15) | 0.0590(17) | 0.0248(11) | 0.0075(11) | 0.0050(10) | 0.0089(13) |
| C16 | 0.0340(12) | 0.0526(15) | 0.0354(12) | 0.0112(11) | 0.0063(10) | –0.0049(11) |
| C17 | 0.0202(10) | 0.0357(12) | 0.0294(11) | 0.0025(9) | 0.0007(8) | –0.0016(9) |
| C18 | 0.0251(11) | 0.0349(12) | 0.0338(11) | 0.0015(9) | -0.0020(9) | –0.0053(9) |
| O5 | 0.0266(7) | 0.0345(8) | 0.0274(7) | –0.0036(6) | 0.0002(6) | –0.0057(6) |
| O6 | 0.0388(10) | 0.0588(11) | 0.0518(10) | 0.0026(9) | 0.0007(8) | -0.0250(9) |
| O7 | 0.0732(15) | 0.0445(12) | 0.0800(15) | 0.0124(10) | 0.0376(12) | 0.0022(10) |

[a] Estimated standard deviations of the least significant digits are given in parentheses.
The form of the anisotropic function is:

$$U = \exp(-2\pi^2[h^2(a^*)^2U_{11} + k^2(b^*)^2U_{22} + l^2(c^*)^2U_{33} + 2(hka^*b^*U_{12} + hla^*c^*U_{13} + klb^*c^*U_{23})]$$

Table 4.4. Selected Interatomic Bond Lengths[a] (Å).

| Atoms | Distance | Atoms | Distance | Atoms | Distance |
|---|---|---|---|---|---|
| Co–O1 | 1.8881(14) | Co–O3 | 1.8897(13) | Co–O5 | 1.8902(14) |
| Co–N1 | 1.9117(16) | Co–N2 | 1.9257(16) | Co–N3 | 1.9177(16) |
| N1–C1 | 1.3309(27) | N2–C7 | 1.3297(25) | N3–C13 | 1.3381(25) |
| C1–C2 | 1.376(3) | C7–C8 | 1.370(3) | C13–C14 | 1.3796(29) |
| C2–C3 | 1.372(3) | C8–C9 | 1.367(3) | C14–C15 | 1.369(3) |
| C3–C4 | 1.374(3) | C9–C10 | 1.378(3) | C15–C16 | 1.383(3) |
| C4–C5 | 1.3712(28) | C10–C11 | 1.3641(29) | C16–C17 | 1.3771(28) |
| C5–N1 | 1.3448(26) | C11–N2 | 1.3433(24) | C17–N3 | 1.3402(26) |
| C5–C6 | 1.4902(29) | C11–C12 | 1.4943(28) | C17–C18 | 1.5024(28) |
| C6–O1 | 1.3016(24) | C12–O3 | 1.2820(25) | C18–O5 | 1.2957(24) |
| C6–O2 | 1.2091(25) | C12–O4 | 1.2131(24) | C18–O6 | 1.2052(25) |

[a] Estimated standard deviations of the least significant digits are given in parentheses.

Table 4.5. Selected Interatomic Bond Angles[a] (°)

| Atoms | Angle | Nature |
|---|---|---|
| O1–Co–N1 | 84.30(7) | chelate ring |
| O3–Co–N2 | 84.79(6) | |
| O5–Co–N3 | 84.54(6) | |
| O1–Co–N2 | 90.47(7) | *cis*-N,O |
| O1–Co–N3 | 95.27(6) | |
| O3–Co–N1 | 88.17(6) | |
| O5–Co–N1 | 97.02(7) | |
| O5–Co–N2 | 88.24(7) | |
| N1–Co–N3 | 92.20(7) | *cis*-N,N |
| N2–Co–N3 | 95.46(7) | |
| O1–Co–O3 | 91.80(6) | *cis*-O,O |
| O3–Co–O5 | 88.41(6) | |
| N1–Co–N2 | 171.09(7) | *trans* |
| O1–Co–O5 | 178.67(6) | |
| O3–Co–N3 | 172.93(7) | |

[a] Estimated standard deviations of the least significant digits are given in parentheses.

Table 4.6. Intermolecular Hydrogen Bonds in $[Co(picoline)_3]\cdot H_2O$ (Å, °).

| D–H···A | d[D–H] | d[H···A] | d[D···A] | ∠[D–H···A] |
|---|---|---|---|---|
| C4–H4···O3[c] | 0.93 | 2.61 | 3.287(2) | 130.4 |
| C7–H7···O4[b] | 0.93 | 2.40 | 3.121(3) | 134.8 |
| C8–H8···O6[d] | 0.93 | 2.71 | 3.423(3) | 134.2 |
| C10–H10···O6[e] | 0.93 | 2.49 | 3.210(3) | 134.8 |
| C13–H13···O2[f] | 0.93 | 2.40 | 3.127(3) | 135.2 |
| C15–H15···O5[g] | 0.93 | 2.73 | 3.436(3) | 132.9 |
| C15–H15···O7[b] | 0.93 | 2.65 | 3.431(3) | 141.9 |
| O7–H7a···O1[a] | 0.96(3) | 1.92(3) | 2.853(3) | 163(2) |
| O7–H7b···O4[b] | 0.90(3) | 1.96(3) | 2.847(3) | 166(3) |

Symmetry codes: (a) x, y, z; (b) x, –y, z–1/2; (c) –x, y, –z+3/2; (d) –x+1/2, –y+1/2, z–1; (e) –x+1/2, y–1/2, –z+3/2; (g) –x, –y, –z+1; (f) x, –y+1, z –1/2

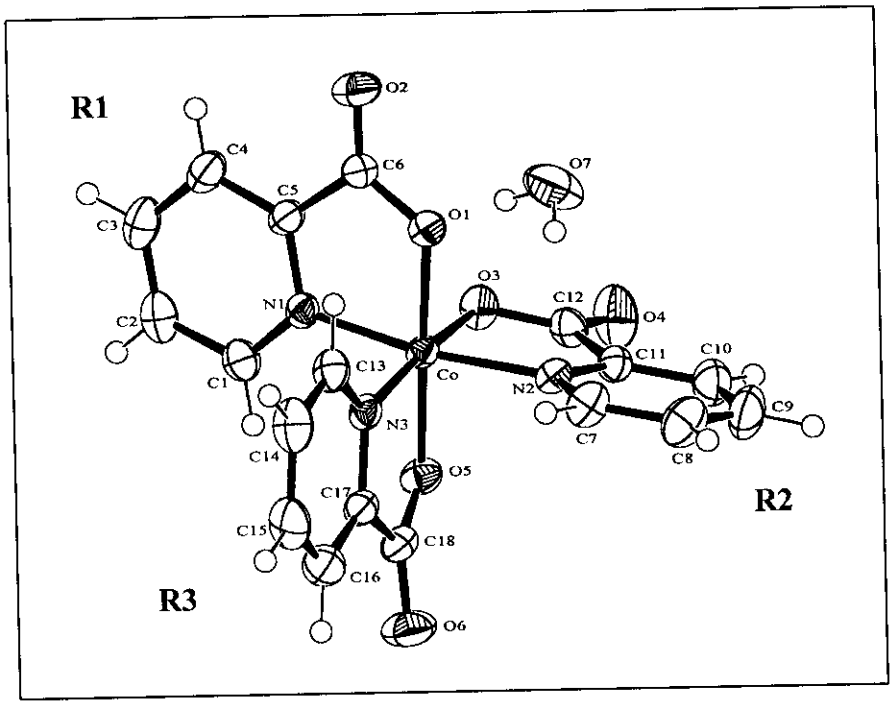


Figure 4.1. Perspective drawing of $[Co(picoline)_3]\cdot H_2O$. Nonhydrogen atoms are represented with 50% probability ellipsoids and hydrogen atoms with arbitrary small spheres for clarity. **R1**, **R2**, and **R3** are used to identity the rings in subsequent discussion.

**$\pi$–$\pi$ Stacking Interactions**

The discrete molecules pack into columns as a series of aryl-aryl offset face-to-face interactions, *off*, propagated in the ***c*** direction by alternating 2-fold axes with distances of 3.465(3) Å between 2-fold related aryl rings from adjacent molecules (the aryl rings are nearly coplanar with a dihedral angle of 1.23(2)°), and inversion sites with distances of 3.420(3) Å between adjacent parallel inversion related aryl rings indicating significant noncovalent $\pi$–$\pi$ stacking interactions (Janiak, 2000), giving rise to an interdigitated double comb motif as shown in Figure 4.2. Projection of the $\pi$–$\pi$ stack perpendicular to the 2-fold axis, as in Figure 4.3, shows that the $\pi$–$\pi$ stacks are bordered by ring **R2**.

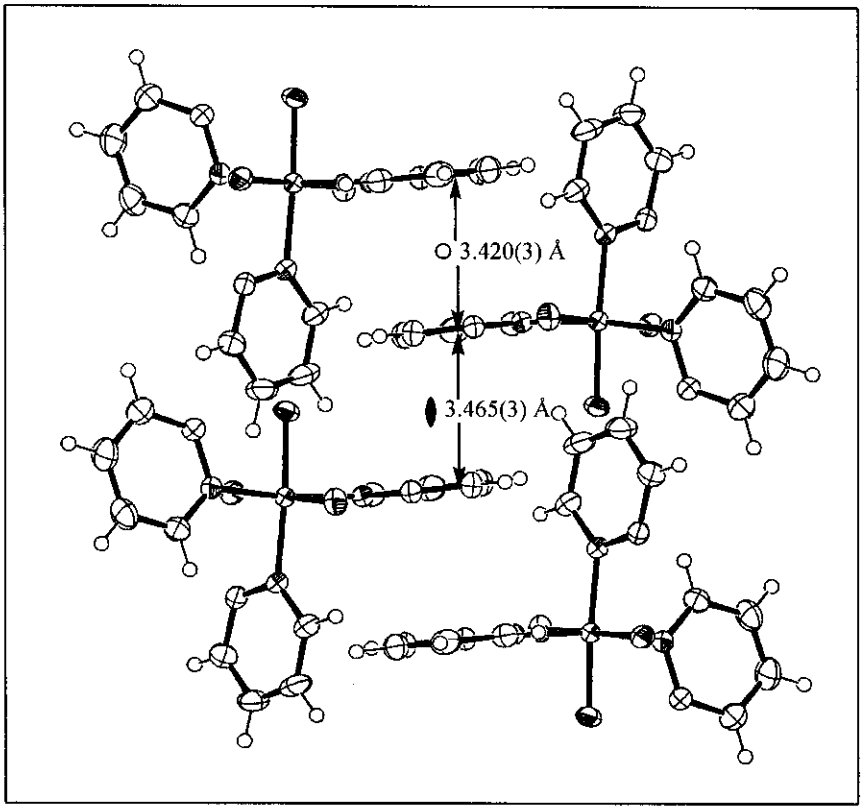


Figure 4.2. Projection diagram down [010] showing the $\pi$–$\pi$ stacking of rings **R1** along *c*. Rings **R2** are oriented in the vertical direction. Water molecules and carbonyl groups were not drawn for clarity.

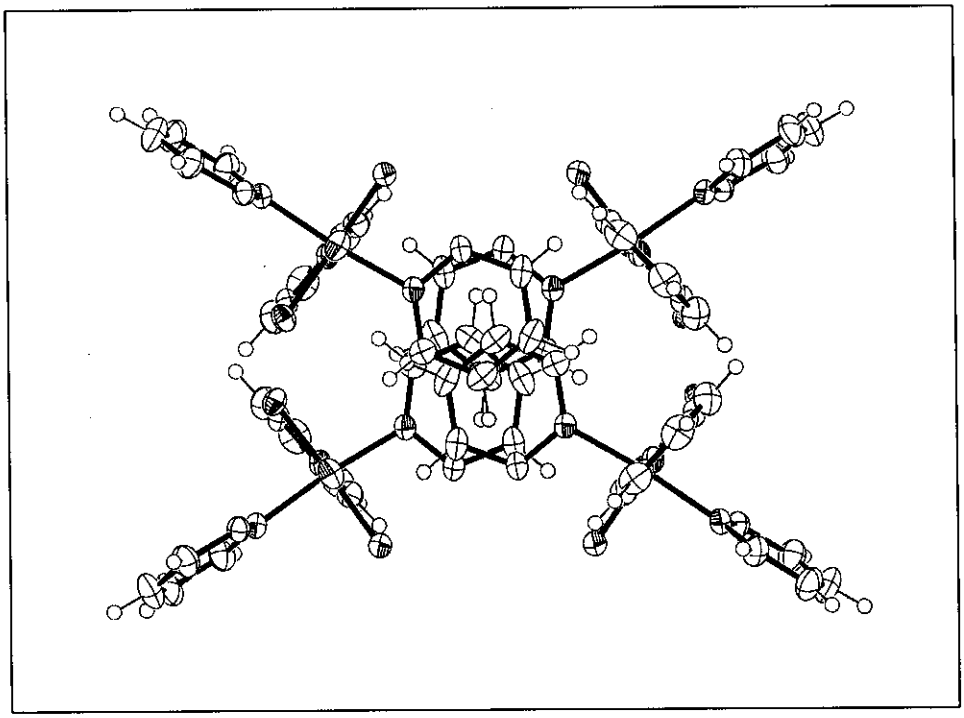

Figure 4.3. Projection diagram down the π–π stacking direction. The portion of the structure illustrated in Figure 4.2 but rotated about the horizontal direction so the structure is projected perpendicular to the 2-fold axis and rings **R2** are perpendicular to the diagram.

**Parallel Fourfold Aryl Embrace (P4AE)**

The **R2** rings reinforce the interdigitated comb structure in the ***c*** direction by additional noncovalent interactions in the form of C–H···π edge-to-face type interactions from hydrogen atoms, H3, of the stacked aryl rings, pointing towards the faces of aryl rings **R2** at a distance of 2.791(2) Å, resulting in centrosymmetric, achiral, parallel fourfold aryl embraces, P4AE, (one *of*f interaction, and two *ef* interactions) as illustrated Figures 4.4 and 4.5. The Co···Co distance across these P4AE is 8.675 Å.

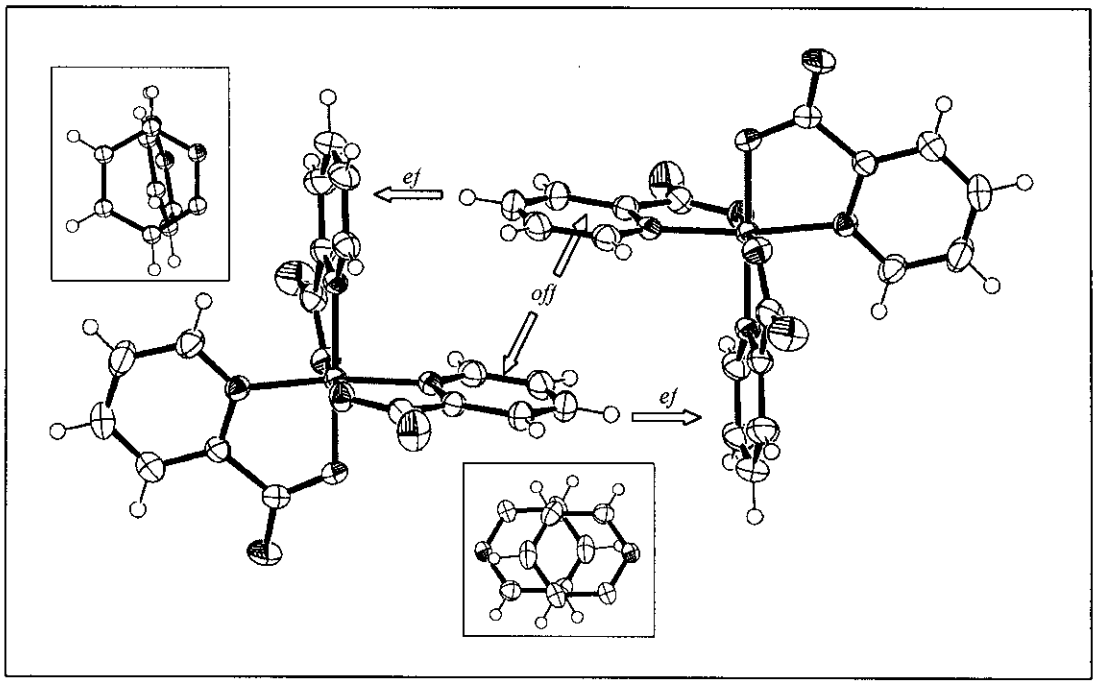


Figure 4.4. P4AE interaction between two [Co(picoline)$_3$] complex molecules. The upper left inset shows the *ef* interaction projected on **R2**. The lower center inset shows the parallel *off* interaction projected on **R1**.

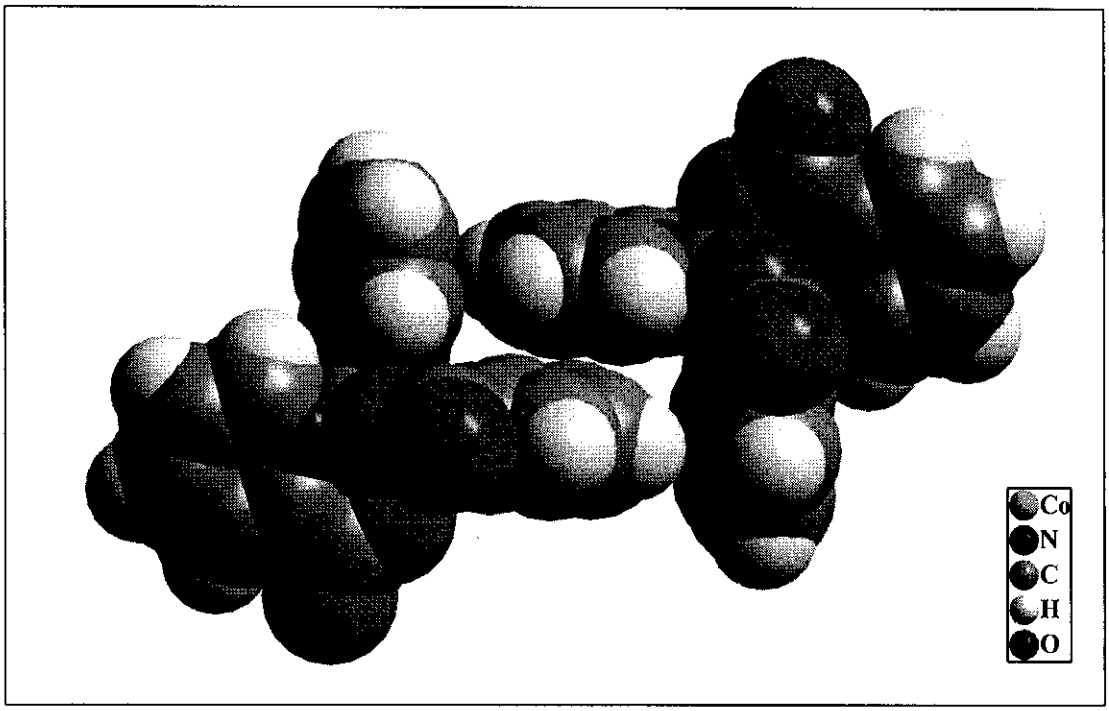


Figure 4. 5. Space-filling model of the P4AE interaction between two [Co(picoline)$_3$] complex molecules. The C–H···$\pi$ *ef* interactions are clearly visible.

**Carbonyl-Carbonyl Interactions**

Carbonyl oxygen atom O2 (x, y, z) forms a 3.391(2) Å antiparallel, Type II (Allen, Baalham, Lommerse & Raithby, 1998) contact with the inversion related carbonyl carbon atom C6 (–x, –y, 1–z) as shown in Figure 4.6. The C–O···C and O···C–O angles of 100.12(4)° and 79.88(4)°, respectively, compare reasonably with the ideal values of 96.5(4)° and 83.5(4)° found by Allen and coworkers. The $C(\delta^+)\cdots O(\delta^-)$ distance is longer than the optimal distance 3.02 Å, but still within the range of distances found by Allen and coworkers, indicating that this is a weak carbonyl-carbonyl interaction. The columns are linked into thick planes by carbonyl-carbonyl interactions between 2-fold related pairs of carboxypyridine ligands of adjacent face-to-face columns (described in π–π stacking part) as shown in the schematic drawing in Figure 4.7.

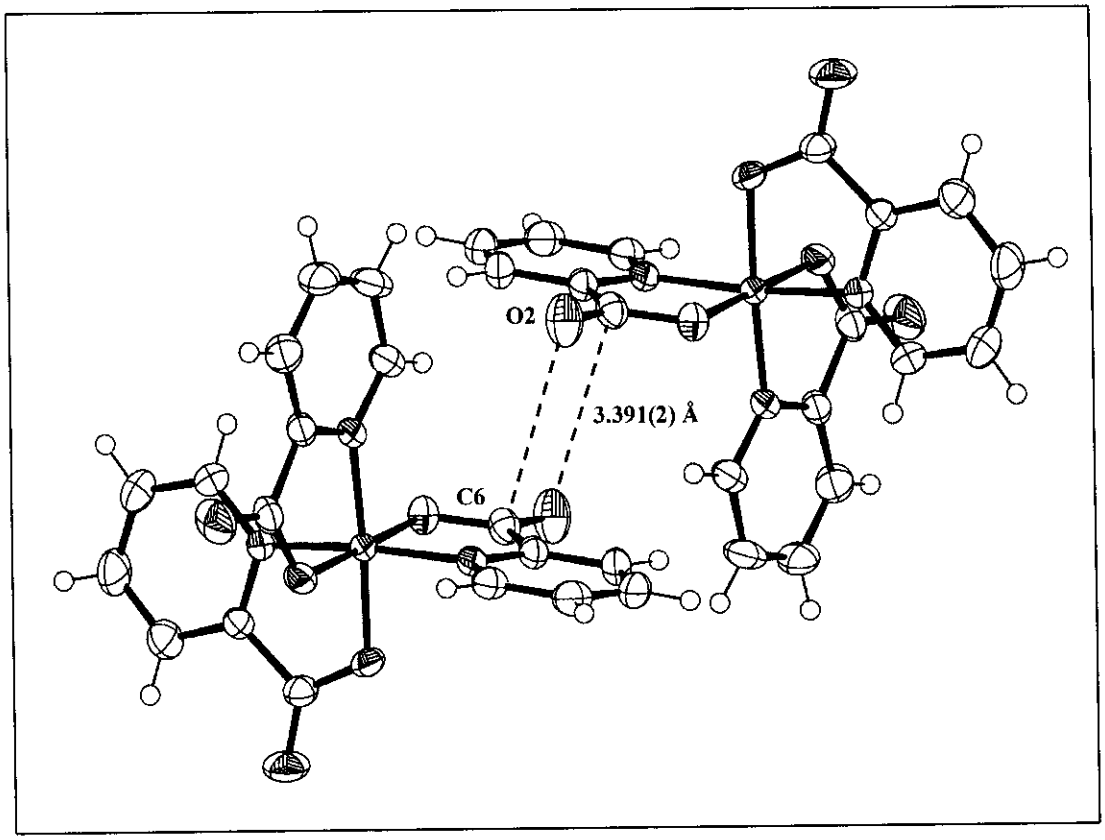


Figure 4.6. Carbonyl-carbonyl antiparallel interaction motif.

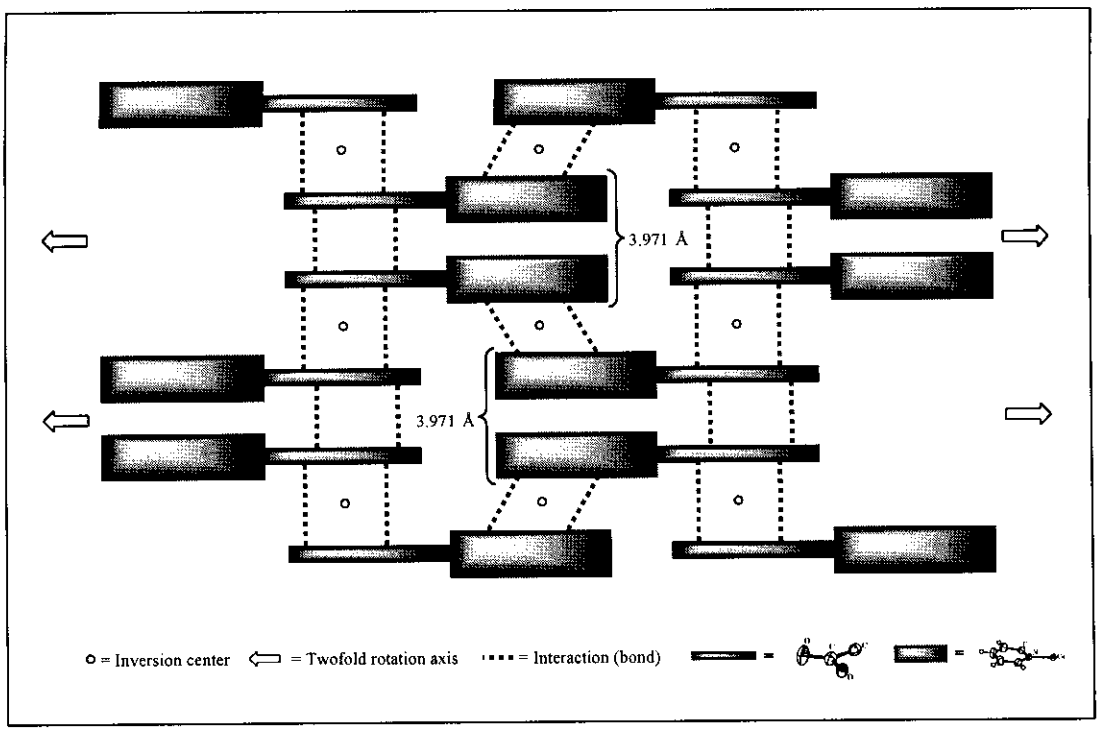


Figure 4.7. Schematic representation of the 2-D carbonyl-carbonyl linked π-stacked columns.

**Strong O–H···O Hydrogen Bonding**

There is also hydrogen bonding involving the [Co(picoline)$_3$] and the solvent water molecule. Adjacent π–π stacked columns are linked together by strong O–H···O hydrogen bonding from the solvate water molecule. Each water molecule forms two donor hydrogen bonds with oxygen atoms of the complex, bridging the carboxylate oxygen, O1 on **R1**, of one molecule to the carbonyl oxygen, O4 (x, –y, z–1/2), on **R2** of another molecule, *via* hydrogen bonds to adjacent π–π stacks, as illustrated in Figure 4.8.

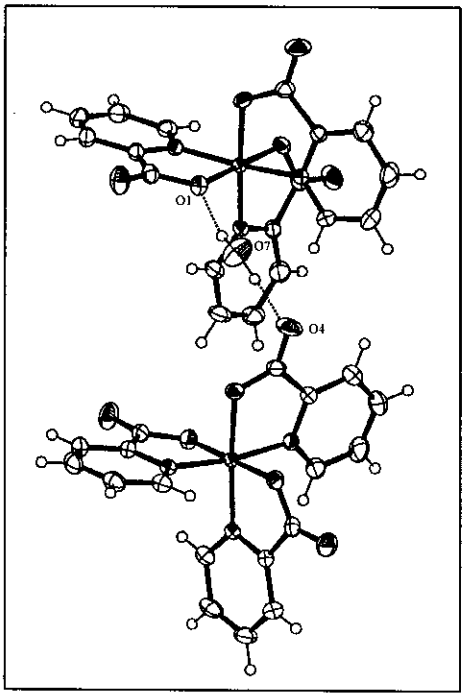


Figure 4.8. Water bridging two molecules, showing strong O–H···O hydrogen bonds.

### Weak C–H···O Hydrogen Bonding

Moreover, extensive intermolecular weak hydrogen bonds are formed between carbon atoms on the aryl rings acting as hydrogen bond donors and carboxylate oxygen atoms as acceptors generating a two-dimensional network as depicted in Figure 4.9. The important hydrogen bonds are listed in the Table 4.6.

## 4.5 Further Physical Characterization

### SEM-EDX analysis

The crystal morphology is shown in Figure 4.10, and the EDX spectrum, confirming presence of cobalt as the only heavy element in the complex, is shown in Figure 4.11.

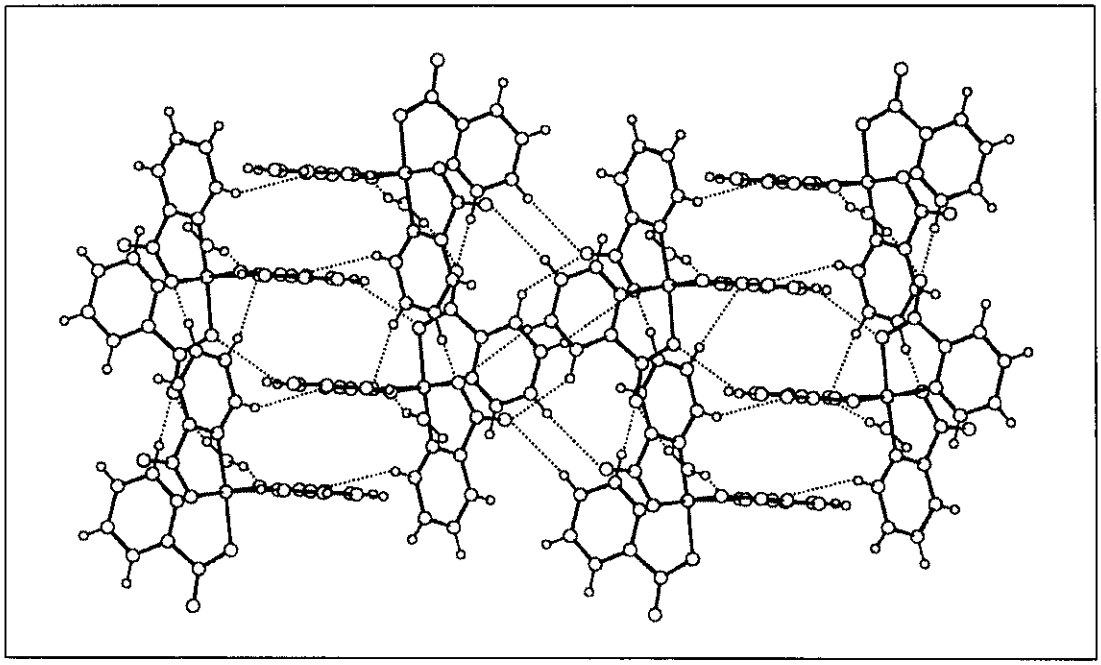

Figure 4. 9. The 2-D network of $[Co(picoline)_3]\cdot H_2O$ connected by hydrogen bonds.

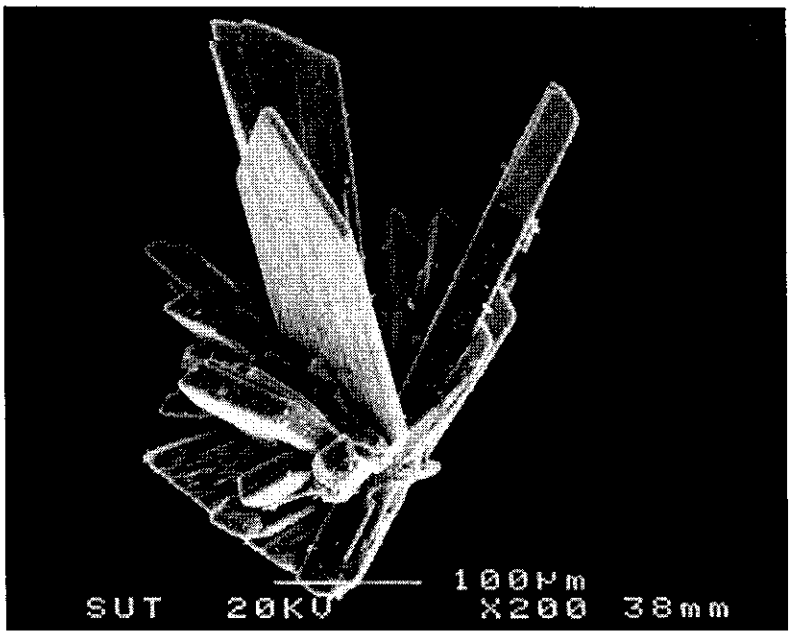


Figure 4.10. SEM picture of $[Co(picoline)_3]\cdot H_2O$.

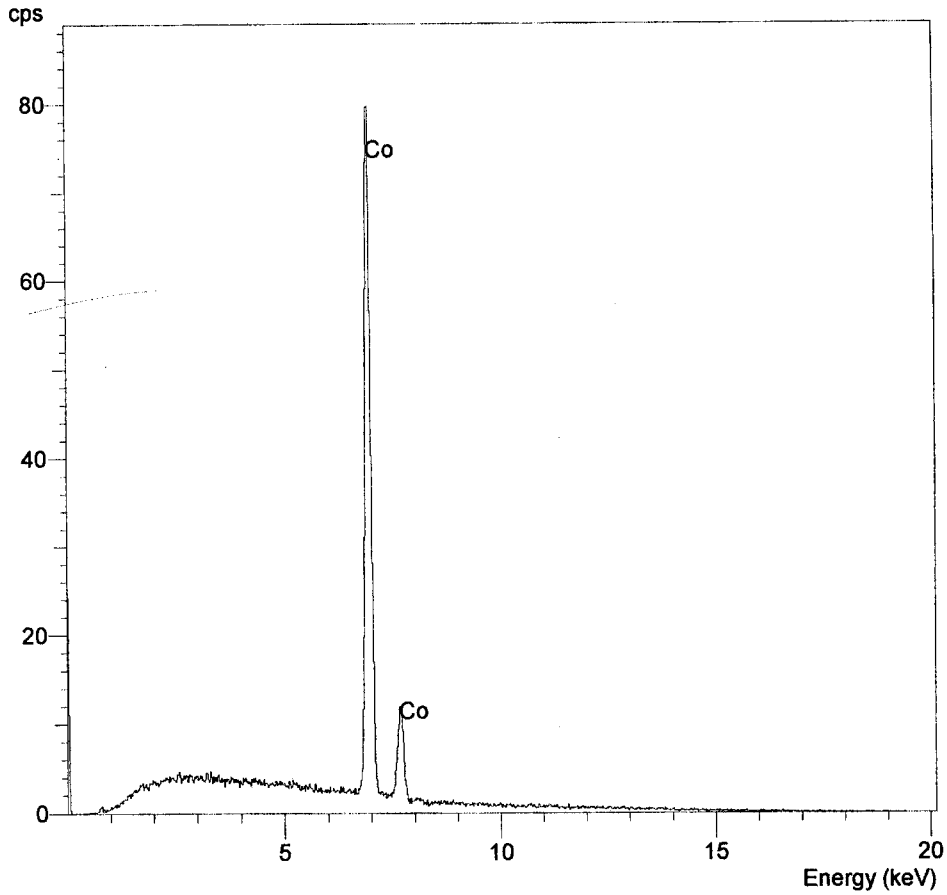


Figure 4.11. EDX spectrum of $[Co(picoline)_3]\cdot H_2O$.

**FTIR analysis**

The IR spectrum of $[Co(pic)_3]\cdot H_2O$ is shown in Figure 4.12. It shows the expected absorptions corresponding to the asymmetric and symmetric carbonyl stretches of picolinate, and uncoordinated water. In the high-frequency region, absorption bands at 3454 and 3520 $cm^{-1}$, where the hydrogen bonding involving the carboxylic acid group and water absorbs, very broad bands due to O–H···O. These bands confirm the presence of water in the complex,.while the bands at 3061 and 3112 $cm^{-1}$ correspond to C–H stretching in aromatic rings. The IR carbonyl –COO stretch of the free ligand gives rise to a strong absorption bands at 1710 $cm^{-1}$, [$\nu_{as}$(COO)] (Goher, Abu-Youssef & Mautner, 1996), which is shifted towards a lower

wave number at 1681 $cm^{-1}$ in this complex indicative of bonding through the carboxylate moiety to the cobalt metal atom. The symmetric carbonyl stretch, [$\nu_s$(COO)] shows peaks at 1380, 1354, and 1333 $cm^{-1}$. The coordination mode of ligands is further supported by the frequencies occurring in the 462-392 $cm^{-1}$ range which have been assigned tentatively to $\nu$(Co–O) or $\nu$(Co–N), (Islam & Uddin, 1993). Tentative assignments for the most important peaks in the 4000-370 $cm^{-1}$ region are summarized in Table 4.7.

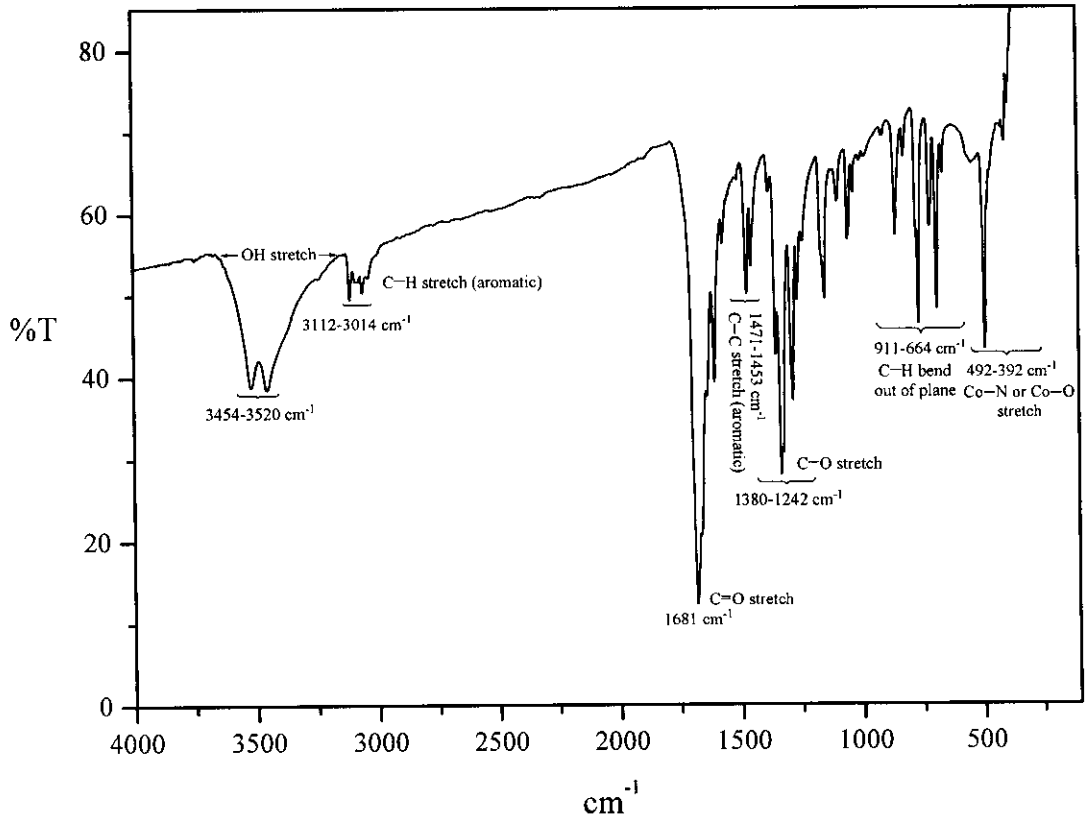


Figure 4.12. FTIR spectrum of [Co(picoline)$_3$]·$H_2O$.

Table 4.7. Vibrational Frequency ($cm^{-1}$) Data of $[Co(picoline)_3]\cdot H_2O$.

| Range ($cm^{-1}$) | Intensity | Assignments |
|---|---|---|
| 392-492 | s | Co–N, Co–O |
| 664-911 | s | C–H bend out of plane (aromatic) |
| 1242-1380 | s | C–O stretch |
| 1453-1471 | m | C–C stretch |
| 1681 | s | C=O stretch (carbonyl) |
| 3112-3061 | s | C–H stretch (aromatic) |
| 3520-3454 | s, br | O–H stretch, H-bonded |

s = strong, m = medium, br = broad

**Thermal Analysis**

Thermal decomposition (TGA) under air shows loss of water from 60-156 °C (4.6% loss) followed by two overlapping steps from 275-~320 °C and ~320-412 °C corresponding to ~15.4% weight loss and 62% weight loss, respectively, as the ligands decompose. Potential decomposition products are listed in Table 4.8, along with their masses and relative percentages of the complex. The TGA spectrum is shown in Figure 4.13.

Table 4.8. Potential Decomposition Products of $[Co(picoline)_3]\cdot H_2O$.

| Fragment | MW, Daltons | Relative Weight % |
|---|---|---|
| $H_2O$ | 18.02 | 4.07 |
| CO | 28.01 | 6.32 |
| $CO_2$ | 44.01 | 9.93 |
| $C_5H_4NCO_2$ | 122.10 | 27.55 |
| $C_5H_4N$ | 78.09 | 17.62 |
| **TGA Waves** | **Weight Loss, %** | **Assignment** | **Relative % Error** |
| 60-156 °C | 4.6 | $H_2O$ | +13 |
| 275-310 °C | 15.4 | 3CO | -18 |
| 320-412 °C | 62 | $3C_5H_4N$ | +17 |

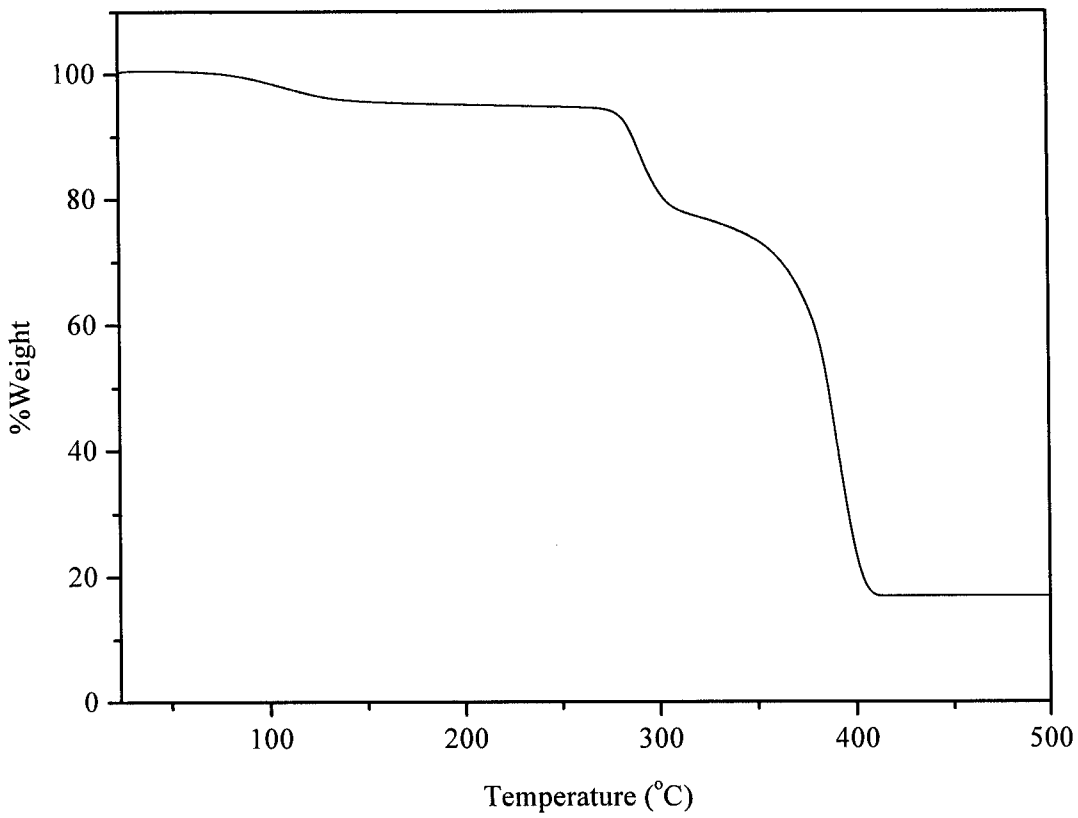


Figure 4.13. TGA curve of $[Co(picoline)_3]\cdot H_2O$.

# Chapter V

# Hydrothermal Synthesis and Characterization of $(H_2dap)^{2+}[(V^{IV}O)_2(V^{V}O_4)_2]^{2-}$

## 5.1 Introduction

In the past decade, design and synthesis of organic-inorganic hybrid materials has received considerable attention, not only to the variety of structural types and bonding geometries, but also due to potential application in fields such as; catalysis (Botella, López-Nieto, Solsona, Mifud & Márquez, 2002), electronic conductivity (Yang, Song, Ngala, Zavalij & Whittingham, 2003), magnetism (Alda, Bazán, Mesa, Pizarro, Arriortua & Rojo, 2003), and medicine (Saha, Padhyde, Anson & Powell, 2002). One of the most powerful methods for the preparation of these hybrid materials and other important solids including microporous crystals (Pertierra, Salvadó, Garcia-Granda, Anatoly, Bortun, Khainakov & García, 2002), complex oxide ceramics (Huang, Xiong, Fang & Feng, 2003), magnetic materials (Yu, Fujino & Yoshimura, 2003), chemical sensors, and electronically conducting solids (Feng & Xu, 2001) is the hydrothermal synthesis technique. The hydrothermal method is particularly suitable for fabrication of organic-inorganic hybrid metal oxide materials since the traditional methods of synthesizing the metal oxide frameworks rely on high temperatures which would destroy the organic template molecules. Organic amines have been used extensively as templates for preparation of many of these hybrid materials under hydrothermal conditions. The organic amine is generally both a

charge-compensating cation and a space-filling moiety, and may also function as a ligand to the metal.

The structure reported in this chapter is a simple hydrated coordination complex. It was the major product of an attempt to synthesize a mixed-valence, organic-inorganic hybrid of vanadium-cobalt oxide employing the hydrothermal method. Characterization of the complex by single X-ray diffraction, FTIR, and thermal analysis is reported herein.

## 5.2 Hydrothermal Crystallization

The attempted synthesis of a cobalt-vanadium oxide compound was carried out under hydrothermal reaction conditions. A mixture of $V_2O_5$ (0.3 mmol, 0.50 g), $CoCl_2 \cdot 6H_2O$ (0.3 mmol, 0.75 g), 1,3-dap (0.6 mmol, 0.46 mL), HCl (0.3 mmol, 0.08 mL), and $H_2O$ (1.6 mol, 30 mL) in a molar ratio of 1:1:2:1:593 was stirred for 30 min in air. The solution/mixture was transferred and sealed in a 125 mL Teflon-lined stainless steel autoclave (Parr bomb), and heated to 180 °C under autogenous pressure for 4 days before cooling to room temperature. The acidity of the medium was constant at pH ~7-8 before and after the reaction. Brown-black crystals were filtered off, washed with water, and air-dried at room temperature. The compound is insoluble in water and common organic solvents (methanol). The yield was 0.40 g, 89% based on vanadium.

## 5.3 X-Ray Crystallographic Study

A single crystal of the compound with size, 0.28 x 0.30 x 0.32 mm was selected and mounted to the end of a hollow glass fiber with cyanoacrylate glue. Reflection intensities were collected on a Bruker-Nonius KappaCCD four-circle area-detector diffractometer using the COLLECT software (Nonius, 1998). The diffractrometer was equipped with a graphite monochromator, a 0.5 mm *ifg* capilliary collimator, and a fine focus X-ray tube (Mo $K_\alpha$ radiation, $\bar{\lambda}$ = 0.71073 Å) operating at 40 kV and 20 mA. The frame images were reduced to intensity data using the EvalCCD package (Duisenberg, Kroon-Batenburg & Schreurs, 2003). The structure was solved by direct methods using SIR97 (Altomare, Burla, Camalli, Cascarano, Giacovazzo, Guagliardi, Moliterni, Polidori & Spagna, 1999) and all the hydrogen atoms easily located from a subsequent difference electron density map. Crystal data and details of the data collection, and structure refinement are summarized in Table 5.1. Fractional monoclinic coordinates and (equivalent) isotropic atomic displacement parameters for the refined atoms are given in Table 5.2. Anisotropic atomic displacement parameters for the nonhydrogen atoms are given in Table 5.3. Selected interatomic bond distances and angles are complied in Table 5.4, and hydrogen bond parameters are given in Table 5.5. Derived hydrogen atom positions and isotropic atomic displacement parameters, torsional angles, principal mean squaare atomic displacements, and mean planes calculated through selected groups of nominally planar atoms are given as supplementary material in Appendix B as Tables B1.1, B1.2, B1.3, and B1.4, respectively.

Table 5.1 Summary of Crystal Data, Data Collection, and Structure Refinement Details for $(H_2dap)^{2+}[(V^{IV}O)_2(V^{V}O_4)_2]^{2-}$.

| | |
|---|---|
| *Crystal data* | |
| Structure formula | $(H_2dap)^{2+}[(V^{IV}O)_2(V^{V}O_4)_2]^{2-}$ |
| Chemical formula | $C_3H_{12}N_2V_4O_{10}$ |
| Chemical formula weight | 439.91 |
| Crystal color / habit | brown-black / hexagonal |
| Crystal size (mm) | 0.28 x 0.30 x 0.32 |
| Crystal system and space group | monoclinic $P2_1/c$ (No. 14) |
| Unit cell $a$ (Å) | 7.975(3) |
| $b$ (Å) | 9.986(2) |
| $c$ (Å) | 15.629(3) |
| $\beta$ (°) | 100.66(3) |
| $V$ (Å$^3$) | 1223.3(6) |
| $Z$ | 4 |
| $D_{calc}$ (Mg m$^{-3}$) | 2.389 |
| Temperature (K) | 298(2) |
| Absorption coefficient, $\mu$ (cm$^{-1}$) | 3.01 |
| *F(000)* | 864 |
| *Data collection* | |
| Diffractometer | Bruker-Nonius KappaCCD |
| Radiation type / Wavelength (Å) | Mo $K_\alpha$ / 0.71073 |
| Generator settings (kV/mA) | 40 / 20 |
| Absorption correction: | multiscan (SADABS; Sheldrick, 1996) |
| | $T_{min}$ = 0.4459, $T_{max}$ = 0.4861 |
| Measured reflections | 16076 |
| Theta range for data collection | 5.15-29.58 |
| $R_{int}$ | 0.0729 |
| Range of *h, k, l* | $-10 \le h \le 10$, $-12 \le k \le 11$, $-20 \le l \le 20$ |

Table 5.1. (Continued)

| | |
|---|---|
| *Refinement* | |
| Refinement on | $F^2$ |
| No. of unique reflections | 2778 |
| No. of observed reflections ($F_o > 4\sigma F_o$) | 2407 |
| Final: *R* indices ($F_o > 4\sigma F_o$) | $R_1 = 0.0384$, $wR_2 = 0.1043$ |
| *R* indices (all data) | $R_1 = 0.0456$, $wR_2 = 0.1111$ |
| goodness of fit | 1.096 |
| Number of variables | 176 |
| Weighting scheme | $w = 1/[\sigma^2 F_o^2 + (0.0610P)^2 + 1.94P]$ where $P = [\max(F_o^2, 0) + 2F_o^2]/3$ |
| $\Delta\rho_{max} / \Delta\rho_{min} / \Delta\rho_{err}$ (e Å$^{-3}$) | 1.116 / –0.865 / 0.143 |
| Refinement program | SHELXL97 (Sheldrick, 1997) |
| Drawing program | ORTEP−III v 1.076 (Farrugia, 1997) (Burnett & Johnson, 1996) Diamond v 2.1e (Brandenburg, 2001) |

Table 5.2. Fractional Monoclinic Coordinates[a] and Isotropic Atomic Displacement Parameters[b] for the Refined Atoms in $(H_2dap)^{2+}[(V^{IV}O)_2(V^{V}O_4)_2]^{2-}$.

| Atom | *x* | *y* | *z* | *U*eq |
|---|---|---|---|---|
| V(1) | 0.11193(6) | 0.26247(4) | 0.04008(3) | 0.00990(15) |
| V(2) | 0.38614(6) | 0.24227(4) | –0.05624(3) | 0.00990(15) |
| V(3) | 0.25934(6) | 0.55542(4) | –0.02747(3) | 0.01047(15) |
| V(4) | 0.24127(6) | –0.04731(4) | 0.02787(3) | 0.01090(15) |
| O(1) | 0.2446(3) | 0.6006(2) | –0.12745(14) | 0.0228(5) |
| O(2) | 0.2341(3) | 0.37350(19) | –0.02344(13) | 0.0151(4) |
| O(3) | 0.0897(3) | 0.6226(2) | –0.00020(14) | 0.0179(4) |
| O(4) | 0.4505(3) | 0.6117(2) | 0.04591(14) | 0.0161(4) |
| O(5) | 0.2079(3) | 0.2916(2) | 0.14155(14) | 0.0217(5) |
| O(6) | 0.3057(3) | 0.2146(2) | –0.15896(14) | 0.0238(5) |

Table 5.2. (Continued)

| | | | | |
|---|---|---|---|---|
| O(7) | 0.2550(3) | 0.12991(19) | 0.00243(14) | 0.0159(4) |
| O(8) | 0.4133(3) | –0.1266(2) | 0.00923(15) | 0.0197(5) |
| O(9) | 0.0497(3) | –0.1181(2) | –0.03778(14) | 0.0169(4) |
| O(10) | 0.2573(3) | –0.0631(2) | 0.13155(14) | 0.0250(5) |
| N(1) | 0.4261(4) | –0.2745(3) | –0.23089(18) | 0.0247(6) |
| N(2) | –0.0786(4) | –0.0777(3) | –0.23529(17) | 0.0262(6) |
| C(1) | 0.3742(5) | –0.1340(4) | –0.2612(2) | 0.0323(8) |
| C(2) | 0.1734(5) | –0.1150(4) | –0.2881(2) | 0.0331(8) |
| C(3) | 0.1153(5) | –0.0925(4) | –0.2104(2) | 0.0301(8) |

[a] Estimated standard deviations of the least significant digits are given in parentheses.
[b] Equivalent isotropic atomic displacement parameters for the atoms refined anisotropically. $U_{eq} = 1/3(U_{11} + U_{22} + U_{33})$

## 5.4 Results and Discussion

### Synthesis

In the synthesis of $(H_2dap)^{2+}[(V^{IV}O)_2(V^{V}O_4)_2]^{2-}$ compound the organic amine acts not only as a charge-compensating, space-filling, and structure-directing cations but also as a reducing agent (Law & Williams, 2000), which is responsible for reaction of $V^{5+}$ to $V^{4+}$. The pH of the reaction system was controlled at ~7–8 to obtain the crystalline title product. The EDX spectrum indicates the presence of both vanadium (96%) and cobalt (4%). There is no evidence for cobalt in the structure from the crystal studied, and all the crystals examined can be related to the same morphology as the data crystal. It is possible that there is a minor solid state product that either deposits on the surface of the crystals, or forms as a minor unobserved noncrystalline deposit along with the crystals. A similar crystal structure was

published by Riou and Férey in 1995, and Zhang, Haushalter, and Clearfield in 1996, but their experimental procedures employ different methodologies than used here. However, many variables in the hydrothermal process, such as the type of starting materials, pH, solvent, reaction time, and temperature can affect the reaction system (Whittingham, Guo, Chen, Chirayil, Janauer & Zavalij, 1995).

Table 5.3. Anisotropic Atomic Displacement Parameters[a] in $(H_2dap)^{2+}[(V^{IV}O)_2(V^{V}O_4)_2]^{2-}$ (Å$^2$).

| Atom | $U_{11}$ | $U_{22}$ | $U_{33}$ | $U_{23}$ | $U_{13}$ | $U_{12}$ |
|---|---|---|---|---|---|---|
| V1 | 0.01021(26) | 0.00540(23) | 0.01585(25) | 0.00002(15) | 0.00674(18) | –0.00008(15) |
| V2 | 0.01112(27) | 0.00507(23) | 0.01536(25) | –0.00067(15) | 0.00729(18) | –0.00014(16) |
| V3 | 0.01200(28) | 0.00398(24) | 0.01760(26) | 0.00121(15) | 0.00838(19) | –0.00013(16) |
| V4 | 0.01159(28) | 0.00429(24) | 0.01883(26) | 0.00201(16) | 0.00807(19) | 0.00080(16) |
| O1 | 0.0337(13) | 0.0155(10) | 0.0225(11) | 0.0044(8) | 0.0143(9) | 0.0004(9) |
| O2 | 0.0172(10) | 0.0048(9) | 0.0279(11) | 0.0005(7) | 0.0162(8) | 0.0010(7) |
| O3 | 0.0156(10) | 0.0101(9) | 0.0321(11) | 0.0033(8) | 0.0150(8) | 0.0021(8) |
| O4 | 0.0155(11) | 0.0085(9) | 0.0269(10) | –0.0016(8) | 0.0107(8) | –0.0021(8) |
| O5 | 0.0249(12) | 0.0212(11) | 0.0196(10) | –0.0038(8) | 0.0057(9) | –0.0031(9) |
| O6 | 0.0318(13) | 0.0209(11) | 0.0203(11) | –0.0038(9) | 0.0092(9) | –0.0021(10) |
| O7 | 0.0166(11) | 0.0057(9) | 0.0298(11) | 0.0017(8) | 0.0162(9) | 0.0012(7) |
| O8 | 0.0152(10) | 0.0104(9) | 0.0377(12) | 0.0045(8) | 0.0155(9) | 0.0021(8) |
| O9 | 0.0160(11) | 0.0077(9) | 0.0297(11) | –0.0010(8) | 0.0114(9) | –0.0023(8) |
| O10 | 0.0333(13) | 0.0226(11) | 0.0229(11) | 0.0054(9) | 0.0150(10) | 0.0078(10) |
| C1 | 0.0360(20) | 0.0264(18) | 0.0403(19) | 0.0008(15) | 0.0219(16) | –0.0057(15) |
| C2 | 0.0388(21) | 0.0346(19) | 0.0289(17) | 0.0056(14) | 0.0144(15) | 0.0051(16) |
| C3 | 0.0380(20) | 0.0271(17) | 0.0268(17) | 0.0006(13) | 0.0103(14) | 0.0006(15) |
| N1 | 0.0226(14) | 0.0287(14) | 0.0245(14) | –0.0027(11) | 0.0090(11) | –0.0041(11) |
| N2 | 0.0362(17) | 0.0209(13) | 0.0253(14) | 0.0019(11) | 0.0159(12) | –0.0000(12) |

[a] Estimated standard deviations of the least significant digits are given in parentheses. The form of the anisotropic function is: $U = \exp(-2\pi^2[h^2(a^*)^2U_{11} + k^2(b^*)^2U_{22} + l^2(c^*)^2U_{33} + 2(hka^*b^*U_{12} + hla^*c^*U_{13} + klb^*c^*U_{23})]$

Table 5.4. Selected Bond Lengths (Å) and Angles (°) for $(H_2dap)^{2+}[(V^{IV}O)_2(V^{V}O_4)_2]^{2-}$.

| | $V(1)O_5$ square pyramidal | | | |
|---|---|---|---|---|
| Atoms | Distance | Type of Oxygen | Atoms | Angles |
| V(1)−O(2) | 1.877(2) | $\mu_3$−O | O(2)−V(1)−O(3) | 87.82(9) |
| V(1)−O(3)[a] | 1.980(2) | $\mu_2$−O | O(2)−V(1)−O(5) | 102.11(10) |
| V(1)−O(5) | 1.654(2) | V=O | O(2)−V(1)−O(7) | 81.28(9) |
| V(1)−O(7) | 1.910(2) | $\mu_3$−O | O(2)−V(1)−O(9) | 147.34(9) |
| V(1)−O(9) | 1.930(2) | $\mu_2$−O | O(3)−V(1)−O(5) | 113.89(11) |
| | | | O(3)−V(1)−O(7) | 143.25(9) |
| | | | O(3)−V(1)−O(9) | 85.76(9) |
| | | | O(5)−V(1)−O(7) | 102.71(11) |
| | | | O(5)−V(1)−O(9) | 109.77(10) |
| | | | O(7)−V(1)−O(9) | 84.93(9) |
| | $V(2)O_5$ square pyramidal | | | |
| Atoms | Distance | Type of Oxygen | Atoms | Angles |
| V(2)−O(2) | 1.919(2) | $\mu_3$−O | O(2)−V(2)−O(4) | 84.98(9) |
| V(2)−O(4)[c] | 1.942(2) | $\mu_2$−O | O(2)−V(2)−O(6) | 102.98(11) |
| V(2)−O(6) | 1.683(2) | V=O | O(2)−V(2)−O(7) | 80.88(9) |
| V(2)−O(7) | 1.884(2) | $\mu_3$−O | O(2)−V(2)−O(8) | 143.00(10) |
| V(2)−O(8)[b] | 1.999(2) | $\mu_2$−O | O(4)−V(2)−O(6) | 110.05(11) |
| | | | O(4)−V(2)−O(7) | 146.21(9) |
| | | | O(4)−V(2)−O(8) | 85.66(9) |
| | | | O(6)−V(2)−O(7) | 102.99(11) |
| | | | O(6)−V(2)−O(8) | 113.85(11) |
| | | | O(7)−V(2)−O(8) | 87.45(9) |
| | $V(3)O_4$ tetrahedron | | | |
| Atoms | Distance | Type of Oxygen | Atoms | Angles |
| V(3)−O(1) | 1.610(2) | V−$O^-$ | O(1)−V(3)−O(2) | 108.82(10) |
| V(3)−O(2) | 1.830(2) | $\mu_3$−O | O(1)−V(3)−O(3) | 102.86(12) |
| V(3)−O(3) | 1.636(2) | $\mu_2$−O | O(1)−V(3)−O(4) | 115.32(11) |
| V(3)−O(4) | 1.819(2) | $\mu_2$−O | O(2)−V(3)−O(3) | 107.27(10) |

Table 5.4. (Continued)

| | | | | |
|---|---|---|---|---|
| | | | O(2)−V(3)−O(4) | 111.71(10) |
| | | | O(3)−V(3)−O(4) | 110.24(11) |
| $V(4)O_4$ tetrahedron | | | | |
| Atoms | Distance | Type of Oxygen | Atoms | Angles |
| V(4)−O(7) | 1.822(2) | $\mu_3$−O | O(7)−V(4)−O(8) | 109.94(10) |
| V(4)−O(8) | 1.656(2) | $\mu_2$−O | O(7)−V(4)−O(9) | 109.42(10) |
| V(4)−O(9) | 1.818(2) | $\mu_2$−O | O(7)−V(4)−O(10) | 108.57(11) |
| V(4)−O(10) | 1.603(2) | V−$O^-$ | O(8)−V(4)−O(9) | 110.60(11) |
| | | | O(8)−V(4)−O(10) | 102.46(12) |
| | | | O(9)−V(4)−O(10) | 115.60(12) |
| 1,3-Diaminopropane molecule | | | | |
| Atoms | Distance | | Atoms | Angles |
| C(1)−C(2) | 1.591(5) | | C(1)−C(2)−C(3) | 105.6(3) |
| C(2)−C(3) | 1.396(2) | | N(1)−C(1)−C(2) | 113.4(3) |
| N(1)−C(1) | 1.514(5) | | C(2)−C(3)−N(2) | 106.0(3) |
| N(2)−C(3) | 1.530(5) | | | |

Symmetry transformations used to generate equivalent atoms: (a) –x, y–½, –z+½; (b) –x, –y, –z; (c) x, y–½, z–½.

**Structure description**

The single crystal structure analysis shows the structure to consist of two dimensional metal oxide layers with 1,3-dap molecules separating adjacent layers. A thermal ellipsoid plot of the asymmetric unit of structure of the compound and the coordination environment around the vanadium atoms is shown in Figure 5.1. In the V–O layer, there are four crystallographically independent vanadium sites, V(1), V(2), V(3), and V(4). The bond valence analysis (Brown & Altermatt, 1985) in Table 5.6, shows that the bond valences for $V(1)O_5$ and $V(2)O_5$ in the square pyramidal sites, and $V(3)O_4$ and $V(4)O_4$ in the tetrahedral sites are 4.17, 4.15, 5.14, and 5.11,

respectively, supporting the assignment of square pyramidal $V^{IV}$ vanadyl and tetrahedral $V^{V}$.

Table 5.5. Intermolecular Hydrogen Bonds in $(H_2dap)^{2+}[(V^{IV}O)_2(V^{V}O_4)_2]^{2-}$ (Å, °).

| D−H···A | Type of Oxygen | d[D−H] | d[H···A] | d[D···A] | ∠[D−H··· |
|---|---|---|---|---|---|
| N1–H1a···O1[a] | $V^{V}-O^{-}$ | 0.85 | 1.86 | 2.670 | 158.3 |
| N1–H1b···O5[b] | $V^{IV}=O$ | 0.85 | 2.16 | 2.998 | 168.3 |
| N1–H1b···O6[c] | $V^{IV}=O$ | 0.85 | 2.57 | 2.985 | 111.1 |
| N1–H1c···O10[d] | $V^{V}-O^{-}$ | 0.85 | 2.02 | 2.985 | 161.1 |
| N2–H2c···O1[e] | $V^{V}-O^{-}$ | 0.80 | 2.14 | 2.911 | 160.6 |
| N2–H2d···O10[f] | $V^{V}-O^{-}$ | 0.80 | 2.01 | 2.741 | 151.6 |
| N2–H2d···O9 | $\mu_2-O$ | 0.80 | 2.62 | 3.093 | 120.0 |
| N2–H2e···O6[e] | $V^{IV}=O$ | 0.80 | 2.28 | 3.034 | 156.7 |
| N2–H2e···O5[f] | $V^{IV}=O$ | 0.80 | 2.47 | 2.886 | 113.4 |

Symmetry transformations used to generate equivalent atoms: (a) x, y–1, z; (b) –x+1, –y, –z; (c) –x+1, y–½, –z–½; (d) x, –y–½, z–½; (e) –x, y–½, –z–½; (f) –x, –y, –z

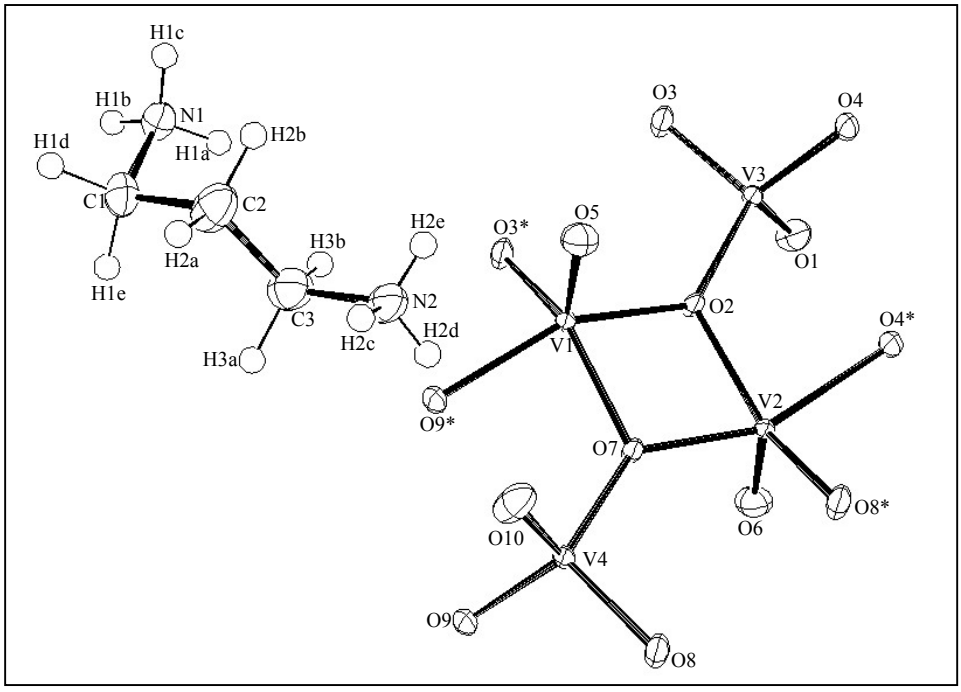


Figure 5.1. ORTEP drawing of $(H_2dap)^{2+}[(V^{IV}O)_2(V^{V}O_4)_2]^{2-}$. V1 and V2 are vanadium(V) while V3 and V4 are vanadium(IV). Thermal ellipsoids are shown at the 50% probability.

In the $\{V^{IV}O_5\}$ square pyramids, the distances of the oxygen atoms in the basal plane from the vanadyl vanadium atom of $\{V^{4.17}(1)O_5\}$ are in the range 1.877(2)–1.980 Å, while the shortest bond distance of 1.654(2) Å formed with the vanadyl oxygen O(5) (V=O), and bond angles from 81.28(9)-147.34(9)°. The $\{V^{4.15}(2)O_5\}$ has its vanadyl oxygen O(6) at a distance of 1.638(2) Å, the V−O bond distances in the basal plane range from 1.884(2)-1.999(2) Å, bond angles from 80.88(9)-146.21(9)°. The $\{V^{V}O_4\}$ is tetrahedrally coordinated with four oxygen atoms, the V−O bond distances are in the range 1.610(2)-1.830(2) Å, and bond angles from 102.86(12)-115.32(11)° correspond to $\{V^{5.14}(3)O_4\}$, while $\{V^{5.12}(4)O_4\}$tetrahedron has bond distance in the range 1.603(2)-1.822(2) Å, and bond angle in the range 102.46(12)-115.60(12)°.

Table 5.6. Bond Valence[a] Sums for $(H_2dap)^{2+}[(V^{IV}O)_2(V^{V}O_4)_2]^{2-}$.

| Atom | Type of Oxygen | V1 | V2 | V3 | V4 |
|---|---|---|---|---|---|
| O1 | $V^{V}–O^{-}$ | − | − | 1.685 | − |
| O2 | $\mu_3$–O | 0.778 | 0.694 | 0.930 | − |
| O3 | $\mu_2$–O | 0.589 | − | 1.570 | − |
| O4 | $\mu_2$–O | − | 0.652 | 0.958 | − |
| O5 | $V^{IV}$=O | 1.421 | − | − | − |
| O6 | $V^{IV}$=O | − | 1.484 | − | − |
| O7 | $\mu_3$–O | 0.711 | 0.763 | − | 0.902 |
| O8 | $\mu_2$–O | − | 0.559 | − | 1.413 |
| O9 | $\mu_2$–O | 0.674 | − | − | 0.912 |
| O10 | $V^{V}–O^{-}$ | − | − | − | 1.631 |
| Σ | | 4.173 | 4.152 | 5.143 | 5.115 |

[a] The results refer to the equation S = exp((Ro−R)/B).

As shown in Figure 5.2, the structure of $(H_2dap)^{2+}[(V^{IV}O)_2(V^{V}O_4)_2]^{2-}$ compound, which shows four-membered-ring and eight-membered-ring channels connected by $\{VO_4\}$ tetrahedra and $\{VO_5\}$ square pyramids. The layers are constructed from an equal number of $\{VO_4\}$ tetrahedra each containing one vanadyl oxygen atom, and $\{VO_5\}$ square pyramids with vanadyl oxygen atoms in the apical positions as illustrated in Figure 5.3. Each oxygen atom shared between the two square pyramids is also shared with one $\{VO_4\}$ tetrahedra ($\mu_3$−O). The remaining four

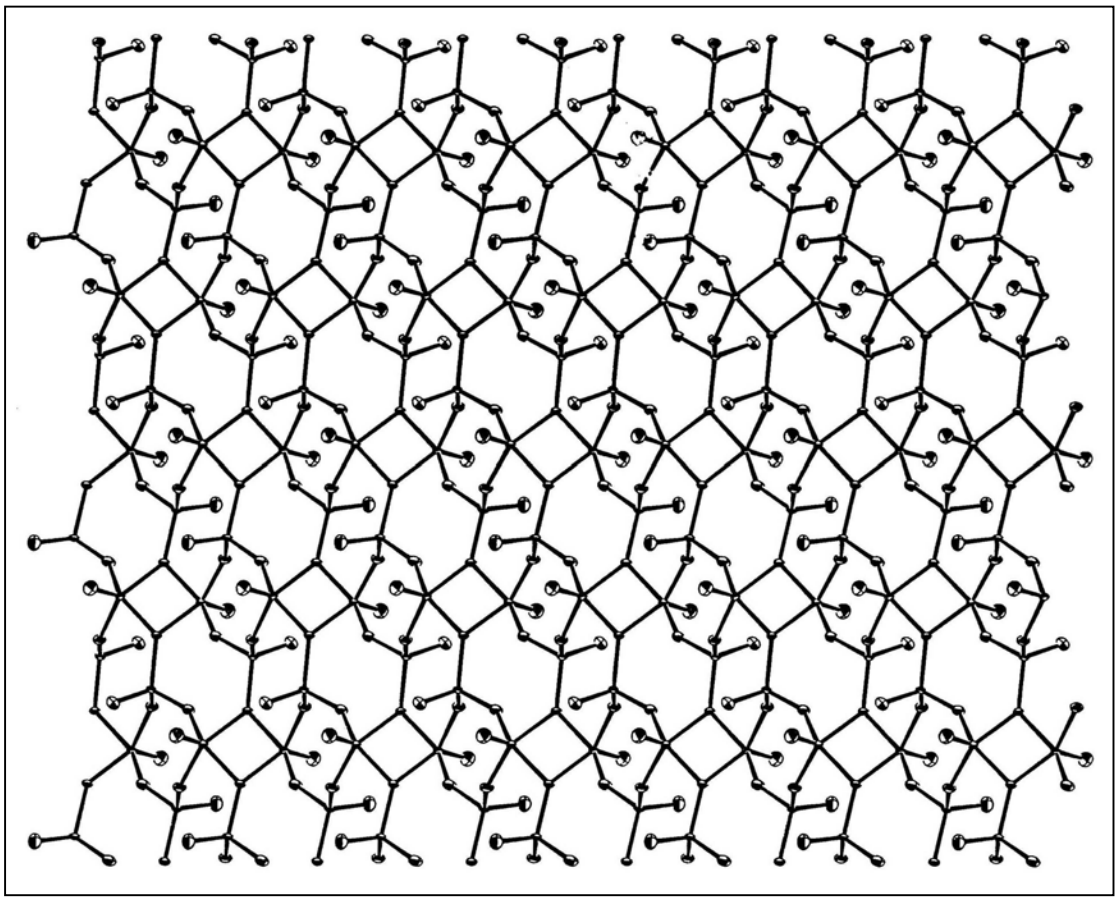

Figure 5.2. View of ball and stick model of the building unit with $\{V_4O_{10}\}^{2-}$.

oxygen atoms of the basal planes are also shared with {$VO_4$} tetrahedra ($\mu_2$−O). It can be seen that the nonbridging apical positions (the vanadyl groups) of both the tetrahedra and square pyramids alternate above and below the plane as one moves across the layer. In each pair of edge-sharing pyramids the two terminal oxygen atoms are oriented toward opposite sides of the plane of the layers. Two square pyramids share an edge in such a way that in one pyramid the two different positions are labeled "up" and "down", for the pyramids and the tetrahedra. The last vertex of each tetrahedron protrudes into the two–dimensional inorganic network where it participates in hydrogen bonding holding the layers together. The arrangement of tetrahedra along the rows of tetrahedra is alternating in antiparallel directions, up/down/up/down…. In rows of the pyramidal units the arrangement of the pyramids is alternatively up/down/up/down…. The resulting network is illustrated as a polyhedral representation in Figure 5.4. The polyhedra in the present compound are closely related to those found in the structure of $Cd[C_3N_2H_{11}]_2[V_8O_{20}]$ (Zhang, Shi, Yang, Chen & Feng, 2000) but the relative orientations of polyhedra are quite different.

A view of the two-dimensional character of the layers of vanadium oxide and the organic amine cations, ($NH_3^+CH_2CH_2CH_2NH_3^+$) located in the interlayer regions are indicated in Figure 5.5. Vanadyl groups are good hydrogen bond acceptors, so it is not surprising to find extensive hydrogen bonding between the N−H groups from the organic template cation, ($-NH_3^+$) and the oxygen atoms from the inorganic anion chains such that all six hydrogen bond donors are utilized. Three of the hydrogen bonds involve two oxygen atoms (bifurcated hydrogen bonds) and three involve single oxygen atoms. The N−H···O interatomic distances for the hydrogen bonds are

in the range 2.670-3.093 Å (Table 5.4). The hydrogen bond interactions are illustrated in Figure 5.6.

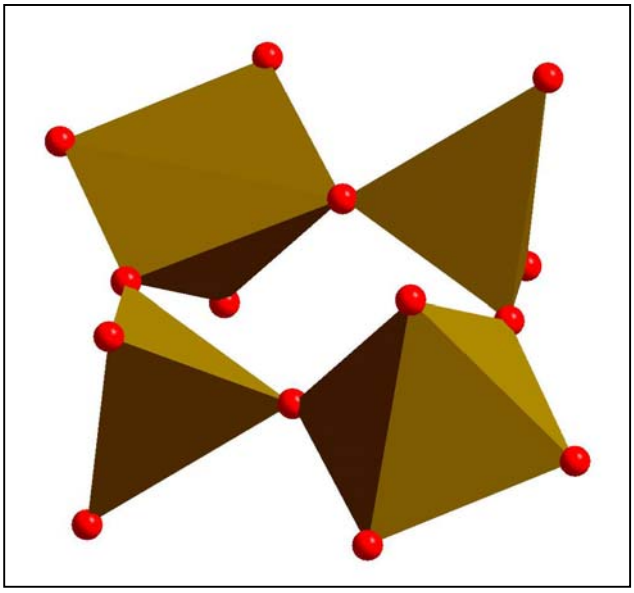

Figure 5.3. A polyhedral representation of one unit of the tetravanadate network.

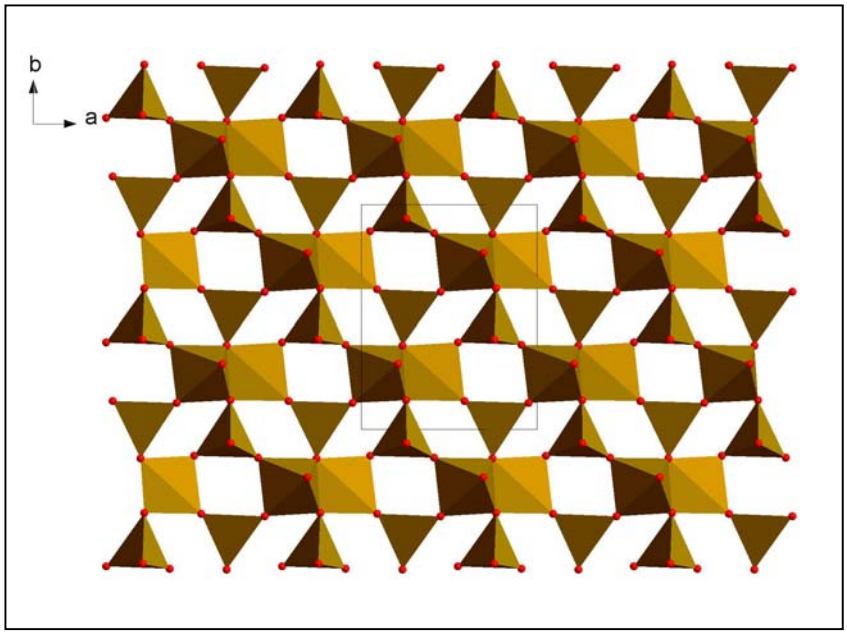


Figure 5.4. The 2-D single layer structure of $\{V_4O_{10}\}^{2-}$.

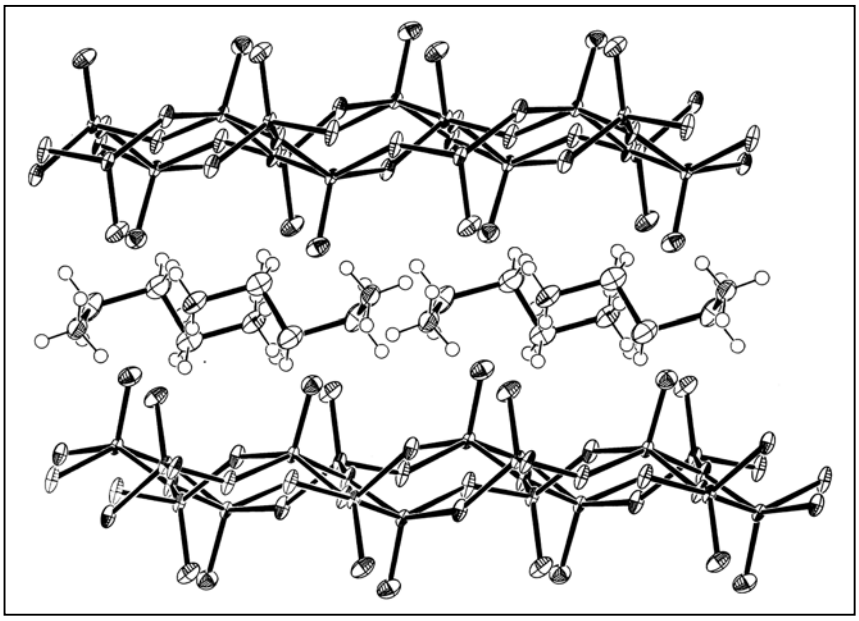

Figure 5.5. View along the *b* axis of the alternating layers of anionic vanadium oxide and organic amine cations in the interlayer spaces.

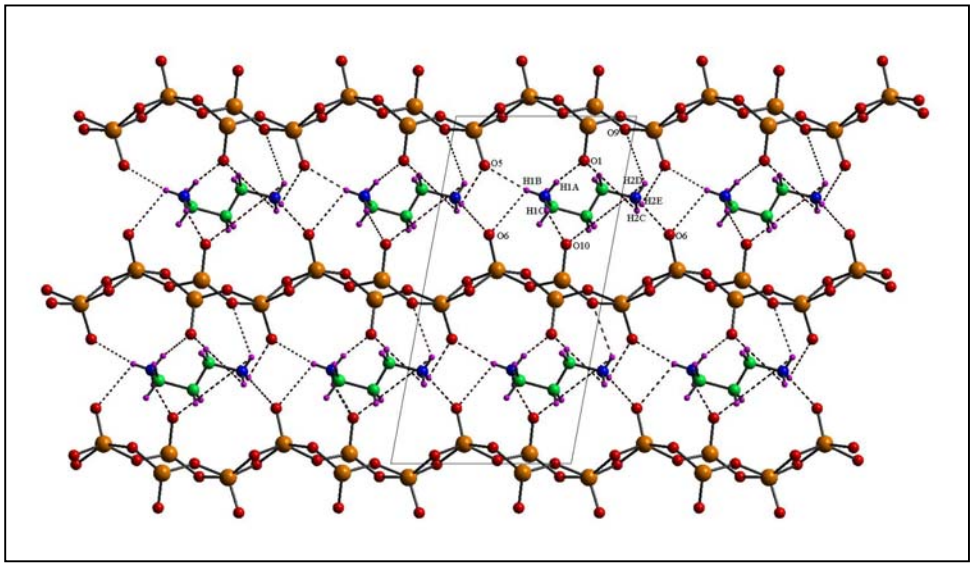


Figure 5.6. Edge view of the layers of $(H_2dap)^{2+}[(V^{IV}O)_2(V^{V}O_4)_2]^{2-}$. The hydrogen bonding interactions between protonated amines and the inorganic framework are indicated as dashed lines.

## 5.5 Further Physical Characterization

### SEM-EDX analysis

The crystal morphology is shown in Figure 5.7, and the EDX spectrum, showing the dominant presence of vanadium (96%) as the heavy element in the compound plus a possible minor cobalt (4%) component is shown in Figure 5.8.

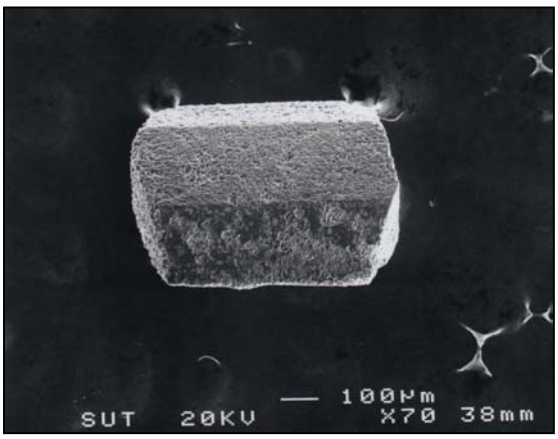


Figure 5.7. SEM picture of $(H_2dap)^{2+}[(V^{IV}O)_2(V^{V}O_4)_2]^{2-}$.

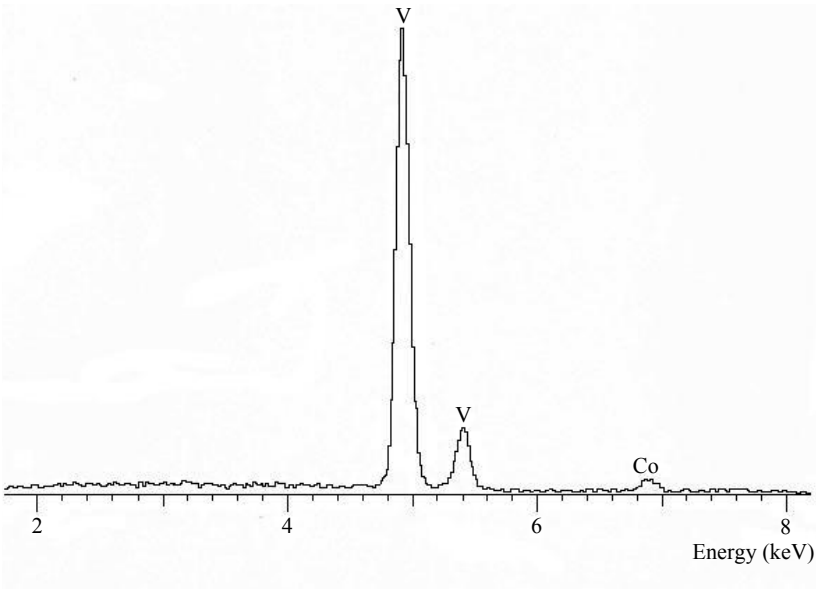


Figure 5.8. EDX spectrum of $(H_2dap)^{2+}[(V^{IV}O)_2(V^{V}O_4)_2]^{2-}$.

**FTIR**

The IR spectrum of $(H_2dap)^{2+}[(V^{IV}O)_2(V^{V}O_4)_2]^{2-}$ is shown in Figure 5.9. The strong band at 971 $cm^{-1}$ is assigned to terminal V=O stretching and bands at 830, 631 and 560 $cm^{-1}$ are consistent with symmetrical and asymmetrical V–O–V stretching. Bands at 1599, 1488, and 1187 $cm^{-1}$ are characteristic of 1,3-dap, and bands in the 3009 and 3450 $cm^{-1}$ region can be attributed to N−H stretching and water, respectively.

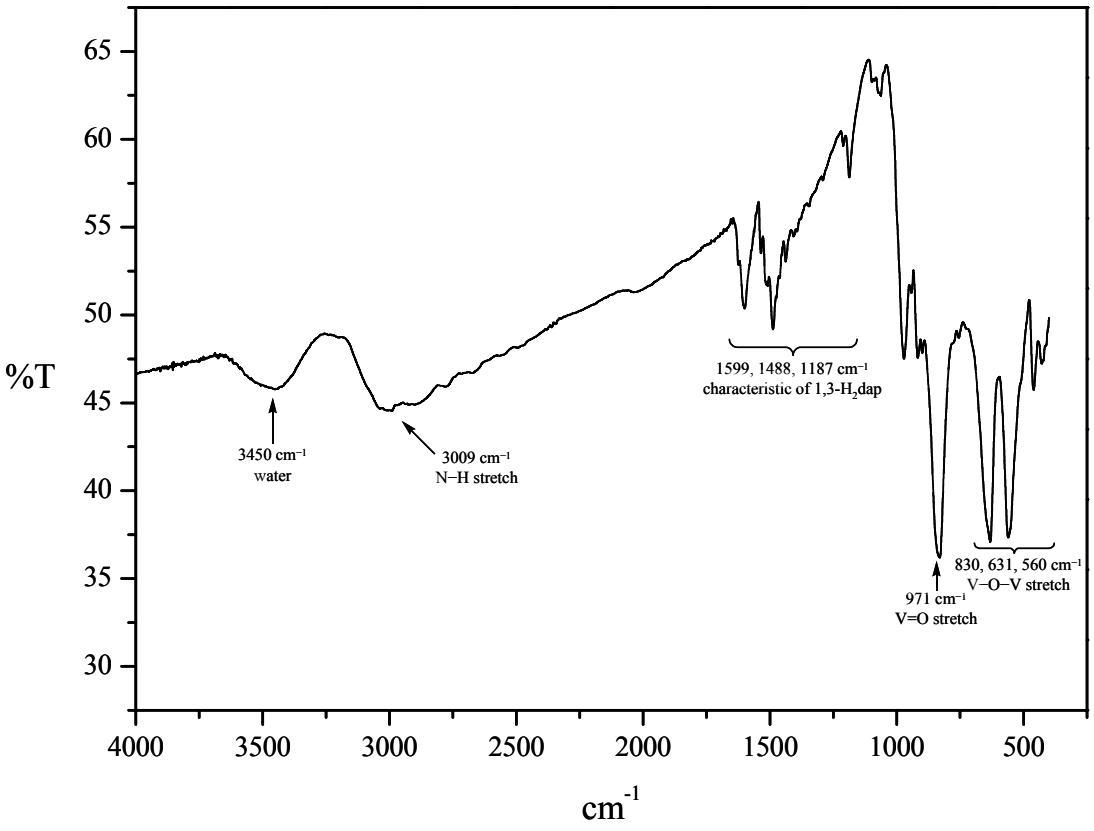


Figure 5.9. FTIR spectrum of $(H_2dap)^{2+}[(V^{IV}O)_2(V^{V}O_4)_2]^{2-}$.

**Thermal analysis**

Thermal gravimetric analysis under air, illustrated in Figure 5.10, shows a weight loss of 18% from 270-325 °C corresponding to loss of the 1,3-dap follows with weight loss of 17.5% from 330-560 °C assigned to loss of the VO. The 1% weight increase from 625-680 °C corresponds to the oxidation of $[(V^{IV}O)_2(V^{V}O_4)_2]^{2-}$ framework from $V^{IV}$ to $V^{V}$ as previously observed in $[Cd(C_3H_{11}N_2)_2V_8O_{20}]$ (Zhang, Shi, Yang, Chen & Feng, 2000), and $[Cu(phen)V_4O_{10}]$ (Cui, Lin & Yang, 2003). Potential decomposition products are listed in Table 5.7, along with their masses and relative percentages of the compound.

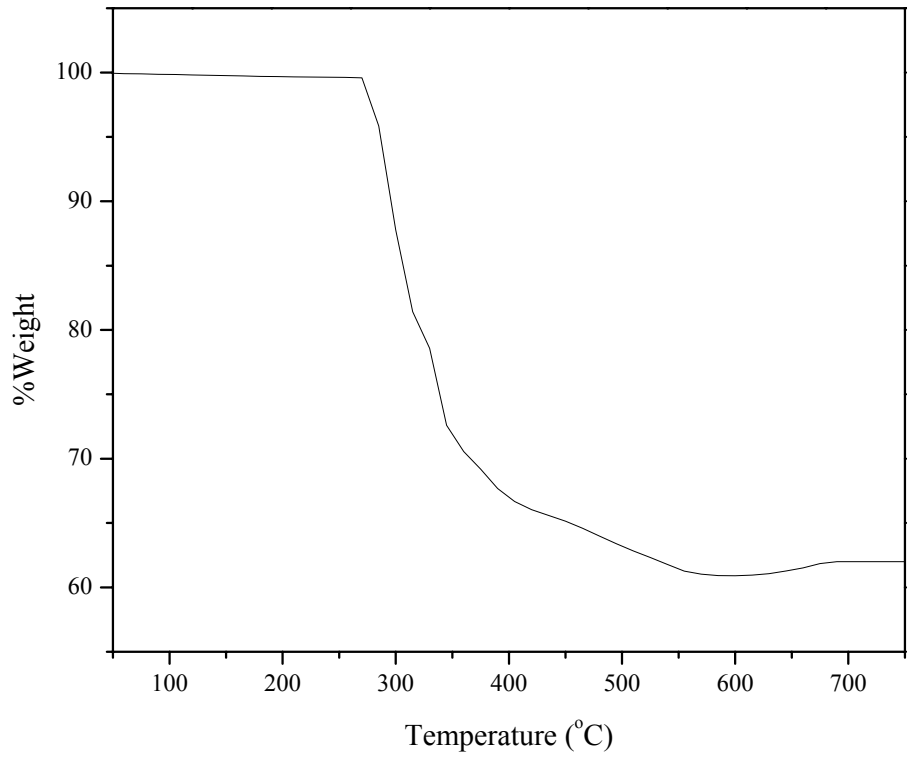


Figure 5.10. TGA curve of $(H_2dap)^{2+}[(V^{IV}O)_2(V^{V}O_4)_2]^{2-}$.

Table 5.7. Potential Decomposition Products of $(H_2dap)^{2+}[(V^{IV}O)_2(V^{V}O_4)_2]^{2-}$.

| Fragment | | MW, Daltons | Weight % of the Compound |
|---|---|---|---|
| $H_3N(CH_2)_3NH_3$ | | 78.16 | 17.78 |
| VO | | 66.94 | 15.22 |
| Add one O atom | | 16.00 | 3.64 |
| TGA Waves | Weight Loss, % | Assignment | Relative % Error |
| 270-570 °C | 18 | $H_3N(CH_2)_3NH_3$ | +2.2 |
| 330-560 °C | 17.5 | VO framework | +23.2 |
| 625-680 °C | 1 | $V^{IV} \rightarrow V^{V}$ | +26.4 |

# Chapter VI

# Conclusions

## 6.1 Conclusions

Hydrothermal synthesis provides a convenient tool for the preparation of coordination complexes and organic-inorganic hybrid materials. This method has been exploited in the synthesis and hydrothermal crystallization of the monohydrate of Co(picoline)$_3$ and $(dapH_2)^{2+}[(V^{IV}O)_2(V^{V}O_4)_2]^{2-}$.

[Co(picoline)$_3$]·$H_2O$ was obtained as the major crystalline product from an attempted synthesis of a cobalt/vanadium framework with 2,5-pyridinedicarboxylic acid linking ligands, and 1,3-diaminopropane template molecules. The structure has distorted octahedral coordination geometry with three *mer* pyridyl nitrogen atoms and three *mer* carboxylate oxygen atoms. The water molecule is not coordinated to the [Co(picoline)$_3$] complex, but is part of the extensive supramolecular interactions, which include π−π stacking, O−H···O, C−H···O, and C−H···π hydrogen bonding interactions, and $C(\delta^+)\cdots O(\delta^-)$ carbonyl-carbonyl dipole-dipole interactions.

The supramolecular architecture is analyzed to be formed from π–π stacked, columns of the complex stacked along the *c* direction, with aryl-aryl offset face-to-face interactions at distances of 3.465(3) Å between 2-fold related aryl rings from adjacent molecules, and aryl-aryl offset face-to-face interactions between adjacent inversion related aryl rings with perpendicular distances of 3.420(3) Å. Other supramolecular interactions can be found; water molecules bridge adjacent π−π stacks with strong intermolecular O−H···O hydrogen bonds to a carboxylate oxygen

atom of one molecule and a carbonyl oxygen atom of another molecule, with O···O distances of 2.847(3) and 2.853(3) Å, respectively. Moreover, there is extensive weak C−H···O hydrogen bonding with the aryl rings acting as hydrogen bond donors and ligand oxygen atoms as acceptors, with C···O distances in the range 3.121(3)-3.436(3) Å, and C−H···π edge-to-face type hydrogen bonding interactions from hydrogen atoms, H3, of the stacked pyridyl rings, pointing towards the faces of other pyridyl rings arranged about the stacked columns at a perpendicular distance of 2.791(2) Å. In addition, weak $C(\delta^+)\cdots O(\delta^-)$ antiparallel carbonyl-carbonyl interactions are also present, with the carbonyl oxygen atom O2 interacting with the inversion related carbonyl carbon atom, C6 (–x, –y, 1–z), at a contact distance of 3.391(2) Å, and with C−O···C and O···C−O angles of 100.12(4)° and 79.88(4)°, respectively.

Further physical characterization techniques have been used to support the crystallographic method. SEM-EDX analysis of the red-violet plate crystals indicates only cobalt. The FTIR spectrum has two O−H stretching bands in the water region at 3454 and 3520 $cm^{-1}$, due to the different character of the two O−H···O interactions to water. The strong band at 1681 $cm^{-1}$ is assigned to carbonyl, and the bands from the 392-462 $cm^{-1}$ range are tentatively assigned to *ν*(Co−O) or *ν*(Co−N) stretching. The TGA curve shows loss of water at 60-156 °C (4.6% loss) followed by broad overlapping steps from 275-412 °C corresponding to 79.8% weight loss as the ligands decompose.

The $(dapH_2)^{2+}[(V^{IV}O)_2(V^{V}O_4)_2]^{2-}$ organic-inorganic hybrid material has also been prepared by hydrothermal crystallization from vanadium(V) oxide, and 1,3-diaminopropane in the presence of cobalt(II) chloride hexahydrate, hydrochloric acid, and water in the molar ratio 1:2:1:1:593. The structure consists of two-

dimensional mixed valence vanadium ($V^{IV}$ and $V^{V}$) oxide layers with $(dapH_2)^{2+}$ dications separating adjacent layers. Vanadium(V) vanadyl groups and vanadium(IV) bound oxide oxygen atoms, which are good hydrogen bond acceptors, protrude from the inorganic vanadium oxide layers into the organic dication layers, and engage in extensive hydrogen bonding with the $-NH_3^+$ groups in the organic layer. All six hydrogen bond donors are utilized, as are all of the vanadyl and oxide oxygen acceptor atoms, leading to nine hydrogen bonds per dication with N−H···O interatomic distances in the range 2.670-3.093 Å. Three of the hydrogen bonds are bifurcated and three involve single oxygen acceptors.

The EDX spectrum indicates the presence of a minor cobalt component (4%), but there is no cobalt in the structure from the crystal studied, and all the crystals examined can be related to the same morphology as the data crystal. The vanadium signal is attributed to the small amount of powder material with the crystals that did not wash away with water. The FTIR spectrum shows bands in the 3009 and 3450 $cm^{-1}$ region which are attributed to N–H stretching and absorbed water, respectively. Bands at 1599, 1488, and 1187 $cm^{-1}$ are characteristic of $(dapH_2)^{2+}$. The strong band at 971 $cm^{-1}$ is assigned to terminal V=O stretching and bands at 830, 631, and 560 $cm^{-1}$ are consistent with symmetrical and asymmetrical V–O–V stretching. TGA shows a weight loss of 39% from 270-570 °C corresponding to loss of the $(dapH_2)^{2+}$ and weight gain from 630-680 °C due to the oxidation of $V^{IV}$ to $V^{V}$.

## 6.2 Suggestions for Future Work

Although the KBr was oven dried and stored in a dessicator, preparation of samples for FTIR spectroscopy was carried out without precautions to exclude water

absorption on the KBr pellet, probably leading to the unexpected result in chapter V, a broad absorption band in the high frequency region at 3450 $cm^{-1}$ attributed to O–H stretching of water. The FTIR analysis does not correspond to the single crystal X-ray result which does not show coordinated water and/or water of solvation in the crystal structure of $(dapH_2)^{2+}[(V^{IV}O)_2(V^{V}O_4)_2]^{2-}$. It is possible that the broad band at 3450 $cm^{-1}$ is from moisture in the air that was absorbed onto the KBr pellet during preparation, or after preparation prior to placing the pellet in the IR spectrometer. In order to prevent water absorption on the KBr all operations must be carried out under controlled atmosphere conditions. This can be accomplished by grinding the KBr and sample in a glove bag, and by using an inert gas blanket or purge for all other steps. The spectrometer should have an inert gas purge so once the sample is in the spectrometer it is protected.

Thermal analysis results are affected by many experimental factors, including heating rate, mass and particle size of sample, atmosphere, buoyancy, convection currents and turbulence, sample container, temperature gradient and reaction extent in various parts of sample vessel, and packing density of sample (Hatakeyama & Liu, 1998). To obtain reliable results all of these factors must be considered. For example, when the heating rate is controlled dynamically and continuously in response to the reaction of the sample, sharper resolution can be observed. Using a lower heating rate can give better resolution of the TG curve than a higher heating rate, as reported in the dehydration of the inorganic salt, $MgSO_4 \cdot 7H_2O$ (Ramalingom, Podder & Kalkura, 2001). The TG curve of $[Co(picoline)_3] \cdot H_2O$ (5 °C/min, chapter IV) shows poor resolution. The decomposition analysis might be easier if a slower heating rate (1-3 °C/min), is used to obtain resolution of the overlapping waves. Moreover, mass and

particle size of the sample are also important factors because these properties affect heat flow. In addition, data resolution can be improved by using smaller samples, increasing specific surface area (grinding), and using a helium purge to improve heat transfer properties (Chung, Wu & Malawer, 1998). Too much grinding, on the other hand, may lead to loss of solvent molecules or other weakly held molecular species.

Design, synthesis, and characterization of organic-inorganic hybrid materials utilizing principles of supramolecular chemistry is still interesting. As already mentioned, there are many variables in the hydrothermal process, such as the type of starting materials, pH, solvent, reaction time, and temperature which can affect the reaction system. The role of the templating organic ions can also be extremely important (Law, Sung & Williams, 2000). There have been suggestions with regard to the role of the templating organic in the formation of various structures, with the pH of the medium and the $pK_a$ of the templating organic as important parameters (Davis & Lobo, 1992, Oliver, Kuperman & Ozin, 1998).

Finally, the key element in understanding of crystal packing into supramolecular interactions that determine the manner in which the contents of unit cells interact with the contents of other unit cells is the energy of the interactions. Single crystal X-ray crystallographic analysis and calculation of the energy of interactions are thus complimentary. Electronic theory such as density functional theory (DFT) would be most useful in the study of the nature of the interactions within complex molecular assemblies.

# References

# References

Alda, E., Bazán, B., Mesa, J. L., Pizarro, J. L., Arriortua, M. I. and Rojo, T. (2003). A new vanadium(III) fluorophosphate with ferromagnetic interactions, $(NH_4)[V(PO_4)F]$. **J. Solid State Chem.** 173(1): 101-108.

Allen, F. H., Baalham, C. A., Lommerse, P. M. J. and Raithby, P. R. (1998). Carbonyl-Carbonyl Interactions can be Competitive with Hydrogen Bonds. **Acta Cryst.** B54: 320-329.

Altomare, A., Burla, M. C., Camalli, M., Cascarano, G. L., Giacovazzo, C. Guagliardi, A. Moliterni, A. G. G., Polidori, G. and Spagna, R. (1999). *SIR*97: A new tool for crystal structure determination and refinement. **J. Appl. Cryst.** 32: 115-119.

Arora, K. K. and Pedireddi, V. R. (2004). Host-guest complexes of 3,5-dinitrobenzo-nitrile: channels and sandwich supramolecular architectures. **Tetrahedron.** 60(4): 919-925.

Benavente, E., Santa Ana, M. A., Mendizábal, F. and GonzHosseini, M. W. (2003). Molecular tectonics: from molecular recognition of anions to molecular networks. **Coord. Chem. Rev.** 240(1-2): 157-166.

Bernstein, J., Etter, M. C. and Leiserowitz, L. (1994). **The Role of Hydrogen Bonding in Molecular Assemblies: Structure Correlation.** Volume 2, Bürgi, H.-B., Dunitz, J. D., Eds., Weinheim, New York, pages 431-500.

Bondi, A. (1964). van der Waals volumes and radii. **J. Phy. Chem.** 68(3): 441-451.

Botella, P., López Nieto, J. M., Solsona, B., Mifsud, A. and Márquez, F. (2002). The Preparation, Characterization, and Catalytic Behavior of MoVTeNbO Catalysts Prepared by Hydrothermal Synthesis. **J. Catal.** 209(2): 445-455.

Braga, D. and Grepioni, F. (2001). Intermolecular interactions in nonorganic crystal engineering. **Acc. Chem. Res.** 33(9): 601-608.

Braga, D., Grepioni, F., Sabatino, P. and Desiraju, G. (1994). Hydrogen bonding in organometallic crystals. 1. From carboxylic acids and alcohols to carbonyl complexes. **Organometallics.** 13(9): 3532-3543.

Braga, D., Grepioni, F. and Desiraju, G. (1998). Crystal engineering and organometal lic architecture. **Chem. Rev.** 98(4): 1375-1405.

Brandenburg, K. (2001). **DIAMOND.** Version 2.1e, Crystal Impact GbR, Bonn, Germany.

Brown, I. D. and Altermatt, D. (1985). Bond-valence parameters obtained from a systematic analysis of the Inorganic Crystal Structure Database. **Acta Cryst.** B41: 244-247.

Bugnet, E. A., Nixon, T. D., Kilner, C. A., Greatrex, R. and Kee. T. P. (2003). Regioselective supramolecular catalysis. Exploiting multiple binding motifs in propanediurea molecular clips. **Tetrahedron Lett.** 44(29): 5491-5494.

Burnett, M. N. and Johnson, C. K. (1996). **ORTEP-III.** Report ORNL-6895, Oak Ridge National Laboratory, Tennessee, USA.

Byrappa, K. and Gopalakrishna, G. S. (1985). A critical survey on the study of alkaline rare earth phosphate and nasicon systems with a special reference to the hydrothermal method. **Prog. Crystal Growth and Charac.** 11(2): 89-107.

Centi, G. and Trifir, F. (1996). Catalytic behavior of V-containing zeolites in the transformation of propane in the presence of oxygen. **Appl. Catal.** A143(1): 3-16.

Chainok, K., Haller, K. J. and Williams, I. D. (2002). Crystal Structure of the Missing [$Cu_2$(terephthalate)$_4$] "Paddle-Wheel" Coordination Polymer. **The 28th Congress on Science and Technology of Thailand**. 24-26 October 2002, Queen Sirikit National Convention Center, Bangkok, Thailand.

Chen, C. (1998). Phase diagram and its application to the crystal growth of high TC oxide superconductors. **Prog. Crystal Growth and Charac.** 36(1-2): 1-97.

Chirayil, T. G., Boylan, E. A., Mamak, M., Zavalij, P. V. and Whittingham, M. S. (1997). $NMe_4V_3O_7$: critical role of pH in hydrothermal synthesis of vanadium oxides. **J. Chem. Soc., Chem. Comm.** (1): 33-34.

Chirayil, T., Zavalij, P. Y. and Whittingham, M. S. (1998). Hydrotermal synthesis of vanadium oxides. **Chem. Mater.** 10(10): 2629-2640.

Chui, S. S.-Y., Lo, S. M.-F., Chrmant, J. P. H., Orpen, A. G. and Williams, I. D. (1999). A chemically functionalizable nanoporous material [$Cu_3$(TMA)$_2$ ($H_2O$)$_3$]$_n$, **Science.** 283: 1148-1150.

Chung, K. H., Wu, C. S. and Malawer, E. G. (1989). Thermomagnetometry and thermogravimetric analysis of carbonyl iron powder. **Thermochim. Acta.** 154(2): 195-204.

Cotton, F. A., Lin, C. and Murillo, C. A. (2001). Supramolecular arrays based on dimetal building units. **Acc. Chem. Res.** 43(10): 759-771.

Császár, A. G. and Mills, I. M. (1997). Vibrational energy levels of water. **Spectrochim. Acta.** A53(8): 1101-1122.

Cui, X.- B., Lin, Z.-E. and Yang, G.-Y. (2003). A novel interpenetrating 2-D brush-like structure: hydrothermal synthesis and crystal structure of [Cu(phen)$V_4O_{10}$] (phen=1,10-phenanthroline). **Solid State Sci.** 5(2): 311-315.

Dance, I. and Scudder, M. (1995). The sextuple phenyl embrace, a ubiquitous concerted supramolecular motif. **J. Chem. Soc., Chem. Comm.** (10): 1039-1040.

Dance, I. and Scudder, M. (1996a). Concerted supramolecular motifs: linear columns and zigzag chains of multiple phenyl embraces involving $Ph_4P^+$ cations in crystals. **J. Chem. Soc., Dalton Trans.** (19): 3755-3769.

Dance, I. and Scudder, M. (1996b). Supramolecular motifs: concerted multiple phenyl embraces between $Ph_4P^+$ cations are attractive and ubiquitous. **Chem. Eur. J.** 2(5): 481-486.

Dance, I. and Scudder, M. (1998). Supramolecular motifs: Sextuple aryl embraces in crystalline [M(2,2´-bipy)$_3$] and related complexes. **J. Chem. Soc., Dalton Trans.** (8): 1341-1350.

Dann, S. E. (2000). **Reactions and Characterization of Solids.** Cambridge, UK, pages 91-94.

Demianets, L. N. (1991). Hydrothermal synthesis of new compounds. **Prog. Crystal Growth and Charac.** 21(1-4): 299-355.

Desiraju, G. R. (2002). Hydrogen bridges in crystal engineering: interactions without borders. **Acc. Chem. Res.** 35(7): 565-573.

Desiraju, G. R. (2003). Crystal engineering. From molecules to materials. **J. Mol. Struc.** 656(1-3): 5-15.

Davis, M. E. and Lobo, R. F. (1992). Zeolite and molecular sieve synthesis. **Chem. Mater.** 4(4): 756-768.

Dickert, F. L. and Sikorski, R. (1999). Supramolecular strategies in chemical sensing. **Mater. Sci. Eng.** C10(1-2): 39-46.

Dinolfo, P. H. and Hupp, J. T. (2001). Supramolecular coordination chemistry and functional microporous molecular materials. **Chem. Mater.** 13(10): 3113-3125.

Douglas, B., McDaniel, D. and Alexander, J. (1994). **Concepts and Models of Inorganic Chemistry.** 3rd edition, Wiley, New York, pages 9-13.

Duisenberg, A. J. M., Kroon-Batenburg, L. M. J. and Schreurs, A. M. M. (2003). An intensity evaluation method: EVAL-14. **J. Appl. Cryst.** 36: 220-229.

El-Sonbati, A. Z., El-Bindary, A. A. and Diab, M. A. (2003). Polymer complexes: Supramolecular assembly on coordination models of mixed-valence-ligand poly[1-acrylamido-2-(2-pyridyl)ethane] complexes. **Spectrochim. Acta.** A58(3): 443-454.

Enoki, T. (2004). Intercalation and guest-host interaction in nano-graphite. **J. Phys. Chem. Solids.** 65(2-3): 103-108.

Erxleben, A. (2003). Structures and properties of Zn(II) coordination polymers. **Coord. Chem. Rev.** 246(1-2): 203-228.

Farrugia, L. J. (1997). ORTEP-3 for Windows - a version of ORTEP-III with a Graphical User Interface (GUI). **J. Appl. Cryst.** 30: 565.

Feng, S. and Xu, R. (2001). New materials in hydrothermal synthesis. **Acc. Chem. Res.** 34(3): 239-247.

Férey, G. (1998). The new microporous compounds and their design. **Solid State Chemistry and Crystal Chemistry.** 1-13.

Ferrer, M., Rodriguez, L. and Rossell, O. (2003). Study of the self-assembly reactions between the organic linker 1,4-bis(4-pyridyl)butadiyne and the metal-containing corners (diphosphine)M(II) (M = Pd, Pt; diphosphime = dppp, dppf, depe, dppbz). **J. Organomet. Chem.** 681(1-2): 158-166.

Giacovazzo, C., Monaco, M. L., Artioli, G., Viterbo, D., Ferraris, G., Gilli, G., Zanotti, G. and Catti, M. (2002). **Fundamentals of Crystallography.** 2nd edition, Oxford, New York.

Godzisz, D., Ilczyszyn, M. M. and M. Ilczyszyn. (2002). Classification and nature of hydrogen bonds to betaine. X-ray, $^{13}C$ CP MAS and IR description of low barrier hydrogen bonds**. J. Mol. Struc.** 606(1-3): 123-137.

Goher, M. A. S., Abu-Youssef, M. A. M. and Mautner, F. A. (1996). Synthesis, spectra and structural characterization of a monomeric chloro complex of zinc(II) with picoline acid, $[Zn(C_5H_4NCO_2H)(C_5H_4NCO_2)Cl]$. **Polyhedron.** 15(3): 453-457.

Gopalakrishnan, J. (1995). Chimie douce approaches to the synthesis of metastable oxide materials. **Chem. Mater.** 7(7): 1265-1275.

Grabowski, S. J. (2001). A new measure of hydrogen bonding strength – *ab initio* and atoms in molecules studies. **Chem. Phys. Lett.** 338(4-6): 361-366.

Gu, W., Bian, H.-D., Xu, J.-Y., Yan, S.-P., Liao, D.-Z. and Jiang, Z.-H. (2003). Hydrothermal synthesis, structure, spectroscopic and magnetic properties of a hexanuclear cluster: $[\{Mn(2,2'\text{-bipy})_2\}_2V_4O_{12}]$. **Inorg. Chem. Commun.** 6(2): 217-220.

Islam, M. S. and Uddin, M. M. (1993). Preparation and characterization of some complexes of chromium(III), cobalt(III) and rhodium(III) ions containing 1,4,8,12-tetra-azacyclopentadecane. **Polyhedron.** 12(4): 423-426.

Hagrman, P. J., Finn, R. C. and Zubieta, J. (2001). Molecular manipulation of solid state structure: Influences of organic components on vanadium oxide architectures **Solid State Sci.** 3(7): 74-774.

Haitao, X., Nengwu, Z., Hanhuia, X., Yonggang, W., Ruyi, Y., Enyi, Y. and Xianglin, J. (2002). **J. Mol. Struc.** 610(1-3): 47-52.

Hellman, S., (1996). Röentgen centennial lecture: Discovering the past, inventing the future. **Int. J. Radiation Oncology Biol. Phys.** 35(1): 15-20.

Horn, C., Scudder, M. L. and Dance, I. (2001). Contrasting crystal supramolecularity for $[Fe(phen)_3]_{18}$ and $[Mn(phen)_3]_{18}$: Complementary orthogonality and comple-menttary helicity. **Cryst. Eng. Comm.** (1): 1-8.

Hosseini, M. W. (2003). Molecular tectonics: from molecular recognition of anions to molecular networks. **Coord. Chem. Rev.** 240(1-2): 157-166.

Hou, Y., Shen, E., Wang, S., Wang, E., Xiao, D., Li, Y., Xu, L and Hu, C. (2003). Hydrothermal synthesis and crystal structure of a metal-organic coordination polymer with double-helical structure: $[Fe(phen)(ipt)]_n$, (ipt = isophthalate, phen = 1,10-phenanthroline). **Inorg. Chem. Commun.** 6(10): 1347-1349.

Huang, J. R., Xiong, Z. X., Fang, C. and Feng, B. L. (2003). Hydrothermal synthesis of $Ba_2Ti_9O_{20}$ nano-powder for microwave ceramics. **Mater. Sci. Eng.** B99 (1-3): 226-229.

Hunter, C. A., Lawson, K. V.,Perkins, J. and Urch, C. J. (2001). Aromatic interactions. **J. Chem. Soc., Perkin Trans.** 2(5): 651-669.

Hunter, C. A. and Sanders, J. K. M. (1990). The nature of π–π interactions. **J. Am. Chem. Soc.** 112(14): 5525-5534.

Huyskens, P., Sobczyk, L. and Majerz, I. (2002). On a hard/soft hydrogen bond interaction. **J. Mol. Struc.** 615(1-3): 61-72.

Janiak, C. (2000). A critical account on π–π stacking in metal complexes with aromatic nitrogen-containing ligands. **J. Chem. Soc., Dalton Trans.** (21): 3885-3896.

Kaya, C., Hea, J. Y., Gub, X. and Butlera, E. G. (2002). Nanostructured ceramic powders by hydrothermal synthesis and their applications **Micropor. Mesopor. Mater.** 54(1-2): 37-49.

Kollman, P. A. (1977). Noncovalent interaction. **Acc. Chem. Res.** 10: 365-371.

Krachodnok, S. and Haller, K. J. (2004). The crystal structure of pyridine-3,5-dicarboxylic acid. **The Sixth Conference of the Asian Crystallographic Association**. 27-30 June 2004, The Hong Kong University of Science and Technology, Hong Kong, China.

**Kuleshova, L. N. and Zorkii, P. M. (1980). Graphical enumeration of hydrogen-bonded structure. Acta Cryst. B36: 2113-2115.**

LaDuca, R. L., Finn, R. and Zubieta, J. (1999). A two-dimensional organic-inorganic material constructed from copper-dipyridylamine and vanadate chains: [Cu(dpa)$VO_3$]. **J. Chem. Soc., Chem. Comm.** (17): 1669-1670.

LaDuca, R. L., Raring, R. S. and Zubieta, J. (2001). Hydrothermal synthesis of organic-inorganic hybrid materials: Network structures of the bimetallic oxides [M(Hdpa)2V4O12] (M = Co, Ni, dpa = 4,4'-dipyridylamine). **Inorg. Chem.** 40(4): 607-612.

Lahiri, S., Thompson, L. J. and Moore, J. S. (2000). Solvophobically driven π-stacking of phenylene ethynylene macrocycles and oligomers. **J. Am. Chem. Soc.** 122(46): 11315-11319.

Law, T. S-C., Sung, H. H.-Y. and Williams, I. D. (2000). A porous organo-ceramic solid with cyclo-tetravanadate units, $[H_2pn][Mn_2(C_2O_4)(V_4O_{12})]$. **Inorg. Chem. Commun.** 3(8): 420-423.

Law, T. S-C. and Williams, I. D. (2000). Organo-directed synthesis of manganese vanadates with variable stoichiometry and dimensionality: 1-D $[(Hen)_2Mn(VO_3)_4]$, 2-D $[H_2en]_2[Mn(VO_3)_6]$, and 3-D $[H_2en][MnF(VO_3)_3]$. **Chem. Mater.** 12(8): 2070-2072.

Leininger, S., Olenyuk, B. and Stang, P. J. (2000). Self-assembly of discrete cyclic nanostructure mediated by transition metals. **Chem. Rev.** 100(3): 853-908.

Lehn, J.-M. (1988). Supramolecular chemistry-scope and perspectives molecules, supermolecules, and molecular devices (Nobel Lecture). **Angew. Chem., Int. Ed. Engl.** 27: 89-112.

Leonard, N. J. (1979). **Trimethylene bridges as synthetic spacers for the detection of intramolecular interactions**. **Acc. Chem. Res.** 12(12): 423-429.

Lincoln, S. F. (1997). Mechanistic studies of some macrocyclic complexes. **Coord. Chem. Rev.** 166: 255-285.

Linton, B. and Hamilton, A. D. (1999). Host-guest chemistry: Combinatorial receptors. **Curr. Opin. Chem. Biol.** 3(3): 307-312.

Liu, C.-M., Hou, Y.-L., Zhang, J. and Gao, S. (2002). Hydrothermal synthesis and crystal structure of a novel two-dimensional vanadium oxide complex with a

6,14-net sinusoidal ruffling anionic layer: [Ni(phen)$_2$V$_4$O$_{11}$] (phen = 1,10-phenanthroline). **Inorg. Chem.** 41(1): 140-143.

Lobachev, A. N. (1973). (ed.). **Hydrothermal Synthesis of Crystals.** Consultants Bureau: New York.

Lu, J., Paliwala, T., Lim, S. C., Yu, C., Niu, T. and Jacobson, A. J. (1997). Coordination polymers of Co(NCS)$_2$ with pyrazine and 4,4'-bipyridine: syntheses and structures. **Inorg. Chem.** 36(5): 923-929.

Lutz, H. D. (2003). Structure and strength of hydrogen bonds in inorganic solids. **J. Mol. Struc.** 646(1-3): 227-234.

Lutz, H. D. and Haeuseler, H. (1999). Infrared and Raman spectroscopy in inorganic solids research. **J. Mol. Struc.** 511-512: 69-75.

Ma, C. J. and Dougherty, D. A. (1997). The cation–π interaction. **Chem. Rev.** 97(5): 1301-1324.

Mambote, R. C. M., Reuter, M. A., Krijgsman, P. and Schuiling, R. D. (2000). Hydrothermal metallurgy: an overview of basic concepts and applications. **Miner. Eng.** 13(8-9): 803-822.

Matsuda, K., Stone, M. T. and Moore, J. S. (2002). Helical pitch of *m*-phenylene ethynylene poldamers by double spin labeling. **J. Am. Chem. Soc.** 124(40): 11836-11837.

Min, D. and Lee, S. W. (2002). Terbium-oxalate-pyridinedicarboxylate coordination polymers suggesting the reductive coupling of carbon dioxide ($CO_2$) to oxalate ($C_2O_4^{2-}$): [Tb$_2$(3,5-pdc)$_2$(H$_2$O)$_4$(C$_2$O$_4$)]·2H$_2$O and [Tb$_2$(2,4-pdc)(H$_2$O)(C$_2$O$_4$)]$_{0.5}$] (pdc = pyridinedicarboxylate). **Inorg. Chem. Commun.** 5(11): 978-983.

Millero, F. J. (1982). The effect of pressure on the solubility of minerals in water and seawater. **Geochim. Cosmochim. Acta.** 46(1): 11-22.

Min, D., Yoon, S. S., Lee, J. H., Suh, M. and Lee, S. W. (2001). A three-dimensional cobalt(II)-coordination polymer based on 3,5-pyridinedicarboxylate. **Inorg. Chem. Commun.** 4(6): 297-300.

Min, D., Yoon, S. S., Jung, D.-Y., Lee, C. Y., Kim, Y., Han, W. S. and Lee, S. W. (2001). One-dimensional copper-pyridinedicarboxylate polymer containing square-planar Cu(II) centers exhibiting antiferromagnetic coupling **Inorg. Chim. Acta.** 324(1-2): 293-299.

Morey; G. W., (1953). The System $H_2O$-$NaPO_3$. **J. Am. Chem. Soc.** 75(23): 5794-5797.

Morey, G. W. and Niggli, P. (1913). The hydrothermal formation of silicates, a review. **J. Am. Chem. Soc.** 35(9): 1086-1130.

Moulton, B. and Zaworotko, M. J. (2001). From molecules to crystal engineering: Supramolecular isomerism and polymorphism in network solids. **Chem. Rev.** 101(6): 1629-1658.

Müller, A. and Roy, S. (2003). En route from the mystery of molybdenum blue via related manipulatable building blocks to aspects of materials science. **Coord. Chem. Rev.** 245(1-2): 153-166.

Natarajan, S. (2003). Hydrothermal synthesis and crystal structure of a two-dimensional zinc vanadate, $[(NH_3(CH_2)_3NH)Zn]_2^{3+}[V_4O_{13}]^{6-}$. **Inorg. Chim. Acta.** 348: 233-236.

Nonius BV. (1998). **COLLECT: KappaCCD software**, Nonius BV, Delft, The Netherlands.

Oliver, S., Kuperman, A. and Ozin, G. A. (1998). A New Model for Aluminophosphate Formation: Transformation of a Linear Chain Aluminophosphate to Chain, Layer, and Framework Structures. **Angew. Chem. Int. Ed. Engl.** 37(1/2): 46-62.

Papaefstathiou, G. S. and MacGillivray, L. R. (2003). Inverted metal-organic frameworks: Solid-state hosts with modular functionality. **Coord. Chem. Rev.** 246(1-2): 169-184.

Pauling, L. (1945). **The Nature of the Chemical Bond**. Cornell University Press, USA.

Pech, R. and Pickardt, J. (1988). Aatena-Triaqua-$\mu$-[1,3,5-benzenetricarboxylato(2-)]copper(II). **Acta Cryst.** C44: 992-994.

Pejov, L. (2002). On a quantum theoretical basis for determination of the dependence of the intermolecular X–H(D) potential on the hydrogen bond strength. **J. Mol. Struc. (Theochem).** 498(1-3): 29-35.

Peppas, E., Anastassopoulou, J. and Theophanides, T. (2001). Supramolecular interaction between a barbiturate copper(II) complex and 2,6-bis(alconoylamino) pyridines. **J. Mol. Struc.** 559(1-3): 219-225.

Pertíerra, P., Salvadó, M. A., García-Granda, S., Bortun, A. I., Khainakov, S. A. and García, J. R. (2002). Hydrothermal synthesis and structural characterization of framework microporous mixed tin-zirconium silicates with the structure of umbite. **Inorg. Chem. Commun.** 5(10): 824-827.

Plater, M. J., Howie, R. A. and Lachowski, E. E. (1998). Hydrothermal synthesis and characterization of M(pdc)·2$H_2O$ (pdc = 3,5-pyridinedicaboxylate). A two-dimensional coordination polymer. **J. Chem. Res.** (S): 754-755.

Plater, M. J., Foreman, M. R. St. J., Howie, R. A. and Lachowski, E. E. (1998). Hydrothermal synthesis and characterization of M(pdc)·3$H_2O$ (pdc = 2,5-pyridinedicaboxylate); M = Co, Ni, $Co_xNi_y$ (x = 0.4-0.6, y = 0.6-0.4). **J. Chem. Res.** (S): 754-755.

Plater, M. J., Roberts, A. J. and Howie, R. A. (1998). Hydrothermal synthesis of Co(pdc)·2$H_2O$ (pdc = 3,5-pyridinedicarboxylate). A two-dimensional coordination polymer. **J. Chem. Res.** (S): 240-241.

Polak, E., Munn, J., Barnes, P. and Tarling, S. E. (1990). Time-resolved neutron diffraction analyses of hydrothermal syntheses using a novel autoclave cell. **J. Appl. Cryst.** 23: 258-262.

Rabenau, A. (1985). The Role of Hydrothermal Synthesis in Preparative Chemistry. **Angew. Chem. Int. Ed. Engl.** 24: 1026-1040.

Ramalingom, S., Podder, J. and Kalkura, S. N. (2001). Crystallization and Characterization of Orthorhombic $\beta$- $MgSO_4$·7$H_2O$. **Crys. Res. and Technol.** 36(12): 1357-1364

Rao, K. J., Vaidhyanathan, B., Ganguli, M. and Ramkrishnan, P. A. (1999). Synthesis of inorganic solids using microwaves. **Chem. Mater.** 11(4): 882-895.

Rathore, R., Lindeman, S. V. and Kochi, J. K. (1997). Charge-transfer probes for molecular recognition *via* steric hindrance in donor-acceptor pairs. **J. Am. Chem. Soc.** 119(40): 9393-9404.

Riou, D. and Férey, G. (1995). Intercalated Vanadyl Vanadate ($V^{IV}O$)[$V^{V}O_4$] 0.5[$C_3N_2H_{12}$]: Hydrothermal Synthesis, Crystal Structure, and Structural Correlations with $V_2O_5$ and Other Vanadyl Compounds. **J. Solid State Chem.** 120(1): 137-145.

Rizzarelli, E. and Vecchio, G. (1999). Metal complexes of functionalized cyclodextrins as enzyme models and chiral receptors. **Coord. Chem. Rev.** 188(1): 343-364.

Rowland, R. S. and Taylor, R. (1996). Intermolecular nonbonded contact distances in organic crystal structures: Comparison with distances expected from van der Waals radii. **J. Phys. Chem.** 100(18): 7384-7391.

Russell, V. M., Scudder, M. and Dance, I. (2001). The crystal supramolecularity of metal phenanthroline complexes. **J. Chem. Soc., Dalton Trans.** (6): 789-799.

Saha, D. K., Padhye, S., Anson, C. E. and Powell, A. K. (2002). Hydrothermal synthesis, crystal structure, spectroscopy, electrochemistry and antimycobacterial evaluation of the copper(II) ciprofloxacin complex: $[Cu(cf)_2(BF_4)_2]\cdot 6H_2O$. **Inorg. Chem. Commun.** 5(12): 1022-1027.

Schmaltz, B., Jouaiti, A., Hosseini, M. W. and Cian, A. D. (2001). Double stranded interwound infinite linear silver coordination network. **J. Chem. Soc., Chem. Comm.** (14): 1242-1243.

Scudder, M. and Dance, I. (1998). Crystal supramolecular motifs. Ladders, layers and labyrinths of $Ph_4P^+$ cations engaged in fourfold phenyl embraces. **J. Chem. Soc., Dalton Trans.** (19): 3155-3165.

Scudder, M. and Dance, I. (2002). Dimorphic intra- and intermolecular aryl motifs in symmetrical hexafaceted molecules $(Ar_nX)_3Y\text{-}Z\text{-}Y(XAr_n)_3$. **Chem. Eur. J.** 8(23): 5456-5468.

Scudder, M., Goodwin, H. A. and Dance, I. D. (1999). Crystal supramolecular motifs: two-dimensional grids of terpy embraces in $[ML_2]^z$ complexes (L = terpy or aromatic $N_3$-tridentate ligand). **New J. Chem.** (2): 695-705.

Serrano, L. J. and Sierra, T. (2003). Helical supramolecular organizations from metal-organic liquid crystals. **Coord. Chem. Rev.** 242(1-2): 73-85.

Sheldrick, G. M. (1996). **SADABS**. University of Göttingen, Germany.

Sheldrick, G. M. (1997). **SHELXL97. Program for the Refinement of Crystal Structures.** University of Göttingen, Germany.

Shimidzu, T. (1996). Porphyrin arrays connected with molecular wire. **Syn. Mat.** 81(2-3): 235-241.

Sōmiya, S. and Roy, R. (2000). Hydrothermal synthesis of fine oxide powders. **Bull. Mater. Sci.** 23(6): 453-460.

Sreekanth, A., Kala, U. L., Nayar, C. R. and Kurup, M. R. P. (2004). Cobalt(III) complexes of 2-hydroxyacetophenone N(4)-phenyl semicarbazone containing heterocyclic coligands: Syntheses, structure and spectral studies. **Polyhedron.** 23(1): 41-47.

Stang, P. J. and Olenyuk, B. (1997). Self-assembly, symmetry, and molecular architecture: coordination as the motif in the rational design of supramolecular metallacyclic polygons and polyhedra. **Acc. Chem. Res.** 30(12): 502-518.

Steed, J. W. (2001). First- and second-sphere coordination chemistry of alkali metal crown ether complexes. **Coord. Chem. Rev.** 215(1): 171-221.

Steed, J. W. and Atwood, J. L. (2000). **Supramolecular Chemistry.** Chichester: England.

Stout, G. H. and Jensen, L. H. (1989). **X-ray Structure Determination: A Practical Guide**. 2nd Edition, Wiley: New York.

Sun, S.-S. and Lees, A. J. (2002). Transition metal based supramolecular systems: Synthesis, photophysics, photochemistry and their potential applications as luminescent anion chemosensors. **Coord. Chem. Rev.** 230(1-2): 170-192.

Sun, C., Zheng, X. and Jin, L. (2003). Supramolecular formation via hydrogen bonding in the Zn(II), Mn(II), and Cu(II) complexes with 3-hydroxypicolinic acid. **J. Mol. Struc.** 646(1-3): 201-210.

Swiegers, G. F. and Malefetse, T. S. (2000). New self-assembled structural motifs in coordination chemistry. **Chem. Rev.** 100(9): 3483-3537.

Tobe, Y., Utsui, N., Kawabata, K., Nagano, A., Adechi, K., Araki, S., Sonoda, M., Hirose, K. and Naemura, K. (2002). *m*–Diethynylbezene macrocycles syntheses and self-association behavior in solution. **J. Am. Chem. Soc.** 124(19): 5350-5364.

Vögtle, F., Gestermann, S., Hesse, R., Schwierz, H. and Windisch, B. (2000). Functional dendrimers. **Prog. Polym. Sci.** 25(7): 987-1041.

Yuan, H., Thomas, L. and Woo, L. K. (1996). Synthesis and characterization of mono-, bis-, and tetrakis-pyridyltriarylporphyrin Pd(II) and Pt(II) supramole cular assemblies. Molecular structure of a Pd-linked bisporphyrin complex. **Inorg. Chem.** 35(10): 2808-2817.

Ward, M. D. (2000). Supramolecular coordination chemistry. **Annu. Rep. Prog. Chem., Sect.** A96: 345-385.

Waters, M. L. (2002). Aromatic interactions in model systems. **Curr. Opin. Chem. Biol.** 6(6): 736-741.

Whitfield, T., Zheng, L.-M., Wang, X. and Jacobson, A. J. (2001). Syntheses and characterization of Co(pydc)($H_2O$)$_2$ and Ni(pydc)($H_2O$) (pdyc = 3,5-pyridine-dicarboxylate. **Solid State Sci.** 3(8): 829-835.

Whittingham, M. S., Guo, J.-D., Chen, R., Chirayil, T., Janauer, G. and Zavalij, P. (1995). The hydrothermal synthesis of new oxide materials. **Solid State Ionics.** 75: 257-268.

Williams, I. D. (2004). **Personal communication.**

Yang, S., Song, Y., Ngala, K., Zavalij, P. Y. and Whittingham, M. S. (2003). Performance of $LiFePO_4$ as lithium battery cathode and comparison with manganese and vanadium oxides. **J. Power Sources.** 119-121: 239-246.

Yu, S.-H., Fujino, T. and Yoshimura, M. (2003). Hydrothermal synthesis of $ZnFe_2O_4$ ultrafine particles with high magnetization. **J. Magn. Magn. Mater.** 256(1-3): 420-424.

Zhang, Y., Haushalter, R. C. and Clearfield, A. (1996). Hydrothermal synthesis and structural characterization of layered vanadium oxides incorporating organic cations: $\alpha$-, $\beta$-($H_3N(CH_2)_2NH_3[V_4O_{10}]$ and $\alpha$-, $\beta$-($H_3N(C_2H_4)_2NH_3[V_4O_{10}]$. **Inorg. Chem.** 35(17): 4950-4956.

Zhang, F., Ngala, K. and Whittingham, M. S. (2000). Synthesis and electrochemistry of a vanadium pillared manganese oxide. **Elec. Commun.** 2(6): 445-447.

Zhang, L., Shi, Z., Yang, G., Chen, X. and Feng, S. (2000). Hydrothermal synthesis and crystal structure of a layered vanadium oxide with an interlayer metal co-ordination complex: $Cd[C_3N_2H_{11}]_2[V_8O_{20}]$. **J. Chem. Soc., Dalton Trans.** (3): 275-278.

Zheng, Y.-Q., Sun, J. and Lin, J.-L. (2003). Hydrogenmaleato bridged supramolecular double chains via π–π stacking interactions: syntheses, crystal structures and magnetic properties of $^{1}_{\infty}[Cu(phen)X(HL)_{2/2}]$ with $X=Cl^{-}$ (1), $NO_3^{-}$ (2) and $H_2L$=maleic acid. **J. Mol. Struc.** 650(1-3): 49-56.

# Appendices

# Appendix A

# Supplementary Material for [Co(picoline)$_3$]·H$_2$O

Table A1.1. Derived Fractional Monoclinic Coordinates[a] and Isotropic Atomic Displacement Parameters[b] (Å$^2$) for the Unrefined Hydrogen Atoms in [Co(picoline)$_3$]·H$_2$O.

| Atom | *x* | *y* | *z* | $U_{iso}$ |
|---|---|---|---|---|
| H1 | 0.07429 | 0.54979 | 0.61946 | 0.03771 |
| H2 | 0.00317 | 0.65358 | 0.62597 | 0.04651 |
| H3 | −0.05786 | 0.48689 | 0.62956 | 0.04970 |
| H4 | –0.04654 | 0.21865 | 0.62678 | 0.04307 |
| H7 | 0.17979 | 0.02151 | 0.52081 | 0.04288 |
| H8 | 0.24350 | −0.11939 | 0.57190 | 0.05489 |
| H9 | 0.26938 | −0.12273 | 0.73530 | 0.05843 |
| H10 | 0.22805 | 0.00393 | 0.84584 | 0.04764 |
| H13 | 0.07334 | 0.08861 | 0.42858 | 0.03735 |
| H14 | 0.08547 | 0.14215 | 0.26980 | 0.04825 |
| H15 | 0.13697 | 0.33186 | 0.23666 | 0.05268 |
| H16 | 0.17445 | 0.47160 | 0.36554 | 0.04855 |

Table A1.2. Selected Torsion Angles[a] (°) for [Co(picoline)3]·$H_2O$.

| | | | |
|---|---|---|---|
| O1−Co−N1−C1 | −178.11(0.17) | O5−Co−O1−C6 | 178.50(99.99) |
| O3−Co−N1−C1 | 89.91(0.17) | N1−Co−O1−C6 | −8.14(0.14) |
| O5−Co−N1−C1 | 1.74(0.17) | N3−Co−O1−C6 | −99.84(0.14) |
| N3−Co−N1−C1 | −83.03(0.17) | N2−Co−O1−C6 | 164.63(0.14) |
| N2−Co−N1−C1 | 127.59(0.43) | O1−Co−N2−C7 | 81.78(0.19) |
| O1−Co−N1−C5 | 7.36(0.13) | O3−Co−N2−C7 | 173.54(0.19) |
| O3−Co−N1−C5 | −84.62(0.13) | O5−Co−N2−C7 | −97.90(0.19) |
| O5−Co−N1−C5 | −172.79(0.13) | N1−Co−N2−C7 | 135.70(0.42) |
| N3−Co−N1−C5 | 102.44(0.13) | N3−Co−N2−C7 | −13.55(0.19) |
| N2−Co−N1−C5 | −46.94(0.51) | O1−Co−N2−C11 | −100.37(0.14) |
| C5−N1−C1−C2 | 0.36(0.29) | O3−Co−N2−C11 | −8.61(0.13) |
| Co−N1−C1−C2 | −173.83(0.15) | O5−Co−N2−C11 | 79.95(0.14) |
| N1−C1−C2−C3 | −0.20(0.31) | N1−Co−N2−C11 | −46.45(0.51) |
| C1−C2−C3−C4 | 0.01(0.32) | N3−Co−N2−C11 | 164.30(0.14) |
| C2−C3−C4−C5 | 0.02(0.32) | C11−N2−C7−C8 | −0.12(0.33) |
| C1−N1−C5−C4 | −0.33(0.28) | Co−N2−C7−C8 | 177.59(0.18) |
| Co−N1−C5−C4 | 174.72(0.15) | N2−C7−C8−C9 | −1.86(0.38) |
| C1−N1−C5−C6 | 179.40(0.18) | C7−C8−C9−C10 | 2.03(0.40) |
| Co−N1−C5−C6 | −5.55(0.20) | C8−C9−C10−C11 | −0.30(0.38) |
| C3−C4−C5−N1 | 0.14(0.30) | C7−N2−C11−C10 | 1.97(0.31) |
| C3−C4−C5−C6 | −179.57(0.20) | Co−N2−C11−C10 | −176.15(0.17) |
| N1−C5−C6−O2 | 179.27(0.20) | C7−N2−C11−C12 | −177.00(0.18) |
| C4−C5−C6−O2 | –1.00(0.33) | Co−N2−C11−C12 | 4.87(0.21) |
| N1−C5−C6−O1 | −0.81(0.25) | C9−C10−C11−N2 | −1.75(0.34) |
| C4−C5−C6−O1 | 178.92(0.18) | C9−C10−C11−C12 | 177.12(0.22) |
| O2−C6−O1−Co | −173.09(0.18) | N2−C11−C12−O4 | −177.29(0.20) |
| C5−C6−O1−Co | 6.99(0.21) | C10−C11−C12−O4 | 3.75(0.34) |
| O3−Co−O1−C6 | 79.83(0.14) | N2−C11−C12−O3 | 4.16(0.27) |
| C10−C11−C12−O3 | −174.80(0.21) | N3−C13−C14−C15 | −0.12(0.34) |
| O4−C12−O3−Co | 170.16(0.19) | C13−C14−C15−C16 | −1.04(0.36) |
| C11−C12−O3−Co | −11.38(0.23) | C14−C15−C16−C17 | 0.93(0.36) |

Table A1.2. (Continued)

| | | | |
|---|---|---|---|
| O1−Co−O3−C12 | 101.72(0.15) | C13−N3−C17−C16 | −1.54(0.31) |
| O5−Co−O3−C12 | −76.97(0.15) | Co−N3−C17−C16 | 179.18(0.17) |
| N1−Co−O3−C12 | −174.05(0.16 | C13−N3−C17−C18 | 178.46(0.18) |
| N3−Co−O3−C12 | −80.93(0.57) | Co−N3−C17−C18 | −0.82(0.22) |
| N2−Co−O3−C12 | 11.41(0.15) | C15−C16−C17−N3 | 0.36(0.34) |
| O1−Co−N3−C13 | 7.78(0.18) | C15−C16−C17−C18 | −179.64(0.21) |
| O3−Co−N3−C13 | −169.57(0.47) | N3−C17−C18−O6 | 172.54(0.21) |
| O5−Co−N3−C13 | –173.54(0.18) | C16−C17−C18−O6 | −7.46(0.35) |
| N1−Co−N3−C13 | −76.70(0.18) | N3−C17−C18−O5 | −7.34(0.26) |
| N2−Co−N3−C13 | 98.76(0.18) | C16−C17−C18−O5 | 172.66(0.20) |
| O1−Co−N3−C17 | −173.02(0.14) | O6−C18−O5−Co | −167.80(0.19) |
| O3−Co−N3−C17 | 9.63(0.61) | C17−C18−O5−Co | 12.08(0.22) |
| O5−Co−N3−C17 | 5.66(0.14) | O1−Co−O5−C18 | 71.49(2.59) |
| N1−Co−N3−C17 | 102.50(0.14) | O3−Co−O5−C18 | 170.19(0.14) |
| N2−Co−N3−C17 | −82.04(0.14) | N1−Co−O5−C18 | −101.85(0.14) |
| C17−N3−C13−C14 | 1.41(0.31) | N3−Co−O5−C18 | −10.30(0.14) |
| Co−N3−C13−C14 | −179.44(0.15) | N2−Co−O5−C18 | 85.36(0.14) |

[a]Estimated standard deviations of the least significant digits are given in parentheses.

Table A1.3. Principal Mean Square Atomic Displacements *U* (in Å$^2$) for [Co(picoline)$_3$]·H$_2$O.

| Atom | minimum | intermediate | maximum |
|---|---|---|---|
| Co | 0.0282 | 0.0219 | 0.0184 |
| N1 | 0.0308 | 0.0220 | 0.0217 |
| C1 | 0.0339 | 0.0309 | 0.0295 |
| C2 | 0.0555 | 0.0339 | 0.0268 |
| C3 | 0.0657 | 0.0360 | 0.0225 |
| C4 | 0.0510 | 0.0343 | 0.0223 |
| C5 | 0.0372 | 0.0233 | 0.0225 |
| C6 | 0.0389 | 0.0283 | 0.0240 |
| O1 | 0.0381 | 0.0283 | 0.0240 |
| O2 | 0.0791 | 0.0481 | 0.0230 |
| N2 | 0.0319 | 0.0254 | 0.0189 |
| C7 | 0.0494 | 0.0322 | 0.0256 |
| C8 | 0.0635 | 0.0503 | 0.0234 |
| C9 | 0.0694 | 0.0567 | 0.0199 |
| C10 | 0.0525 | 0.0397 | 0.0269 |
| **C11** | **0.0306** | **0.0257** | **0.0234** |
| C12 | 0.0353 | 0.0348 | 0.0233 |
| O3 | 0.0471 | 0.0285 | 0.0206 |
| O4 | 0.0874 | 0.0478 | 0.0209 |
| N3 | 0.0309 | 0.0255 | 0.0190 |
| C13 | 0.0396 | 0.0304 | 0.0235 |
| C14 | 0.0622 | 0.0373 | 0.0212 |
| C15 | 0.0648 | 0.0437 | 0.0232 |
| C16 | 0.0588 | 0.0365 | 0.0261 |
| C17 | 0.0369 | 0.0288 | 0.0199 |
| C18 | 0.0401 | 0.0328 | 0.0218 |
| O5 | 0.0377 | 0.0298 | 0.0215 |
| O6 | 0.0773 | 0.0511 | 0.0219 |
| **O7** | **0.1056** | **0.0500** | **0.0360** |

Table A1.4. Mean Planes Calculated for $[Co(picoline)_3]\cdot H_2O$.
Least-squares planes (x,y,z in crystal coordinates) and deviations from them
(* indicates atom used to define plane)

Plane 1: 21.797(19)x -5.789(6)y -0.301(12)z = 0.971(6)

*  0.0092 (0.0013) N3
*  -0.0044 (0.0015) C13
*  -0.0041 (0.0016) C14
*  0.0077 (0.0017) C15
*  -0.0030 (0.0017) C16
*  -0.0055 (0.0015) C17
-2.7915 (0.0025) H3_$3
0.0266 (0.0027) Co
-0.0245 (0.0033) C18
-0.1758 (0.0033) O5
0.0942 (0.0039) O6
-0.0141 (0.0017) H13
-0.0119 (0.0018) H14
0.0225 (0.0018) H15
-0.0083 (0.0018) H16

Rms deviation of fitted atoms = 0.006

Plane 2: 19.65(.5)x -6.309(18)y +0.88(5)z = 1.02(4)

Angle to Plane 1 = 7.05(27)

*  0.0000 (0.0000) C18
*  0.0000 (0.0000) O5
*  0.0000 (0.0000) O6
0.3619 (0.0056) Co
0.1612 (0.0110) N3
0.1489 (0.0168) C13
0.0045 (0.0204) C14
-0.1313 (0.0182) C15
-0.1424 (0.0122) C16
0.0029 (0.0088) C17

Table A1.4. (Continued)

Plane 3: 1.044(23)x + 0.092(8)y +13.672(3)z = 12.007(4)

* -0.0018 (0.0013) N1_$2
* 0.0013 (0.0014) C1_$2
* -0.0001 (0.0014) C2_$2
* -0.0006 (0.0015) C3_$2
* 0.0002 (0.0015) C4_$2
* 0.0010 (0.0013) C5_$2

Rms deviation of fitted atoms = 0.0010

Plane 4: 1.044(23)x -0.092(8)y +13.672(3)z = 8.501(3)

Angle to Plane 3 = 1.23 ( 0.02 )

* 0.0018 (0.0013) N1
* -0.0013 (0.0014) C1
* 0.0001 (0.0014) C2
* 0.0006 (0.0015) C3
* -0.0002 (0.0015) C4
* -0.0010 (0.0013) C5
0.1625 (0.0026) Co
-0.0112 (0.0033) C6
-0.0326 (0.0033) O1
-0.0020 (0.0039) O2
-0.0045 (0.0016) H1
0.0008 (0.0016) H2
0.0015 (0.0016) H3
-0.0001 (0.0016) H4
3.4646 (0.0034) C5_$2
-3.4203 (0.0030) C5_$3

Rms deviation of fitted atoms = 0.0010

Table A1.4. (Continued)

Plane 5: 1.044(23)x -0.092(8)y +13.672(3)z = 5.079(5)

* -0.0018 (0.0013) N1_$3
* 0.0013 (0.0014) C1_$3
* -0.0001 (0.0014) C2_$3
* -0.0006 (0.0015) C3_$3
* 0.0002 (0.0015) C4_$3
* 0.0010 (0.0013) C5_$3

Rms deviation of fitted atoms = 0.0010

Plane 6: -17.030(23)x +6.624(6)y -2.830(5)z = 2.246(5)

* 0.9242 (0.0022) H1_$3
* -0.9562 (0.0019) H2_$3
* -0.8811 (0.0020) H3_$3
* 1.0807 (0.0020) H4_$3
* 0.1689 (0.0014) H1_$2
* -0.3364 (0.0014) H2_$2
-2.4697 (0.0034) H3_$2
-4.0617 (0.0029) H4_$2

Rms deviation of fitted atoms = 0.8015

# Appendix B

# Supplementary Material for $(H_2dap)^{2+}[(V^{IV}O)_2(V^{V}O_4)_2]^{2-}$

Table B1.1. Derived Fractional Monoclinic Coordinates[a] and Isotropic Atomic Displacement Parameters[b] ($Å^2$) for the Hydrogen Atoms in $(H_2dap)^{2+}[(V^{IV}O)_2(V^{V}O_4)_2]^{2-}$.

| Atom | *x* | *y* | *z* | $U_{iso}$ |
|---|---|---|---|---|
| H1a | 0.37525(250) | −0.29628(104) | −0.18978(141) | 0.02713 |
| H1b | 0.53321(257) | −0.27721(62) | −0.21290(144) | 0.02713 |
| H1c | 0.39888(271) | −0.32875(137) | −0.27298(105) | 0.02713 |
| H1d | 0.42658 | −0.11225 | −0.31076 | 0.03557 |
| H1e | 0.41771 | −0.07143 | −0.21490 | 0.03557 |
| H2a | 0.14668 | −0.03922 | −0.32705 | 0.03637 |
| H2b | 0.12087 | –0.19458 | −0.31692 | 0.03637 |
| H2c | −0.10116(72) | −0.02097(233) | −0.27176(149) | 0.02878 |
| H2d | −0.11653(112) | −0.05702(245) | −0.19320(112) | 0.02878 |
| H2e | −0.11952(118) | −0.14739(191) | −0.25395(155) | 0.02878 |
| H3a | 0.16581 | −0.01175 | −0.18224 | 0.03310 |
| H3b | 0.14468 | −0.16731 | −0.17082 | 0.03310 |

Table B1.2. Selected Torsion Angles[a] (°) for $(H_2dap)^{2+}[(V^{IV}O)_2(V^{V}O_4)_2]^{2-}$.

| | | | |
|---|---|---|---|
| O5−V1−V2−O6 | −179.46(0.11) | O9_$a−V1−O2−V3 | 128.81(0.16) |
| O2−V1−V2−O6 | −87.63(0.13) | O3_$b−V1−O2−V3 | 50.13(0.17) |
| O7−V1−V2−O6 | 87.97(0.13) | V2−V1−O2−V3 | −162.21(0.23) |
| O9_$a−V1−V2−O6 | 56.61(0.12) | O5−V1−O2−V2 | 98.36(0.11) |
| O3_$b−V1−V2−O6 | −48.67(0.12) | O7−V1−O2−V2 | −2.87(0.09) |
| O5−V1−V2−O7 | 92.57(0.13) | O9_$a−V1−O2−V2 | −68.98(0.19) |
| O2−V1−V2−O7 | −175.61(0.13) | O3_$b−V1−O2−V2 | −147.66(0.10) |
| O9_$a−V1−V2−O7 | −31.36(0.13) | O6−V2−O2−V3 | −91.94(0.16) |
| O3_$b−V1−V2−O7 | −136.64(0.13) | O7−V2−O2−V3 | 166.72(0.16) |
| O5−V1−V2−O2 | −91.83(0.13) | O4_$d−V2−O2−V3 | 17.51(0.14) |
| O7−V1−V2−O2 | 175.61(0.13) | O8_$c−V2−O2−V3 | 93.47(0.18) |
| O9_$a−V1−V2−O2 | 144.24(0.13) | V1−V2−O2−V3 | 163.81(0.21) |
| O3_$b−V1−V2−O2 | 38.97(0.13) | O6−V2−O2−V1 | 104.25(0.11) |
| O5−V1−V2−O4_$d | −53.16(0.11) | O7−V2−O2−V1 | 2.91(0.09) |
| O2−V1−V2−O4_$d | 38.67(0.13) | O4_$d−V2−O2−V1 | −146.30(0.11) |
| O7−V1−V2−O4_$d | −145.73(0.13) | O8_$c−V2−O2−V1 | −70.35(0.16) |
| O9_$a−V1−V2−O4_$d | −177.09(0.09) | O1−V3−O3−V1_$b | −3.01(0.25) |
| O3_$b−V1−V2−O4_$ | 77.63(0.11) | O4−V3−O3−V1_$b | 120.48(0.22) |
| O5−V1−V2−O8_$c | 47.89(0.12) | O2−V3−O3−V1_$b | −117.69(0.22) |
| O2−V1−V2−O8_$c | 139.72(0.13) | O1−V3−O4−V2_$d | 27.47(0.21) |
| O7−V1−V2−O8_$c | −44.67(0.13) | O3−V3−O4−V2_$d | −88.44(0.18) |
| O9_$1−V1−V2−O8_$c | −76.04(0.11) | O2−V3−O4−V2_$d | 152.40(0.15) |
| O3_$2−V1−V2−O8_$c | 178.69(0.09) | O10−V4−O7−V2 | 125.11(0.19) |
| O1−V3−O2−V1 | −136.87(0.17) | O8−V4−O7−V2 | 13.77(0.22) |
| O3−V3−O2−V1 | −26.25(0.19) | O9−V4−O7−V2 | −107.89(0.19) |
| O4−V3−O2−V1 | 94.66(0.17) | O10−V4−O7−V1 | −53.48(0.17) |
| O1−V3−O2−V2 | 65.08(0.17) | O8−V4−O7−V1 | −164.82(0.13) |
| O3−V3−O2−V2 | 175.70(0.14) | O9−V4−O7−V1 | 73.53(0.15) |
| O4−V3−O2−V2 | −63.39(0.16) | O6−V2−O7−V4 | 77.01(0.20) |
| O5−V1−O2−V3 | −63.85(0.18) | O2−V2−O7−V4 | 178.34(0.21) |
| O7−V1−O2−V3 | −165.08(0.19) | O4_$d−V2−O7−V4 | −115.19(0.20) |

Table B1.2. (Continued)

| | | | |
|---|---|---|---|
| O8_$c−V2−O7−V4 | −36.89(0.19) | O2−V1−O7−V2 | 2.92(0.09) |
| V1−V2−O7−V4 | −178.80(0.25) | O9_$a−V1−O7−V2 | 153.23(0.11) |
| O6−V2−O7−V1 | −104.19(0.12) | O3_$b−V1−O7−V2 | 77.28(0.16) |
| O2−V2−O7−V1 | −2.86(0.09) | O10−V4−O8−V2_$c | 8.11(0.27) |
| O4_$d−V2−O7−V1 | 63.61(0.19) | O9−V4−O8−V2_$c | −115.66(0.24) |
| O8_$c−V2−O7−V1 | 141.91(0.10) | O7−V4−O8−V2_$c | 123.39(0.23) |
| O5−V1−O7−V4 | 81.43(0.15) | O10−V4−O9−V1_$a | −32.41(0.23) |
| O2−V1−O7−V4 | −178.03(0.16) | O8−V4−O9−V1_$a | 83.42(0.20) |
| O9_$a−V1−O7−V4 | −27.72(0.14) | O7−V4−O9−V1_$a | −155.33(0.17) |
| O3_$b−V1−O7−V4 | −103.67(0.16) | N1−C1−C2−C3 | 82.52(0.38) |
| V2 −V1−O7−V4 | 179.05(0.20) | C1−C2−C3−N2 | −178.58(0.26) |
| O5−V1−O7−V2 | −97.62(0.11) | | |

Symmetry transformations used to generate equivalent atoms:

(a) –x, –y, –z; (b) –x, 1–y, –z; (c) 1–x, –y, –z; (d) 1–x, 1–y, –z

[a]Estimated standard deviations of the least significant digits are given in parentheses.

Table B1.3. Principal Mean Square Atomic Displacements *U* (in Å$^2$) for $(H_2dap)^{2+}[(V^{IV}O)_2(V^{V}O_4)_2]^{2-}$.

| atom | minimum | intermediate | maximum |
|---|---|---|---|
| V1 | 0.0175 | 0.0068 | 0.0054 |
| V2 | 0.0178 | 0.0069 | 0.0050 |
| V3 | 0.0203 | 0.0074 | 0.0037 |
| V4 | 0.0210 | 0.0077 | 0.0040 |
| O1 | 0.0376 | 0.0191 | 0.0115 |
| O2 | 0.0339 | 0.0068 | 0.0046 |
| O3 | 0.0361 | 0.0097 | 0.0080 |
| O4 | 0.0292 | 0.0112 | 0.0078 |
| O5 | 0.0275 | 0.0211 | 0.0165 |
| O6 | 0.0333 | 0.0221 | 0.0160 |
| O7 | 0.0351 | 0.0069 | 0.0056 |
| O8 | 0.0410 | 0.0097 | 0.0085 |
| O9 | 0.0318 | 0.0119 | 0.0069 |
| O10 | 0.0418 | 0.0185 | 0.0148 |
| N1 | 0.0326 | 0.0240 | 0.0175 |
| N2 | 0.0407 | 0.0215 | 0.0163 |
| C1 | 0.0512 | 0.0290 | 0.0168 |
| C2 | 0.0460 | 0.0312 | 0.0220 |
| C3 | 0.0389 | 0.0271 | 0.0243 |

Table B1.4. Mean Planes Calculated for $(H_2dap)^{2+}[(V^{IV}O)_2(V^{V}O_4)_2]^{2-}$.
Least-squares planes (x,y,z in crystal coordinates) and deviations from them
(* indicates atom used to define plane)

Plane 1: 1.319(6)x +1.984(9)y +14.359(9)z = 0.672(2)

*  0.0415 (0.0011) O2
* -0.0427 (0.0012) O7
*  0.0396 (0.0011) O9_$1
* -0.0384 (0.0011) O3_$2
  0.5722 (0.0012) V1
 -0.4893 (0.0023) V2
  0.3779 (0.0031) V3
 -0.0471 (0.0030) V4
  2.2137 (0.0026) O5
 -2.1252 (0.0033) O6
 -0.0427 (0.0012) O7
  0.0415 (0.0011) O2
  0.1641 (0.0038) O4_$4
  0.2208 (0.0039) O8_$3

Rms deviation of fitted atoms = 0.0406

Plane 2: 0.740(6)x +1.921(8)y +14.737(8)z = 0.509(3)

Angle to Plane 1 = 4.22(7)

* -0.0351 (0.0011) O7
*  0.0361 (0.0012) O2
* -0.0332 (0.0011) O4_$4
*  0.0323 (0.0011) O8_$3
  0.6685 (0.0022) V1
 -0.5868 (0.0012) V2
  0.3449 (0.0029) V3
 -0.0108 (0.0031) V4
  0.0361 (0.0012) O2
 -0.0351 (0.0011) O7
  0.2376 (0.0038) O9_$1
  0.1523 (0.0038) O3_$2
  2.2908 (0.0031) O5
 -2.2132 (0.0027) O6

Rms deviation of fitted atoms = 0.0342

Table B1.4. (Continued)

Plane 3: 1.028(4)x + 2.046(7)y + 14.530(8)z = 0.678(2)

* -0.0141 (0.0017) O2
* -0.1152 (0.0018) O7
* 0.0610 (0.0013) O9_$1
* 0.0045 (0.0013) O3_$2
* 0.0140 (0.0013) O4_$4
* 0.0497 (0.0013) O8_$3
0.5561 (0.0011) V1
-0.6029 (0.0012) V2
0.3257 (0.0024) V3
-0.1223 (0.0025) V4
2.1887 (0.0025) O5
-2.2346 (0.0027) O6

Rms deviation of fitted atoms = 0.0576

# Appendix C

# Submitted Abstracts and Presentations

1. Kunapongkitti, S., Chainok, K. and Haller, K. J. Synthesis and Characterization of Four-Coordinate Nickel Nitrosyl Bis-Triphenyl Phosphine Halide Complexes. **The 27th Congress on Science and Technology of Thailand.** 16-18 October 2001, Hadyai, Songkla, Thailand.
2. Chainok, K., Haller, K. J. and Williams, I. D. Crystal Structure of the Missing $[Cu_2(terephthalate)_4]$ "Paddle-Wheel" Coordi nation Polymer. **The 28th Congress on Science and Technology of Thailand.** 24-26 October 2002, Queen Sirikit National Convention Center, Bangkok, Thailand.
3. Chainok, K. and Haller, K. J. Hydrothermal Synthesis and Characterization of a Microporous Vanadium Oxide Crystal and Molecular Structure of 2-Hydroxy-N-(2-Aminosalicylidene)Aniline. **The 3rd National Symposium on Graduate Research.** 18-19 August 2002, Suranaree University of Technology, Nakhon Ratchasima, Thailand.
4. Chainok, K., Krachodnok, S. and Haller, K. J. Hydrothermal Synthesis and Characterization of $(NH_3CH_2CH_2CH_2NH_3)^{2+}[(VO)_2(VO_4)_2]^{2-}$. **The 29th Congress on Science and Technology of Thailand.** 20-22 October 2003, Golden Jubilee Convention Hall, Khon Kean University, Thailand.
5. Chainok, K. and Haller, K. J. Hydrothermal Synthesis and Characterization of a Microporous Cobalt Vanadium Oxide Framework Compound. **The 10th Tri-**

**University International Joint Seminar & Symposium 2003: Role of Asia in the World**. 18-21 October 2003, Mie University, Japan.

6. Chainok, K. and Haller, K. J. Hydrothermal Synthesis, Characterization, and Supramolecular Structure of $[Co(C_6H_4O_2N)_3]\cdot H_2O$. **The Sixth Conference of the Asian Crystallographic Association, AsCA'04.** 27-30 June 2004, Hong Kong University of Science and Technology, Hong Kong, China.
7. Chainok, K. and Haller, K. J. Supramolecular Interactions in $[Co(picoline)_3]\cdot H_2O$. **The 4th National Symposium on Graduate Research.** 10-11 August 2004, Lotus Pang Suan Keaw, Chaing Mai, Thailand.
8. Chainok, K., Haller, K. J., Sung, H. H.-Y. and Williams, I. D. Supramolecular Structure of $[(ImH)^+]_2[Co(H_2O)_6]^{2+}[Co(H_2O)_6]^{2+}[Co(TMA)_2(H_2O)_4]^{4-}$. **The 30th Congress on Science and Technology of Thailand.** 19-21 October 2004, Impact Exhibition and Convention Center, Mueng Thong Thani, Bangkok, Thailand.

# Curriculum Vitae

**KITTIPONG CHAINOK**

**Born**: May 26, 1977, Nakhon Ratchasima, Thailand

**Citizenship**: Thai

**Martial Status**: Single

---

**Degree**:

2004 M. Sc., Chemistry
Suranaree University of Technology, Nakhon Ratchasima, Thailand

2000 B. Sc., Chemistry
Ramkhamheang University, Bankok, Thailand

**Relevant Experience**:

2001 Research Assistant: Assoc. Prof. Dr. Kenneth J. Haller

**Publication**:

1. Chainok, K. and Haller, K. J. (2003). Hydrothermal Synthesis and Characterization of a Microporous Cobalt Vanadium Oxide Framework Compound. **Proceedings of the 10th Tri-University International Joint Seminar & Symposium 2003: Role of Asia in the World**. Mie University, Japan. p. 373-376.

**Scholarships, Honors, and Awards**:

**Research Grant,** Suranaree University of Technology for M.Sc. degree study.

**Travel Grant,** Suranaree University of Technology for The Tri-University International Joint Seminar & Symposium 2003, Mie University, Japan.

**IUCr Young Scientist Grant,** to present paper at the Asian Crystallographic Association meeting, AsCA'04, Hong Kong.

**International Union of Crystallography Presentation Prize**, student competition for best presentation, Asian Crystallographic Association meeting, AsCA'04, Hong Kong.